

## 6. The finite element process of solution

At this point it should be clear that the principle of virtual work is an integral form of expressing equilibrium, and when we introduce the other two basic requirements to be satisfied, namely, compatibility and the constitutive behavior into the virtual work statement, we have the mathematical model formulated in integral form. It is then called the variational formulation of the problem.

The question that might be asked is: what is the practical value of the principle of virtual work formulation? For the differential formulation of problems, there are methods of finding analytical solutions. However, for the virtual work formulation no method of solution has been presented so far.

As an example, let us recall our model problem – the 1-D bar problem. Examining the formulation given by equation (5.20), we recognize that even for this problem – the simplest problem – there is no systematic method of finding a displacement field  $u(x)$  which would satisfy equation (5.20) for every virtual displacement  $\delta u(x)$ . On the other hand, we know how to find the solution  $u(x)$  for the differential formulation. Therefore, if our objective were to only solve the bar problem, there would be no point in exploring the principle of virtual work as a basis of solution. However, as we step up our ladder of hierarchical mathematical models, *i.e.*, as we consider increasingly more complex models, we realize that to find the analytical solution of the differential formulation of these models becomes increasingly more difficult and indeed impossible, for example, for 3-D geometrically complex problems.

Of course, the principle of virtual work formulations of such problems would not offer an easier route for an exact analytical solution. However, as it will be seen shortly, the principle of virtual work formulation provides an effective basis for a numerical solution – namely, the finite element solution. We introduce next the finite element formulation starting with the solution of the 1-D bar problem.

### 6.1 Finite element formulation of 1-D bar problem

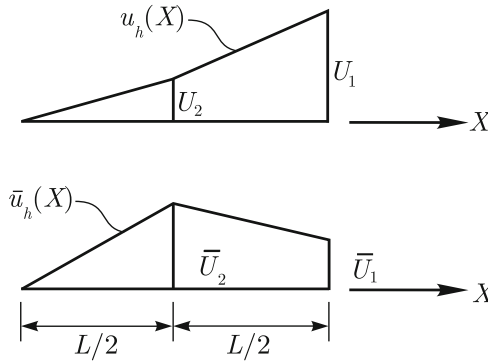
Let us consider the principle of virtual work formulation for the bar problem as given in equation (5.20), with the notation  $\bar{u}(x) = \delta u(x)$ . Let the exact solution be  $u(X)$  where  $X$  is the global longitudinal coordinate. We use

this principle to establish a finite element solution  $u_h(X)$  which, if properly constructed, can be as close as we wish to the exact solution  $u(X)$ . The governing equation to find  $u_h(X)$  is

$$\int_0^L EA \frac{d\bar{u}_h}{dX} \frac{du_h}{dX} dX = \int_0^L f\bar{u}_h dX + R\bar{u}_h |_{X=L} \tag{6.1}$$

for all  $\bar{u}_h(X)$  with  $\bar{u}_h(0) = 0$ .

To proceed further we need to assume a spatial variation for  $u_h(X)$  and  $\bar{u}_h(X)$ . Let us assume the functional form of  $u_h(X)$  and  $\bar{u}_h(X)$  shown in Figure 6.1.



**Fig. 6.1.** Definition of  $u_h(X)$  and  $\bar{u}_h(X)$

As implicitly defined in the Figure 6.1,  $u_h(X)$  and  $\bar{u}_h(X)$  have the following properties:

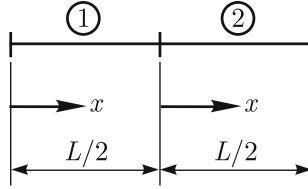
- They are zero at  $X = 0$ .
- They assume the values of  $U_2, \bar{U}_2$  at  $X = L/2$  and  $U_1, \bar{U}_1$  at  $X = L$ .
- They are linear for  $0 \leq X \leq L/2$  and  $L/2 \leq X \leq L$ .

Hence the values  $U_1, U_2$  and  $\bar{U}_1, \bar{U}_2$  completely define  $u_h(X)$  and  $\bar{u}_h(X)$ .

Before further developing the discussion, let us analytically characterize  $u_h(X)$  and  $\bar{u}_h(X)$ . In Figure 6.1, we consider two subdomains: subdomain (1) corresponding to  $0 \leq X \leq L/2$  and subdomain (2) corresponding to  $L/2 \leq X \leq L$ . Figure 6.2 shows these subdomains and also defines domain local coordinate systems represented by  $x$ .

Consider  $u^{(1)}(x)$  as the  $u_h(X)$  for subdomain (1) and  $u^{(2)}(x)$  as the  $u_h(X)$  for subdomain (2). Likewise  $\bar{u}^{(1)}(x), \bar{u}^{(2)}(x)$  represent  $\bar{u}_h(X)$  for subdomains (1) and (2). From this point onwards, we refer to the subdomain ( $m$ ) as element ( $m$ ) and use the superscript ( $m$ ). We have

$$u^{(1)} = \left[ \begin{array}{c} 0 \\ \frac{x}{(L/2)} \end{array} \right] \left[ \begin{array}{c} U_1 \\ U_2 \end{array} \right] = \mathbf{H}^{(1)}\mathbf{U} \tag{6.2}$$



**Fig. 6.2.** Subdivision of the domain for bar problem

$$u^{(2)} = \left[ \frac{x}{(L/2)} \quad 1 - \frac{x}{(L/2)} \right] \begin{bmatrix} U_1 \\ U_2 \end{bmatrix} = \mathbf{H}^{(2)}\mathbf{U} \tag{6.3}$$

where  $\mathbf{U}^T = [U_1 \quad U_2]$  and the  $\mathbf{H}^{(1)}$  and  $\mathbf{H}^{(2)}$  are the displacement interpolation matrices. Similarly

$$\bar{u}^{(1)} = \mathbf{H}^{(1)}\bar{\mathbf{U}} \quad \bar{u}^{(2)} = \mathbf{H}^{(2)}\bar{\mathbf{U}} \tag{6.4}$$

where  $\bar{\mathbf{U}}^T = [\bar{U}_1 \quad \bar{U}_2]$ .

The strains in each element are

$$\varepsilon^{(1)}(x) = \frac{du^{(1)}(x)}{dx} = \left[ 0 \quad \frac{1}{L/2} \right] \begin{bmatrix} U_1 \\ U_2 \end{bmatrix} = \mathbf{B}^{(1)}\mathbf{U} \tag{6.5}$$

$$\varepsilon^{(2)}(x) = \frac{du^{(2)}(x)}{dx} = \left[ \frac{1}{L/2} \quad -\frac{1}{L/2} \right] \begin{bmatrix} U_1 \\ U_2 \end{bmatrix} = \mathbf{B}^{(2)}\mathbf{U}. \tag{6.6}$$

These expressions give the strain interpolation matrices  $\mathbf{B}^{(m)}$ ,  $m = 1, 2$ . The virtual strains are given by

$$\bar{\varepsilon}^{(1)} = \mathbf{B}^{(1)}\bar{\mathbf{U}} \tag{6.7}$$

$$\bar{\varepsilon}^{(2)} = \mathbf{B}^{(2)}\bar{\mathbf{U}}. \tag{6.8}$$

Substituting (6.2) to (6.8) into (6.1) yields

$$\begin{aligned} & \int_0^{L/2} EA\bar{\varepsilon}^{(1)}\varepsilon^{(1)} dx + \int_0^{L/2} EA\bar{\varepsilon}^{(2)}\varepsilon^{(2)} dx \\ &= \int_0^{L/2} \bar{u}^{(1)} f^{(1)} dx + \int_0^{L/2} \bar{u}^{(2)} f^{(2)} dx + R\bar{u}^{(2)}|_{x=L/2} \end{aligned}$$

or

$$EA \int_0^{L/2} \bar{\mathbf{U}}^T \mathbf{B}^{(1)T} \mathbf{B}^{(1)} \mathbf{U} dx + EA \int_0^{L/2} \bar{\mathbf{U}}^T \mathbf{B}^{(2)T} \mathbf{B}^{(2)} \mathbf{U} dx$$

$$= \int_0^{L/2} \bar{\mathbf{U}}^T \mathbf{H}^{(1)T} f^{(1)} dx + \int_0^{L/2} \bar{\mathbf{U}}^T \mathbf{H}^{(2)T} f^{(2)} dx + \bar{\mathbf{U}}^T R \mathbf{H}^{(2)T} \Big|_{x=L/2} \quad (6.9)$$

where we used  $f^{(m)}$  to express the function  $f(X)$  in the element  $(m)$  local coordinate  $x$ . Defining

$$\mathbf{K}^{(1)} = EA \int_0^{L/2} \mathbf{B}^{(1)T} \mathbf{B}^{(1)} dx \quad (6.10)$$

$$\mathbf{K}^{(2)} = EA \int_0^{L/2} \mathbf{B}^{(2)T} \mathbf{B}^{(2)} dx \quad (6.11)$$

$$\mathbf{R}_B^{(1)} = \int_0^{L/2} \mathbf{H}^{(1)T} f^{(1)} dx \quad (6.12)$$

$$\mathbf{R}_B^{(2)} = \int_0^{L/2} \mathbf{H}^{(2)T} f^{(2)} dx \quad (6.13)$$

$$\mathbf{R}_C = R \mathbf{H}^{(2)T} \Big|_{x=L/2} = R \begin{bmatrix} 1 \\ 0 \end{bmatrix} = \begin{bmatrix} R \\ 0 \end{bmatrix} \quad (6.14)$$

equation (6.9) can be re-written as

$$\bar{\mathbf{U}}^T \left[ (\mathbf{K}^{(1)} + \mathbf{K}^{(2)}) \mathbf{U} - (\mathbf{R}_B^{(1)} + \mathbf{R}_B^{(2)}) - \mathbf{R}_C \right] = 0. \quad (6.15)$$

Defining

$$\mathbf{K} = \mathbf{K}^{(1)} + \mathbf{K}^{(2)} = \frac{EA}{(L/2)} \begin{bmatrix} 1 & -1 \\ -1 & 2 \end{bmatrix} \quad (6.16)$$

$$\mathbf{R}_B = \mathbf{R}_B^{(1)} + \mathbf{R}_B^{(2)} = \left[ \int_0^{L/2} \frac{x}{L/2} f^{(1)} dx + \int_0^{L/2} \left(1 - \frac{x}{L/2}\right) f^{(2)} dx \right] \quad (6.17)$$

(6.15) becomes

$$\bar{\mathbf{U}}^T [\mathbf{K}\mathbf{U} - \mathbf{R}_B - \mathbf{R}_C] = 0. \quad (6.18)$$

The fact that  $\bar{u}_h(X)$  is arbitrary, provided it obeys the functional form given in Figure 6.1, is guaranteed by letting  $\bar{\mathbf{U}}$  be an arbitrary vector. The only way for the product of the row matrix  $\bar{\mathbf{U}}^T$  by the column matrix  $[\mathbf{K}\mathbf{U} - \mathbf{R}_B - \mathbf{R}_C]$  to be zero, with  $\bar{\mathbf{U}}$  arbitrary is to have

$$\mathbf{K}\mathbf{U} = \mathbf{R}_B + \mathbf{R}_C. \quad (6.19)$$

Equation (6.19) represents two linear algebraic equations to be solved for  $U_1$  and  $U_2$ , which give  $u_h(X)$  by equations (6.2) and (6.3).

We have shown that by choosing a functional form for both the solution sought and the virtual displacements, we can find a solution that satisfies the virtual work statement (equation (6.1) within the assumed displacement field).

Considering equation (6.19), we realize that these equations correspond to those of the truss model shown in Figure 6.3 when the nodal forces are applied at the truss nodes according to (6.14) and (6.17). The  $\mathbf{K}$  matrix

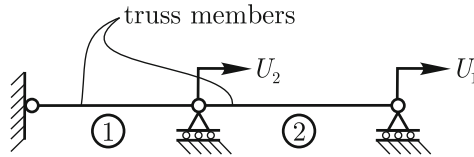


Fig. 6.3. Truss model

of equation (6.16) has the natural interpretation of a stiffness matrix. The column matrices  $\mathbf{R}_B$  and  $\mathbf{R}_C$  collect nodal loads. In fact,  $\mathbf{R}_B$  is lumping the force per unit length to the nodes.

Of course, the principle of virtual work in (6.1) also holds when the bar is unrestrained at the left end. Hence, the problem can be solved by using this principle for the unrestrained bar and then imposing the restraint prior to solving the matrix equations. In this case, we would consider  $u_h$  and  $\bar{u}_h$  as defined in Figure 6.4.

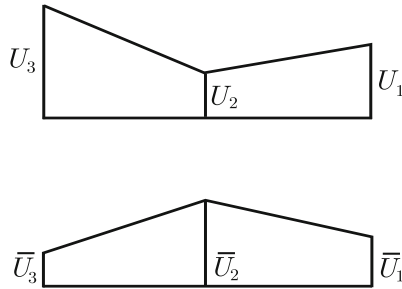


Fig. 6.4. Alternative definition of  $u_h(x)$  and  $\bar{u}_h(x)$

The derivations would be as above, but using  $\mathbf{U}^T = \begin{bmatrix} U_1 & U_2 & U_3 \end{bmatrix}$ ,  $\bar{\mathbf{U}}^T = \begin{bmatrix} \bar{U}_1 & \bar{U}_2 & \bar{U}_3 \end{bmatrix}$  and

$$\mathbf{H}^{(1)} = \begin{bmatrix} 0 & \frac{x}{(L/2)} & 1 - \frac{x}{(L/2)} \end{bmatrix}$$

$$\mathbf{H}^{(2)} = \begin{bmatrix} \frac{x}{(L/2)} & 1 - \frac{x}{(L/2)} & 0 \end{bmatrix}$$

$$\mathbf{B}^{(1)} = \begin{bmatrix} 0 & \frac{1}{(L/2)} & -\frac{1}{(L/2)} \end{bmatrix}$$

$$\mathbf{B}^{(2)} = \begin{bmatrix} \frac{1}{(L/2)} & -\frac{1}{(L/2)} & 0 \end{bmatrix}$$

leading to

$$\mathbf{K}^{(1)} = \frac{EA}{(L/2)} \begin{bmatrix} 0 & 0 & 0 \\ 0 & 1 & -1 \\ 0 & -1 & 1 \end{bmatrix} \quad (6.20)$$

$$\mathbf{K}^{(2)} = \frac{EA}{(L/2)} \begin{bmatrix} 1 & -1 & 0 \\ -1 & 1 & 0 \\ 0 & 0 & 0 \end{bmatrix} \quad (6.21)$$

and the matrices of equation (6.19) would be

$$\mathbf{K} = \frac{EA}{(L/2)} \begin{bmatrix} 1 & -1 & 0 \\ -1 & 2 & -1 \\ 0 & -1 & 1 \end{bmatrix} \quad (6.22)$$

$$\mathbf{R}_B = \begin{bmatrix} \int_0^{L/2} \frac{x}{L/2} f^{(2)} dx \\ \int_0^{L/2} \frac{x}{L/2} f^{(1)} dx + \int_0^{L/2} \left(1 - \frac{x}{L/2}\right) f^{(2)} dx \\ \int_0^{L/2} \left(1 - \frac{x}{L/2}\right) f^{(1)} dx \end{bmatrix} \quad (6.23)$$

and

$$\mathbf{R}_C = \begin{bmatrix} R \\ 0 \\ R_b \end{bmatrix}. \quad (6.24)$$

Here  $R_b$  is the reaction at  $X = 0$ . We would now impose  $U_3 = 0$  and solve the equations for  $U_1$  and  $U_2$ .

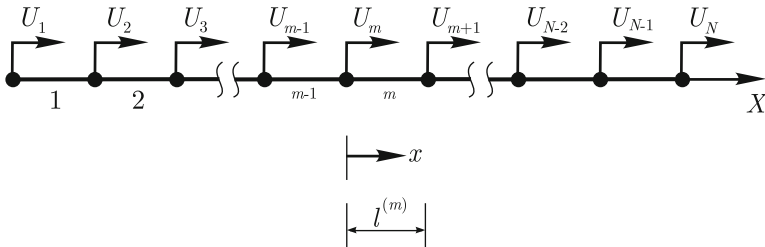
We note that if  $f = 0$ , the solutions based on the virtual work approach and that of the truss model of Figure 6.3 are the same. In fact, the matrices  $\mathbf{K}$  and  $\mathbf{R}_C$  are exactly the same for both approaches and  $\mathbf{R}_B = \mathbf{0}$ . Since the truss

model solution is exact for forces applied to the nodes only, the solution of the virtual work approach is also exact in such a case. Of course, this happens since the functional assumption for the displacements (see Figure 6.1) is the functional form of the analytical solution and, in fact, only one element gives the exact solution when  $f = 0$ .

When  $f(x) \neq 0$  the integration of the differential equation (5.7) gives a  $u(X)$  which is not linear in  $X$ . Hence, since  $u_h(X)$  is piecewise linear, as described in Figure 6.1, the method can not give the exact displacement and stress solution for all points in the bar (unless the procedure described in Section 6.4.2 is used as well, see also Bathe, 1996). We address this issue in more detail later on.

When we anticipate that the exact solution  $u(X)$  is not piecewise linear, it is intuitive to subdivide the original domain into more than two subdomains, *i.e.*, to consider more elements. In such way, the  $u_h(X)$  – although still piecewise linear – may be closer to  $u(X)$ .

Let us consider the subdivision of the original domain into more than two subdomains (elements) as schematically represented in Figure 6.5. In



**Fig. 6.5.** Bar problem discretized by several elements

this figure we also give the nodal points and nodal degrees of freedom. The function  $u_h(X)$  will be defined to be linear in each element and at nodal point  $i$  of coordinate  $X_i$ ,  $u_h(X_i) = U_i$ . Therefore

$$u^{(m)}(x) = U_m \left(1 - \frac{x}{l^{(m)}}\right) + U_{m+1} \frac{x}{l^{(m)}} \quad (6.25)$$

where  $l^{(m)}$  is the length of element ( $m$ ). Note that this displacement interpolation can represent the rigid body motion of the element, which is indeed a fundamental requirement for displacement interpolations, see Bathe, 1996. Letting

$$\mathbf{U}^T = \left[ U_1 \quad U_2 \quad \dots \quad U_N \right]$$

we can define  $\mathbf{H}^{(m)}$

$$u^{(m)} = \mathbf{H}^{(m)} \mathbf{U} \quad (6.26)$$

and  $\mathbf{B}^{(m)}$

$$\varepsilon^{(m)} = \mathbf{B}^{(m)} \mathbf{U} \quad (6.27)$$

where  $\mathbf{H}^{(m)}$  and  $\mathbf{B}^{(m)}$  are

$$\mathbf{H}^{(m)} = \begin{bmatrix} 0 & \dots & 0 & \left(1 - \frac{x}{l^{(m)}}\right) & \frac{x}{l^{(m)}} & 0 & \dots & 0 \end{bmatrix}$$

$$\mathbf{B}^{(m)} = \begin{bmatrix} 0 & \dots & 0 & -\frac{1}{l^{(m)}} & \frac{1}{l^{(m)}} & 0 & \dots & 0 \end{bmatrix}$$

with only two non-zero entries. The virtual quantities are also defined by

$$\bar{u}^{(m)} = \mathbf{H}^{(m)} \bar{\mathbf{U}} \quad (6.28)$$

$$\bar{\varepsilon}^{(m)} = \mathbf{B}^{(m)} \bar{\mathbf{U}} \quad (6.29)$$

where

$$\bar{\mathbf{U}}^T = \begin{bmatrix} \bar{U}_1 & \bar{U}_2 & \dots & \bar{U}_N \end{bmatrix}$$

is the column matrix of virtual nodal displacements.

Let  $\mathbf{R}_C$  collect the nodal concentrated forces corresponding to  $\mathbf{U}$

$$\mathbf{R}_C^T = \begin{bmatrix} R_{C_1} & R_{C_2} & \dots & R_{C_N} \end{bmatrix}. \quad (6.30)$$

Of course, many entries might be zero. Also some entries might correspond to unknown nodal reactions associated with the degrees of freedom for which the displacements are prescribed.

Substituting (6.26) to (6.30) into the virtual work expression (6.1), we obtain

$$\begin{aligned} & \sum_{m=1}^{n_e} \int_0^{l^{(m)}} \bar{\mathbf{U}}^T \mathbf{B}^{(m)T} E^{(m)} A^{(m)} \mathbf{B}^{(m)} \mathbf{U} \, dx \\ &= \sum_{m=1}^{n_e} \int_0^{l^{(m)}} \bar{\mathbf{U}}^T \mathbf{H}^{(m)T} f^{(m)} \, dx + \bar{\mathbf{U}}^T \mathbf{R}_C \end{aligned}$$

where  $n_e$  is the number of elements, and  $E^{(m)}$  and  $A^{(m)}$  are the Young's modulus and the cross-sectional area of element  $(m)$ . This equation can be re-written as

$$\begin{aligned} & \bar{\mathbf{U}}^T \left( \sum_{m=1}^{n_e} \int_0^{l^{(m)}} \mathbf{B}^{(m)T} E^{(m)} A^{(m)} \mathbf{B}^{(m)} \, dx \right) \mathbf{U} \\ &= \bar{\mathbf{U}}^T \left( \sum_{m=1}^{n_e} \int_0^{l^{(m)}} \mathbf{H}^{(m)T} f^{(m)} \, dx + \mathbf{R}_C \right). \end{aligned}$$



Defining

$$\mathbf{K}^{(m)} = \int_0^{l^{(m)}} \mathbf{B}^{(m)T} E^{(m)} A^{(m)} \mathbf{B}^{(m)} dx \quad (6.31)$$

$$\mathbf{R}_B^{(m)} = \int_0^{l^{(m)}} \mathbf{H}^{(m)T} f^{(m)} dx \quad (6.32)$$

$$\mathbf{K} = \sum_{m=1}^{n_e} \mathbf{K}^{(m)} \quad (6.33)$$

$$\mathbf{R}_B = \sum_{m=1}^{n_e} \mathbf{R}_B^{(m)} \quad (6.34)$$

we obtain

$$\bar{\mathbf{U}}^T [\mathbf{K}\mathbf{U} - \mathbf{R}_B - \mathbf{R}_C] = 0.$$

We should impose that  $\bar{\mathbf{U}}^T$  is arbitrary to reflect the condition that  $\bar{u}_h(X)$  is any function which obeys the specified functional form (linear in each element). Using the same arguments as before, this condition implies that

$$\mathbf{K}\mathbf{U} = \mathbf{R} \quad (6.35)$$

with  $\mathbf{R} = \mathbf{R}_B + \mathbf{R}_C$ .

Equation (6.35) is a system of  $N$  algebraic equations to be solved for the nodal displacements. We note that at least one nodal displacement should be prescribed to prevent rigid body motion.

The matrix  $\mathbf{K}^{(m)}$ , which can be interpreted as the element ( $m$ ) stiffness matrix, can be evaluated in closed form due to the simplicity of the element used. In fact, from equation (6.31), we can write

$$\mathbf{K}^{(m)} = \frac{E^{(m)} A^{(m)}}{l^{(m)}} \left[ \begin{array}{ccc} . & & \\ . & & \\ . & & \\ . & & \\ . & & \\ . & & \\ \hline 1 & -1 & \\ \hline -1 & 1 & \\ \hline & & \ddots \\ & & \\ & & \\ \hline & & \\ m & m+1 & \\ \hline & & \end{array} \right]_{(N \times N)}$$

where only the non-zero entries are shown. We observe that this stiffness matrix is exactly the stiffness matrix we would obtain for a truss element if

it were placed linking nodes  $m$  and  $m + 1$  and if only the axial degrees of freedom were considered. The assemblage of the  $\mathbf{K}$  matrix is given by equation (6.33) which is exactly equal to equation (2.49). Recall that equation (2.49), which gives the assemblage of the  $\mathbf{K}$  matrix for trusses, was derived imposing equilibrium and displacement compatibility. In the finite element formulation equation (6.33) is obtained directly from the principle of virtual work. Also

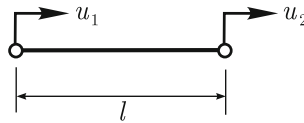
$$\mathbf{R}_B^{(m)} = \begin{bmatrix} \cdot \\ \cdot \\ \cdot \\ \int_0^{l^{(m)}} \left(1 - \frac{x}{l^{(m)}}\right) f^{(m)} dx & m \\ \int_0^{l^{(m)}} \frac{x}{l^{(m)}} f^{(m)} dx & m + 1 \\ \cdot \\ \cdot \\ \cdot \end{bmatrix}$$

where again only the non-zero entries are shown.

In the finite element assemblage, we can define an element matrix containing only the stiffness coefficients associated with the element degrees of freedom in a local numbering as shown in Figure 6.6. Considering element ( $m$ ), the element matrix is given by

$$\mathbf{k}^{(m)} = \frac{EA}{l} \begin{bmatrix} 1 & -1 \\ -1 & 1 \end{bmatrix}$$

where  $E$ ,  $A$  and  $l$  are those for element ( $m$ ).



**Fig. 6.6.** Generic two-node element

The assemblage process implicitly given by equation (6.33) is efficiently performed by using the element matrices corresponding to the local numbering and adding their contributions to the global matrix using the correspondence between local and global degrees of freedom. This assemblage procedure has been discussed in detail in Chapters 2 and 4.

**Example 6.1**

Consider the problem described in Figure 5.1 with  $f(X) = aX$ ,  $L = 2$  m,  $a = 10$  kN/m<sup>2</sup>,  $R = 20$  kN,  $A = 2 \times 10^{-4}$  m<sup>2</sup> and  $E = 2.1 \times 10^8$  kN/m<sup>2</sup>.

- (i) Derive the analytical solution.
- (ii) Detail the solution for a uniform discretization of 2 elements.
- (iii) Formulate and solve the problem for uniform discretizations of 4, 8 and 16 elements.
- (iv) Discuss the stress solutions.

**Solution**

- (i) The analytical solution can be derived by solving the differential formulation which for this case reads (see equations (5.7) to (5.9))

$$EA \frac{d^2 u}{dX^2} + aX = 0$$

$$u(0) = 0$$

$$EA \frac{du}{dX}(L) = R.$$

The solution is given by

$$u(X) = -\frac{a}{6EA} X^3 + \left( \frac{R}{EA} + \frac{aL^2}{2EA} \right) X. \quad (6.36)$$

- (ii) Using equation (6.23), we have

$$\mathbf{R}_B = \begin{bmatrix} \int_0^{L/2} \frac{x}{(L/2)} a \left(x + \frac{L}{2}\right) dx \\ \int_0^{L/2} \frac{x}{(L/2)} ax dx + \int_0^{L/2} \left(1 - \frac{x}{(L/2)}\right) a \left(x + \frac{L}{2}\right) dx \\ \int_0^{L/2} \left(1 - \frac{x}{(L/2)}\right) ax dx \end{bmatrix}$$

where we used the degree of freedom numbering shown in Figure 6.4. Therefore

$$\mathbf{R}_B = \frac{aL^2}{24} \begin{bmatrix} 5 \\ 6 \\ 1 \end{bmatrix}$$

and using (6.22) and (6.24), equation (6.35) reads

$$\frac{EA}{(L/2)} \begin{bmatrix} 1 & -1 & 0 \\ -1 & 2 & -1 \\ 0 & -1 & 1 \end{bmatrix} \begin{bmatrix} U_1 \\ U_2 \\ U_3 \end{bmatrix} = \frac{aL^2}{24} \begin{bmatrix} 5 \\ 6 \\ 1 \end{bmatrix} + \begin{bmatrix} R \\ 0 \\ R_b \end{bmatrix}.$$

Imposing  $U_3 = 0$ , we obtain

$$U_1 = 1.587 \times 10^{-3} \text{ m}, \quad U_2 = 9.127 \times 10^{-4} \text{ m}.$$

The reaction at node 1 is

$$R_b = -40 \text{ kN}$$

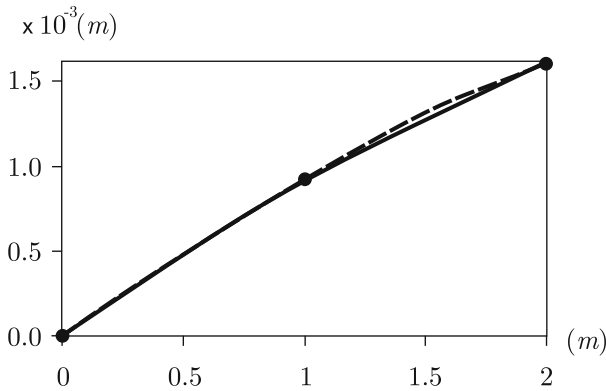
and the solution for each element is

$$u^{(1)}(x) = \frac{x}{(L/2)} U_2$$

and

$$u^{(2)}(x) = \frac{x}{(L/2)} U_1 + \left(1 - \frac{x}{(L/2)}\right) U_2.$$

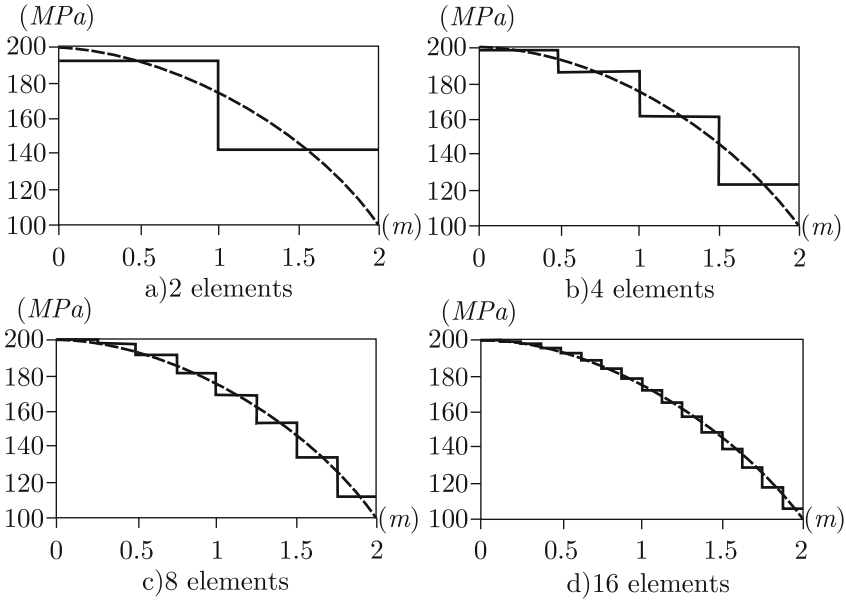
The analytical and finite element solutions are plotted in Figure 6.7.



**Fig. 6.7.** Solutions for displacements are shown for the 2 element mesh (solid line) and the exact solution (dashed line)

(iii) The matrix equation is generically given by





**Fig. 6.8.** Stress solutions. The stepped full line represents the finite element solutions and the dashed line represents the analytical solution

1. Nodal point equilibrium
2. Element equilibrium

We detail below these properties following Bathe, 1996. First, we define the column matrix  $\mathbf{F}^{(m)}$  by

$$\mathbf{F}^{(m)} = \mathbf{K}^{(m)}\mathbf{U} \tag{6.37}$$

which gives the nodal point forces for element  $(m)$ . The nodal displacements given by  $\mathbf{U}$  correspond to the solution of the problem in consideration and, hence, these forces are *acting onto the element* at the element nodal points.

We re-write (6.37) as

$$\mathbf{F}^{(m)} = \mathbf{K}^{(m)}\mathbf{U} = \int_{l^{(m)}} \mathbf{B}^{(m)T} \tau^{(m)} A \, dx$$

where  $\tau^{(m)}$  is the solution for the stress field for element  $(m)$ , *i.e.*,  $\tau^{(m)} = E\mathbf{B}^{(m)}\mathbf{U}$ . From this expression  $\mathbf{F}^{(m)}$  can also be interpreted to be equivalent in the virtual work sense to the element stresses, since we can left multiply the equation above by any finite element virtual displacement field and obtain

$$\bar{\mathbf{U}}^T \mathbf{F}^{(m)} = \int_{l^{(m)}} \bar{\varepsilon}^{(m)} \tau^{(m)} A \, dx. \tag{6.38}$$

Property 1 follows from

$$\sum_{m=1}^{n_e} \mathbf{F}^{(m)} = \sum_{m=1}^{n_e} \mathbf{K}^{(m)} \mathbf{U} = \mathbf{R}$$

$$\sum_{m=1}^{n_e} \mathbf{F}^{(m)} = \mathbf{R}. \quad (6.39)$$

Hence, at each node the sum of the element nodal point forces is in equilibrium with the externally applied nodal loads (which include the lumped distributed forces  $(\mathbf{R}_B)$ ). Here,  $\mathbf{F}^{(m)}$  are the forces that give the stress contribution of element  $(m)$  to the nodal point equilibrium.

To show Property 2 we use equation (6.38) with the nodal virtual displacements

$$\bar{\mathbf{U}}^T = \left[ \Delta \quad \dots \quad \Delta \quad \Delta \quad \dots \quad \Delta \right]$$

where  $\Delta$  is a constant displacement applied to the element nodes, *i.e.*, we are considering a rigid element translation as the virtual displacement field. We obtain

$$\bar{\mathbf{U}}^T \mathbf{F}^{(m)} = 0 \quad (6.40)$$

since  $\bar{\varepsilon}^{(m)} = 0$ . Also

$$\mathbf{F}^{(m)T} = \left[ 0 \quad \dots \quad 0 \quad F_1 \quad F_2 \quad 0 \quad \dots \quad 0 \right]$$

and hence (6.40) yields

$$F_1 = -F_2 \quad (6.41)$$

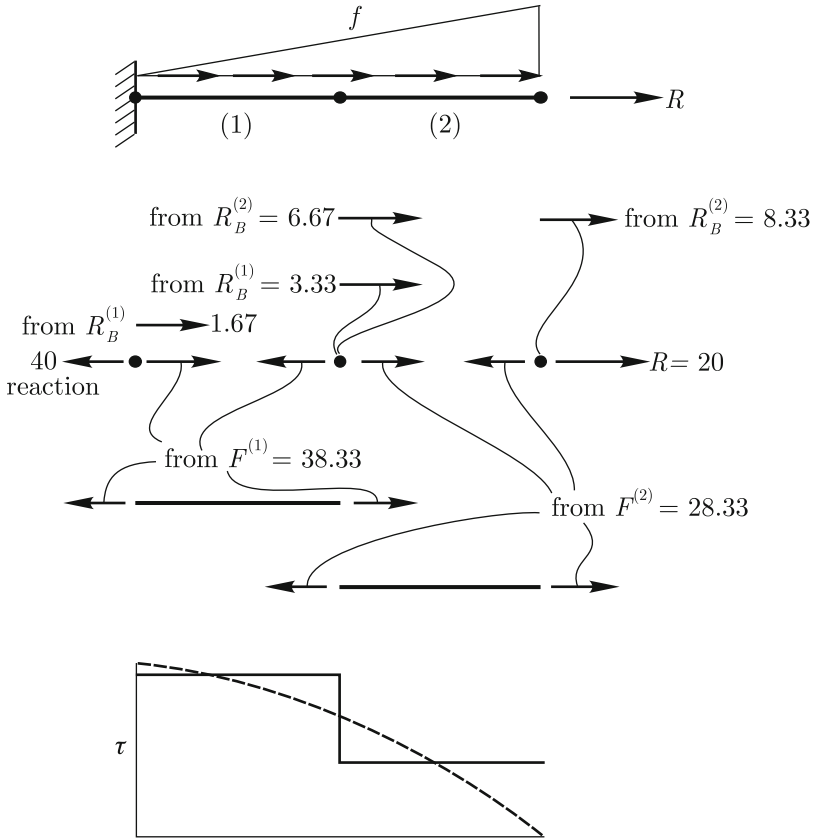
which proves that element  $(m)$  is in equilibrium under its nodal point forces.

In Figure 6.9 we summarize the above results for the two element mesh of Example 6.1. We observe that for all nodes equilibrium is satisfied considering: the external loads; the lumped distributed loads and the element nodal point forces. Actually this is the “pictorial” form of equation (6.39). We also show the element nodal point forces acting on the elements which self-equilibrate (see equation (6.41)).

### Summary of the finite element procedure for 1-D linear elements

Although the bar problem and the finite element solutions using linear elements are a special and simple application, the solution process already displays some key characteristics of the finite element method for structural mechanics:

- The finite element solution is based on the use of the principle of virtual work.
- The problem domain is partitioned into subdomains called elements.



**Fig. 6.9.** Schematic representation of forces/stress variables for bar problem. Values shown are obtained considering  $L = 2$  m,  $A = 2 \times 10^{-4}$  m<sup>2</sup>,  $E = 2.1 \times 10^8$  kN/m<sup>2</sup>,  $f = 10X$  kN/m,  $R = 20$  kN

- A set of points, called nodal points, are defined in each element (the nodal points are at the element end points for the above formulation).
- The unknown displacements (the displacement of the bar sections  $u(X)$  for the above problem) are assumed to have a given functional form through the interpolation functions within each element (linear for the above problem).
- The values of the displacements at every point within the elements are uniquely defined by these interpolation functions and their nodal point values (see equation (6.25) for the above problem).
- Given the values at the nodal points,  $u_h(X)$  is defined for all  $X$ ,  $0 \leq X \leq L$ .
- The principle of virtual work is imposed considering the assumptions for the unknown displacements. The virtual quantities are assumed to have



the same functional form as the real displacements (see equation (6.25) and (6.28) for the above problem).

- The application of the principle of virtual work under these conditions leads to a system of algebraic equations (equation (6.35)).
- The solution of the algebraic equations gives the values of the displacements at the nodes ( $\mathbf{U}$ ).
- Using the displacement nodal values, the displacements throughout the domain are given (use again equation (6.25) for the above problem to obtain  $u_h(X)$ ).
- The finite element solution is an approximation for the exact solution of the problem.
- The finite element solution satisfies: exactly *compatibility*, since the *strain-displacement relation* (equation (6.27) for this case) and the displacement boundary conditions are imposed; exactly the *constitutive relation*, since the stress-strain law ( $\tau^{(m)} = E^{(m)}\varepsilon^{(m)}$  for the above problem) is imposed; approximately equilibrium (see the discussion of “nodal equilibrium” and “element equilibrium”).
- As we consider a finer partition of the domain, *i.e.*, more and smaller elements, the conditions of “nodal equilibrium” and “element equilibrium” (as detailed for the two element bar problem) represent closer and closer differential equilibrium. Therefore, it is intuitive that we can satisfy differential equilibrium as precisely as required, by considering sufficiently small elements. We can therefore arrive at finite element solutions that are as close to the exact solution of the mathematical model as desired.
- A given partition of the domain into elements is referred to as a finite element mesh. The process of further subdividing the domain into more elements is referred to as mesh refinement.

### Quadratic 1-D finite elements

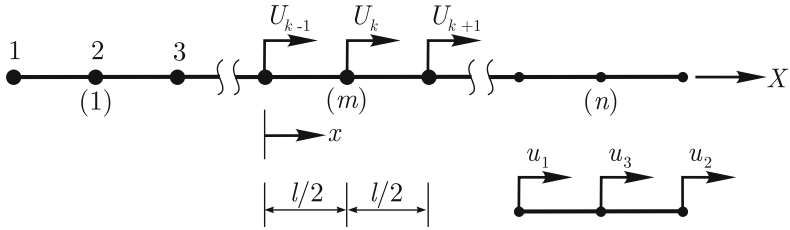
In the previous example we used linear elements, *i.e.*, the displacement interpolation was defined by a linear function in each element. We can define a quadratic element, *i.e.*, an element in which the displacement interpolation is parabolic, but then need to use three-nodes per element.

In Figure 6.10 we show a generic three-node element and also the local numbering of the element degrees of freedom. The interpolation can be defined by

$$u^{(m)}(x) = u_1 h_1(x) + u_2 h_2(x) + u_3 h_3(x). \quad (6.42)$$

Of course,  $U_{k-1} = u_1$ ,  $U_{k+1} = u_2$  and  $U_k = u_3$ . The interpolation functions can be easily derived by observing that each  $h_i(x)$  should be parabolic and should be 1 at the position of the node  $i$  and 0 at the remaining nodal positions, that is

$$u^{(m)}(x = 0) = u_1 = U_{k-1}$$



**Fig. 6.10.** Generic three-node element

$$u^{(m)}(x = l/2) = u_3 = U_k$$

$$u^{(m)}(x = l) = u_2 = U_{k+1}.$$

If these conditions are satisfied, we have that  $u^{(m)}(x)$  is parabolic in  $x$  and we directly obtain

$$h_1(x) = \frac{(x - \frac{l}{2})(x - l)}{(0 - \frac{l}{2})(0 - l)} = \frac{2x^2 - 3xl + l^2}{l^2}$$

$$h_2(x) = \frac{(x - 0)(x - \frac{l}{2})}{(l - 0)(l - \frac{l}{2})} = \frac{2x^2 - xl}{l^2}$$

$$h_3(x) = \frac{(x - 0)(x - l)}{(\frac{l}{2} - 0)(\frac{l}{2} - l)} = -\frac{4(x^2 - xl)}{l^2}$$

Of course,  $l$  varies from element to element and could have been represented by  $l^{(m)}$ .

The interpolation matrix  $\mathbf{H}^{(m)}$  is given by

$$u^{(m)} = \mathbf{H}^{(m)} \mathbf{U}$$

where

$$\mathbf{H}^{(m)} = \begin{bmatrix} 0 & \dots & 0 & h_1 & h_3 & h_2 & 0 & \dots & 0 \end{bmatrix}$$

where  $h_1$  is placed in column  $k - 1$ ,  $h_3$  in  $k$  and  $h_2$  in  $k + 1$ . We note that  $\sum_{i=1}^3 h_i = 1$  which is the requirement that the element can represent a rigid body motion. The derivations leading to  $\mathbf{KU} = \mathbf{R}$  would follow equations (6.26) to (6.35).

**Example 6.2**

Solve the bar problem of Figure 5.1 for  $f(x) = a$  (constant) and  $f(x) = ax$  (linear) with only one three-node element.

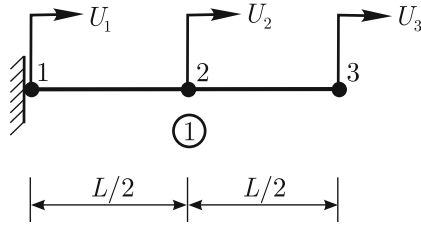


Fig. 6.11. Bar model with one three-node element

**Solution**

Let us consider the finite element model as described in Figure 6.11. Since we have only one element

$$\mathbf{K} = \mathbf{K}^{(1)} = \int_0^{L/2} \mathbf{B}^{(1)T} E^{(1)} A^{(1)} \mathbf{B}^{(1)} dx$$

where

$$\mathbf{B}^{(1)} = \left[ \begin{array}{ccc} \frac{4x}{L^2} - \frac{3}{L} & \frac{-8x}{L^2} + \frac{4}{L} & \frac{4x}{L^2} - \frac{1}{L} \end{array} \right]$$

and therefore

$$\mathbf{K} = \frac{EA}{3L} \begin{bmatrix} 7 & -8 & 1 \\ -8 & 16 & -8 \\ 1 & -8 & 7 \end{bmatrix}$$

Considering first  $f = a$

$$\mathbf{R}_B = \mathbf{R}_B^{(1)} = \int_0^{L/2} \mathbf{H}^{(1)T} f^{(1)} dx$$

$$\mathbf{R}_B = \frac{aL}{3} \begin{bmatrix} \frac{1}{2} \\ 2 \\ \frac{1}{2} \end{bmatrix}$$

and

$$\mathbf{R}_C = R \mathbf{H}^{(1)T} \Big|_{x=L} = R \begin{bmatrix} 0 \\ 0 \\ 1 \end{bmatrix}$$

Considering  $R = 1$  the algebraic system is

$$\frac{EA}{3L} \begin{bmatrix} 7 & -8 & 1 \\ -8 & 16 & -8 \\ 1 & -8 & 7 \end{bmatrix} \begin{bmatrix} U_1 \\ U_2 \\ U_3 \end{bmatrix} = \begin{bmatrix} \frac{aL}{6} \\ \frac{2aL}{3} \\ \frac{aL}{6} + 1 \end{bmatrix}$$

Since  $U_1 = 0$  we are lead to the reduced system

$$\frac{EA}{3L} \begin{bmatrix} 16 & -8 \\ -8 & 7 \end{bmatrix} \begin{bmatrix} U_2 \\ U_3 \end{bmatrix} = \begin{bmatrix} \frac{2aL}{3} \\ \frac{aL}{6} + 1 \end{bmatrix}. \quad (6.43)$$

The solution is

$$\mathbf{U}^T = \left[ 0 \quad \frac{3L^2a+4L}{8EA} \quad \frac{L^2a+2L}{2EA} \right]$$

which leads to

$$u^{(1)}(x) = \mathbf{H}^{(1)}\mathbf{U} = \frac{-ax^2 + 2Lax + 2x}{2EA}$$

since we have only one element

$$u_h(X) = \frac{-aX^2 + 2LaX + 2X}{2EA} \quad (6.44)$$

Since the interpolation is quadratic and the analytical solution is also quadratic in displacements for a constant  $f$ , we should expect the finite element solution to be exact. In fact, substituting (6.44) in the differential equation we have

$$EA \frac{d^2u_h}{dX^2} + f = -a + a = 0.$$

In order to obtain the solution for  $f = ax$  we need only to calculate the corresponding  $\mathbf{R}_B$

$$\mathbf{R}_B = \frac{aL^2}{3} \begin{bmatrix} 0 \\ 1 \\ \frac{1}{2} \end{bmatrix}$$

and solving (6.43) using this  $\mathbf{R}_B$ , we find

$$\mathbf{U}^T = \left[ 0 \quad \frac{11aL^3+24L}{48EA} \quad \frac{aL^3+3L}{3EA} \right].$$

Therefore

$$u_h(X) = \frac{-3X^2aL + 7aL^2X + 12X}{12EA}$$

and substituting into the differential equation

$$EA \frac{d^2 u_h}{dx^2} + f = \frac{-La}{2} + aX \neq 0$$

which shows, as expected, that the differential equation is not exactly satisfied.

□

## 6.2 Convergence properties of 1-D finite element solutions

We introduced the finite element formulation for the 1-D problem in Section 6.1. The fundamental idea was to choose a functional form for the axial displacements and invoke the principle of virtual work. Let us focus, for the moment, on the piecewise linear interpolation of the displacements.

We derived how to obtain the finite element solution  $u_h(x)$  for this problem and pointed out that this solution is in general only an approximation to the exact solution. However, taking into account the compatibility, constitutive and equilibrium conditions that the finite element solution satisfies, we discussed that as we refine the mesh, considering more and more elements, the finite element solution  $u_h(x)$  “converges” to the exact solution, *i.e.*, the finite element solution becomes successively closer to the exact solution, both for displacements and associated stresses. The results of Example 6.1 are an illustration. The objective of this section is to discuss why and how convergence is obtained for 1-D finite element solutions. In Section 6.5.1 we briefly discuss convergence for 2-D and 3-D displacement-based finite element solutions.

The discussion of convergence requires that we measure the “distance” between the finite element and exact solutions and requires some mathematical tools which we shall introduce at the minimum level needed. For a deeper discussion see Bathe, 1996, Chapelle and Bathe, 2010*a* and Grätsch and Bathe, 2005.

Let us define the bilinear form

$$a(g, w) = \int_0^L EA \frac{dg}{dx} \frac{dw}{dx} dx$$

and the linear form

$$(g, w) = \int_0^L gw dx$$

where  $g(x)$  and  $w(x)$  are real valued functions defined on the interval  $[0, L]$ . The constant value  $L$  represents the bar length,  $E$  represents the Young’s modulus and  $A$  the bar cross-sectional area.

Then the principle of virtual work (see equation (5.20)) can be written as:

Find  $u(x)$ ,  $u(0) = 0$ , such that

$$a(u, v) = (f, v) + Rv(L) \quad (6.45)$$

for any  $v(x)$ ,  $v(0) = 0$ .

Until now, the displacement  $u(x)$  and the virtual displacement  $v(x)$  were assumed to be functions defined on the interval  $[0, L]$ . However, we note that not all real functions  $g(x)$  and  $w(x)$  lead to a finite value of  $a(g, w)$ , for example,  $g(x) = x^p$  and  $w(x) = x^q$  with  $p+q \leq 1$  do not. Surely, any possible solution  $u(x)$  should correspond to a finite value of the strain energy given by (see Chapter 2)

$$\mathcal{U}(u(x)) = \frac{1}{2} \int_0^L EA \frac{du}{dx} \frac{du}{dx} dx = \frac{1}{2} a(u, u)$$

where  $u(x)$  is the axial displacement field. Therefore  $a(u, u)$  gives twice the strain energy associated with the displacement field  $u$ . Now we can restate the problem given by equation (6.45) to include this requirement as:

Find  $u(x) \in V$  such that

$$a(u, v) = (f, v) + Rv(L) \quad (6.46)$$

for any  $v(x) \in V$ , where the space  $V$  is defined as

$$V = \{v/ v : [0, L] \rightarrow \mathbb{R}; a(v, v) < \infty; v(0) = 0\} \quad (6.47)$$

which reflects the fact that we require all functions, that we work with, to correspond to a finite strain energy.

We referred to the set of functions  $V$  defined above as a space. Of course, the reader is familiar with the space of Euclidean vectors for which the addition of vectors and the multiplication of a vector by a scalar (real number) are well defined. A fundamental property is that

$$\alpha \mathbf{x} + \beta \mathbf{y} \quad \text{for any vectors } \mathbf{x} \text{ and } \mathbf{y} \text{ and scalars } \alpha, \beta \quad (6.48)$$

is also a vector.

A set for which we can define, both, addition and multiplications by scalar operations and for which the equivalent of (6.48) also gives an element of the set is called a *linear vector space*<sup>1</sup>.

Considering the usual addition and multiplication operations, it is not difficult to show that  $V$  is a linear vector space.

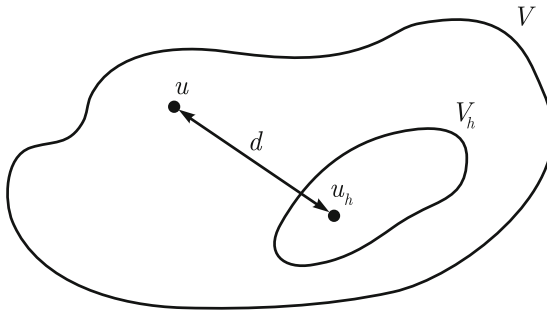
<sup>1</sup> There are other properties that are important to hold in order to work with a linear space (see Bathe, 1996)

The finite element solutions considered in Section 6.2 are then obtained by solving:

Find  $u_h(x) \in V_h$  such that

$$a(u_h, v_h) = (f, v_h) + Rv_h(L) \quad (6.49)$$

for any  $v_h(x) \in V_h$ . Here  $V_h$  is the space of all possible displacement functions  $v_h(x)$ ,  $v_h(x) = 0$ , that can be obtained with the specific mesh used. Of course, we have  $V_h \subset V$  and (6.49) is a restatement of (6.1) in the notation introduced here.



**Fig. 6.12.** Pictorial representation of the exact and finite element solutions

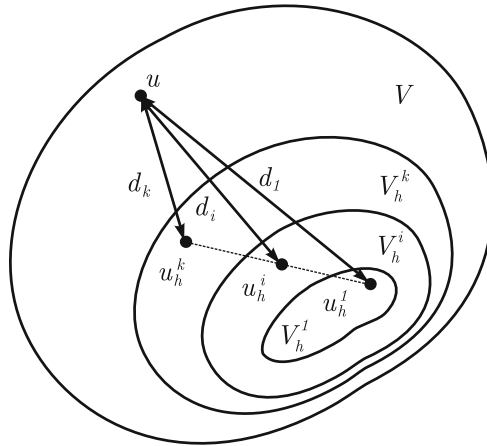
In Figure 6.12 we summarize pictorially the solutions  $u$  and  $u_h$  in the spaces  $V$  and  $V_h$ , with  $V_h \subset V$ . The space  $V_h$  is smaller than  $V$  since  $V$  represents all possible displacement functions and not just the finite element functions contained in  $V_h$ . The exact solution  $u$  lies in general outside  $V_h$ . We also show schematically the “distance”  $d$  between  $u$  and  $u_h$ , still to be defined. Of course, if we choose a coarse mesh,  $V_h$  is “small” and  $u_h$  might be far from the exact solution. As the mesh is refined and  $V_h$  is made larger,  $u_h$  may get closer to  $u$  (*i.e.*, the distance  $d$  may become smaller). The fact that  $u_h$ , indeed, approaches  $u$ , and under what conditions, is discussed below.

In order to introduce the concept of convergence more precisely, let us consider a sequence of meshes, using the same kind of finite elements, starting with mesh 1, which characterizes  $V_h^1$ , and refining sequentially to obtain meshes 2,  $\dots$ ,  $i$ ,  $\dots$ ,  $n$  such that

$$V_h^1 \subset V_h^2 \subset \dots \subset V_h^i \subset \dots \subset V_h^n. \quad (6.50)$$

Here, when refining mesh  $k$  to obtain mesh  $k+1$  the nodal positions of mesh  $k$  shall be preserved which guarantees that  $V_h^k \subset V_h^{k+1}$ .

In Table 6.1 we show some meshes with two-node elements which define finite element spaces that obey condition (6.50). Note that in the left column uniform discretizations are shown, *i.e.*, for each mesh the elements are all



**Fig. 6.13.** Desirable convergence behavior as meshes are refined

**Table 6.1.** Typical mesh refinements for 1-D problem

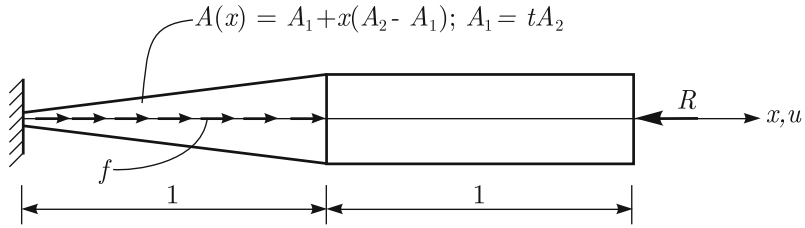
Mesh 1 corresponding to $V_h^1$ 	Mesh 1 corresponding to $V_h^1$ 
Mesh 2 corresponding to $V_h^2$ 	Mesh 2' corresponding to $V_h^{2'}$  16 equal elements
Mesh 4 corresponding to $V_h^4$  32 equal elements	Mesh 2'' corresponding to $V_h^{2''}$ 

of equal length and the next finer mesh is obtained by subdividing every element into two new equal length elements.

In the right column of Table 6.1 we show two possible mesh refinements. Note that the mesh corresponding to  $V_h^{2'}$  is obtained by further subdividing the right half of the domain into 16 equal elements, while to obtain the mesh corresponding to  $V_h^{2''}$ , the left half of the domain is represented by 16 elements of graded lengths.

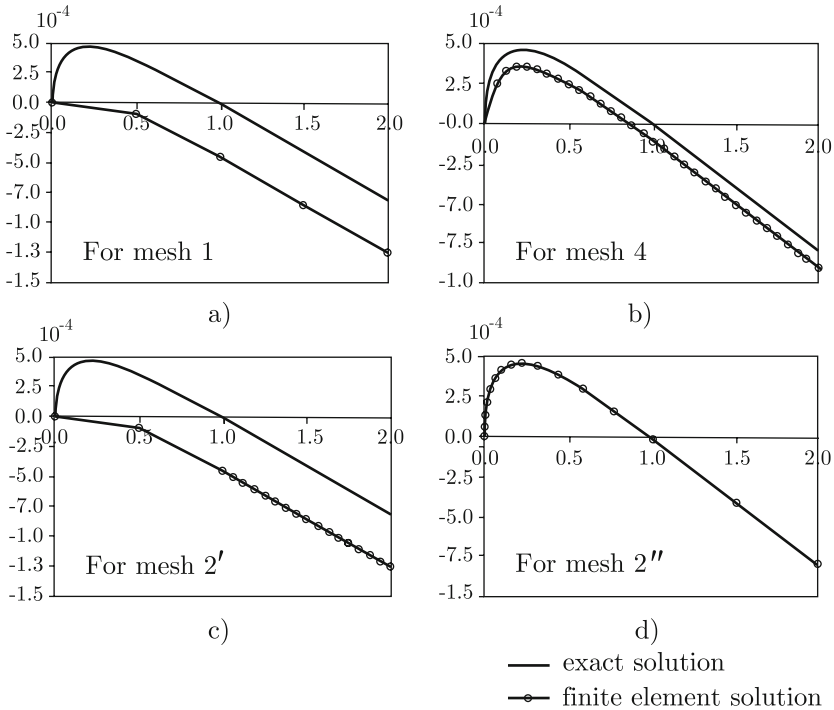
In Figure 6.13 we reproduce Figure 6.12 considering a sequence of finite element spaces. This figure represents what would be the desirable behavior of the finite element solutions, *i.e.*, as we refine the mesh, the finite element solution becomes “closer” to the exact solution. It is also implied that we could obtain a finite element solution as “close” to the exact solution as desired if we sufficiently refine the mesh.





**Fig. 6.14.** Bar problem definition.  $E = 2.0 \times 10^7$  kN/m<sup>2</sup>,  $A_2 = 1$  m<sup>2</sup>,  $t = 0.01$ ,  $R = 15859.075383$  kN. The distributed force  $f = 2.0 \times 10^4$  kN/m is acting only for  $0 \leq x \leq 1$

To illustrate some convergence behaviors, consider the problem definition given in Figure 6.14. The exact solution and the finite element solution for the mesh 1 of Table 6.1 are shown in Figure 6.15a. We see that there is a large error.



**Fig. 6.15.** Finite element and exact solutions for problem of Figure 6.14. The vertical axis shows the axial displacement and the horizontal axis gives the section coordinate, both in meters

In Figure 6.15b we show the finite element solution obtained with mesh 4, *i.e.* with 32 equally spaced elements, *i.e.*, following the refinement of the left column of Table 6.1. Of course, we note a significant improvement in the finite element solution accuracy. But, still, there is a considerable “distance” between the exact and finite element solutions.

In Figure 6.15c we report the finite element solution obtained with mesh 2'. Although we refined the right half of the domain, there is no improvement of the finite element solution, that is,  $u_h^1(x) = u_h^{2'}(x)$ .

In Figure 6.15d we show the finite element solution for the mesh 2'' which is “close” to the exact solution, and in the scale of the figure, we can barely distinguish between the finite element and exact solutions.

Note that the number of degrees of freedom of meshes 2' and 2'' are the same. Nevertheless, the finite element solution accuracies are quite different. Note also that, although the number of degrees of freedom of mesh 2'' is smaller than that of mesh 4 (18 versus 32) the solution  $u_h^{2''}(x)$  is much more accurate than the solution  $u_h^4(x)$ . These numerical results bring up some convergence related issues that we examine next.

### 6.2.1 Convergence conditions

There are two fundamental conditions which should be met to assure that we obtain the desired convergence behavior.

#### Condition 1

*The finite element interpolation should be such that it allows to obtain sequences of finite element spaces as defined in (6.50) for which the space  $V_h^n$  becomes arbitrarily close to any element of  $V$ , *i.e.*, any possible solution.*

By *finite element interpolation* we mean the definition of a generic finite element space  $V_h$ . For example, piecewise continuous linear functions correspond to the finite element interpolation associated with 2-node 1-D elements.

We also note that it is not any strategy of mesh refinement which obeys (6.50) that leads to a space  $V_h^n$  arbitrarily close to any element of  $V$  even when  $n \rightarrow \infty$ . For example, referring to the problem of Figure 6.14, considering the mesh refinement strategy in which only the right half of the domain is subdivided – specifically we use mesh 1, mesh 2', etc. – we can not find a function  $v_h^n(x) \in V_h^n$  arbitrarily close to  $u(x)$  even if we were allowed to freely choose the nodal displacement values. The reason, of course, is that the  $v_h^n(x)$  is piecewise linear in the first half of the domain as given by only 2 elements that are not subdivided in the refinement process, and the analytical solution is far from that assumption.

Of course, it is quite intuitive that if we choose a uniform refinement strategy, we would obtain  $v_h^n(x) \in V_h^n$  arbitrarily close to  $u(x)$ . It would

suffice to make the element small enough and choose as nodal values, the values of  $u(x)$  at the nodal points.

### Condition 2

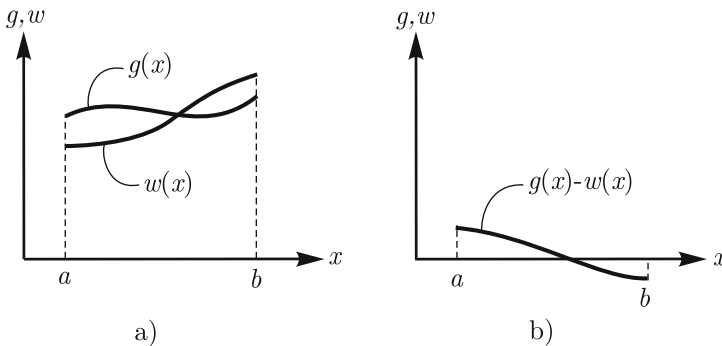
*The finite element solution  $u_h$  is the closest, in some distance measure, to the exact solution among all elements of  $V_h$ .*

It is easy to see that if Conditions 1 and 2 are met, convergence is guaranteed. In fact, Condition 1 assures that we can construct finite element spaces which are arbitrarily close to the exact solution. If we do so, then Condition 2 assures that the finite element solution will be arbitrarily close to the exact solution (since it is the function closest to the exact solution considering all functions in the finite element space).

Our next task is to further discuss Conditions 1 and 2 making them mathematically precise, and for that we first need to introduce some basic definitions.

### 6.2.2 Distances and norms of functions

Of course, the reader is familiar with the concept of the norm of a vector which gives the length of the vector. Let us introduce the concept of the norm of a function because we seek a scalar quantity which gives a measure of the distance between two functions, *i.e.*, how far apart they are. In Figure 6.16a we show two real valued functions  $g(x)$  and  $w(x)$  defined on the domain  $[a, b]$ . It is natural to take the difference of these two functions,  $g(x) - w(x)$ ,



**Fig. 6.16.** Two generic real valued functions

which is plotted in Figure 6.16b. To obtain a scalar, we could integrate this difference function. However, we must avoid that algebraic positive differences are compensated by those which are negative. Therefore, we square the

difference function and then take the square root of the result to arrive at a norm on  $g(x) - w(x)$

$$\|g(x) - w(x)\|_0 = \left( \int_a^b (g(x) - w(x))^2 dx \right)^{1/2}. \quad (6.51)$$

Namely, a norm defined on a linear vector space  $W$  is a function  $\|\cdot\| : W \rightarrow \mathbb{R}^+$  which obeys the following properties

$$\|v\| = 0 \Leftrightarrow v = 0 \quad (6.52)$$

$$\|\alpha v\| = |\alpha| \|v\| \quad \text{for every real number } \alpha \quad (6.53)$$

$$\|v + w\| \leq \|v\| + \|w\| \quad \text{for every } v, w \text{ in } W. \quad (6.54)$$

These properties have a clear geometrical interpretation for Euclidean vectors. The property given in (6.54) is called the triangle inequality since when  $v$  and  $w$  are linearly independent Euclidean vectors it corresponds to the geometrical property that for any triangle the length of a side is smaller than the sum of the other two side lengths.

Based on equation (6.51), we can define a norm of a function  $f(x)$  given in a domain  $[a, b]$  in a linear vector space of functions such as  $V$  ( see (6.47)) by

$$\|f(x)\|_0 = \left( \int_a^b (f(x))^2 dx \right)^{1/2}.$$

It can be shown that this norm definition verifies properties (6.52) to (6.54) and, hence, leads to a valid norm. There are several different norms for spaces of functions. The norm above is referred to as the  $L^2$ -norm or the the 0-norm as the sub-index indicates. The 1-norm can also be defined and it takes into account not only the values of the function but also those of its first derivative leading to

$$\|f(x)\|_1 = \left( \int_a^b \left[ (f(x))^2 + \left( \frac{df(x)}{dx} \right)^2 \right] dx \right)^{1/2}. \quad (6.55)$$

In fact, the  $p$ -norm is defined by

$$\|f(x)\|_p = \left( \int_a^b \left[ (f(x))^2 + \left( \frac{df(x)}{dx} \right)^2 + \left( \frac{d^2f(x)}{dx^2} \right)^2 + \dots + \left( \frac{d^p f(x)}{dx^p} \right)^2 \right] dx \right)^{1/2}$$

where  $p$  is an integer greater than zero. A useful norm in mechanics is the strain energy norm which for a displacement function  $v(x)$  can be defined by

$$\|v(x)\|_E = (a(v, v))^{1/2}.$$

These norms will be sufficient for the convergence study in 1-D. Of course, these concepts can be generalized to obtain norms for spaces of functions defined in several dimensions, see Bathe, 1996.

We can define the distance measured in the norm  $V$  for two real valued functions  $w(x)$  and  $g(x)$  defined in the interval  $[a, b]$  by

$$d(w, v)_V = \|w - v\|_V.$$

Norm  $V$  can be 0, 1,  $E$  or any other norm defined on the vector space considered.

### 6.2.3 Convergence properties

Let us present Condition 1 in a mathematically precise manner. The distance of the exact solution  $u$  of any 1-D bar problem to the finite element space  $V_h^i$  in the norm  $V$  is defined by<sup>2</sup>

$$d(u, V_h^i)_V = \min \{ \|u - v_h^i\|_V \text{ for all } v_h^i \in V_h^i \}. \quad (6.56)$$

We emphasize that norm  $V$  could be the 0-norm, the 1-norm or the energy norm. Note also that (6.56) is the mathematical statement that  $d(u, V_h^i)_V$  is the distance from  $u$  to the closest element of  $V_h^i$  measured in the norm  $V$ .

The Condition 1 would be given by:

There exist sequences of finite element spaces as defined in (6.50) such that

$$d(u, V_h^i)_V \rightarrow 0 \quad \text{when } i \rightarrow \infty \text{ for all } u \in V.$$

Note that Condition 1 is not dependent on the finite element solution. It represents an approximation property that the finite element spaces should satisfy.

The Condition 2 can be defined as:

$$\|u - u_h^i\|_E \leq \|u - v_h^i\|_E \quad \text{for all } v_h^i \in V_h^i \quad (6.57)$$

*i.e.* the finite element solution  $u_h^i$  is the best solution considering all elements of  $V_h^i$  when the distance is measured in the energy norm.

Note that when Condition 1 is satisfied for the energy norm, *Condition 2* gives

$$\|u - u_h^i\|_E \rightarrow 0 \quad \text{when } i \rightarrow \infty$$

which shows that the finite element solution converges in the energy norm to the exact solution.

To obtain the above convergence result for the 1-norm, we consider the norm equivalence given by

<sup>2</sup> Actually, if we would like to be mathematically precise, we should have used the infimum of the set

$$C_1 \|v\|_1 \leq \|v\|_E \leq C_2 \|v\|_1 \quad \text{for all } v \in V \quad (6.58)$$

for positive constants  $C_1$  and  $C_2$ . From (6.57) and (6.58), we can write

$$C_1 \|u - u_h^i\|_1 \leq \|u - u_h^i\|_E \leq \|u - v_h^i\|_E \leq C_2 \|u - v_h^i\|_1 \quad \text{for all } v_h^i \in V_h^i$$

which yields

$$\|u - u_h^i\|_1 \leq C \|u - v_h^i\|_1 \quad \text{for all } v_h^i \in V_h^i \quad (6.59)$$

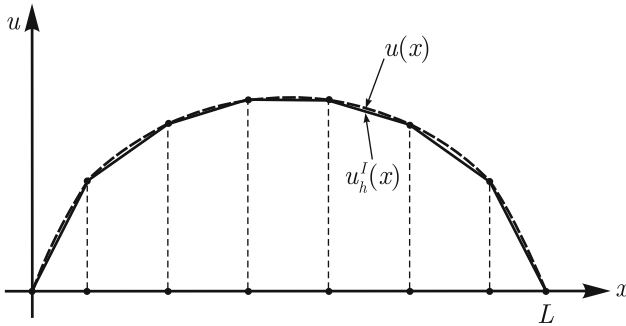
where  $C = C_2/C_1$ .

Equation (6.59) can be interpreted as Condition 2 in the 1-norm and when Condition 1 is satisfied for the 1-norm, we obtain

$$\|u - u_h^i\|_1 \rightarrow 0 \quad \text{when } i \rightarrow \infty \quad (6.60)$$

which shows that the finite element solution converges in the 1-norm to the exact solution.

Let us examine Conditions 1 and 2 for linear finite elements in 1-D for the 1-norm.



**Fig. 6.17.** Typical representation of  $u_h^I(x)$

Let  $u(x)$  be the exact solution of an arbitrary problem given by (6.46) with  $EA$  varying. Of course,  $u$  is a function in  $V$ . Let  $V_h$  be a finite element space implicitly defined by the choice of a finite element mesh. In Figure 6.17 a typical situation is represented where we also show the function  $u_h^I(x)$ . This function is called the interpolant and it is the function in  $V_h$  for which

$$u(x_i) = u_h^I(x_i) \quad i = 1, \dots, n_p$$

where the  $x_i$  are the nodal point coordinates and  $n_p$  is the number of nodal points. Note that the values of the interpolant coincide with the value of  $u(x)$  at the nodal positions. It can be shown (see, for example, Bathe, 1996) that

$$\|u - u_h^I\|_1 \leq C^* h |u|_2$$

where  $h$  is the maximum element length,  $C^*$  is a positive constant independent of  $h$  and  $u(x)$ , and

$$|u|_2 = \left( \int_0^L \left( \frac{d^2 u}{dx^2} \right)^2 dx \right)^{1/2}.$$

Of course, we are assuming that  $u(x)$  is sufficiently smooth such that the above equation is well defined. Since  $u_h^I \in V_h$ , we can write

$$d(u, V_h)_1 \leq \|u - u_h^I\|_1 \leq C^* h |u|_2. \quad (6.61)$$

If we define our sequence of finite element spaces given in (6.50) such that the largest element of mesh  $n$  tends to zero when  $n \rightarrow \infty$ , (6.61) would lead to

$$d(u, V_h)_1 \rightarrow 0 \text{ as } n \rightarrow \infty$$

since  $C |u|_2$  is a positive constant. Therefore, Condition 1 is satisfied.

Related to Condition 2, it can be shown (see, for example, Bathe, 1996) that

$$a(u - u_h, u - u_h) \leq a(u - v_h, u - v_h) \text{ for all } v_h \in V_h$$

where  $u_h$  is the finite element solution for  $V_h$ . Hence

$$\|u - u_h\|_E \leq \|u - v_h\|_E \text{ for all } v_h \in V_h. \quad (6.62)$$

The above equation yields Condition 2 for the energy norm. The property in (6.62) has an important consequence; namely, that when the exact solution is contained in the finite element space, *i.e.*,  $u \in V_h$ , then the finite element solution will be the exact solution, *i.e.*,  $u = u_h$ .

Of course, due to the norm equivalence (6.58) Condition 2 holds for the 1-norm as given in (6.59). Therefore, convergence is assured as given in (6.60).

Since we are considering a specific interpolation, we can obtain an error estimate. In fact, from (6.59)

$$\|u - u_h\|_1 \leq C \|u - u_h^I\|_1 \leq CC^* h |u|_2.$$

Defining  $\tilde{C} = C^* C |u|_2$ , we obtain

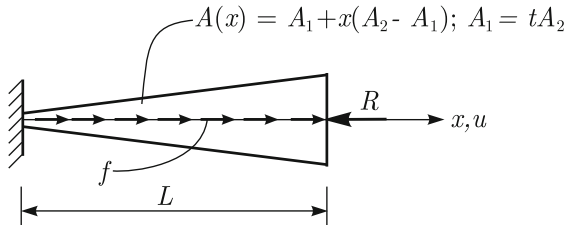
$$\|u - u_h\|_1 \leq \tilde{C} h \quad (6.63)$$

which is a convergence result for the 1-norm for linear finite element approximations of the problem given by (6.46).

Note that (6.63) shows that the error, *i.e.* the distance between the exact solution and the finite element solution, measured in the 1-norm can be made arbitrarily small. It suffices to refine the mesh until  $h$ , the size of the largest element, is small enough. Additionally (6.63) guarantees that not only the function  $u_h(x)$  is close to  $u(x)$  but also its derivative. Since when solving (6.46) we are interested in both displacements and stresses, which are obtained from the derivative of the displacement function, (6.63) is referred to as *the* convergence result. The convergence for linear elements is said to be linear since the error decreases with the first power of  $h$ . If the order of the displacement interpolation is increased, say from linear to quadratic, the convergence is controlled by the second power of  $h$  (in the equivalent of (6.63)) and is then referred to as “quadratic convergence”. The general result is that for piecewise polynomials of order  $p$  the convergence (provided the exact solution  $u$  is sufficiently smooth) is controlled by the  $p$ th power of  $h$ , *i.e.*, the convergence rate is of order  $p$ .

### Example 6.3

Study the convergence of the finite element solutions to the exact solution for the problem described in Figure 6.18. Consider uniform mesh refinements.



**Fig. 6.18.** Bar problem definition.  $E = 2.0 \times 10^7$  kN/m<sup>2</sup>,  $A_2 = 1$  m<sup>2</sup>,  $t = 0.01$ ,  $L = 1$  m,  $R = 15859.075383$  kN,  $f = 2.0 \times 10^4$  kN/m

### Solution

The differential formulation for this problem is given in equations (5.25) to (5.27). The exact solution is

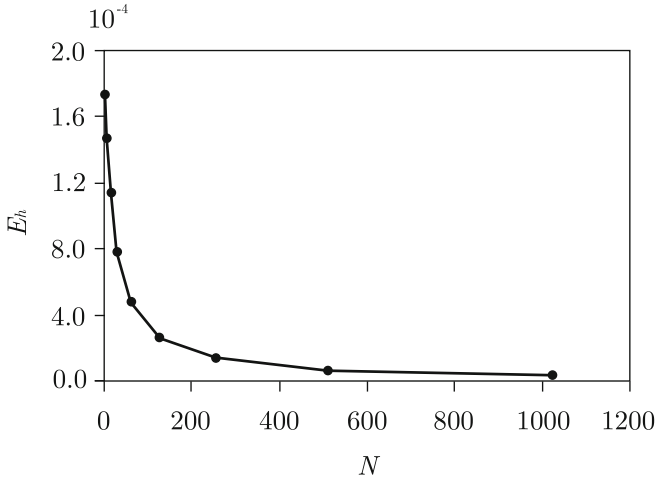
$$u(x) = -\frac{1}{1980} \frac{2x \ln(2) + 2x \ln(5) - \ln(1 + 99x)}{\ln(2) + \ln(5)}. \quad (6.64)$$

The sequence of finite element spaces is obtained by starting with a mesh of two 2-node elements of equal length and subdividing in each mesh refinement every element into two new elements of equal length. Our most refined mesh has 1024 elements. We measure the error in the 1-norm, that is,

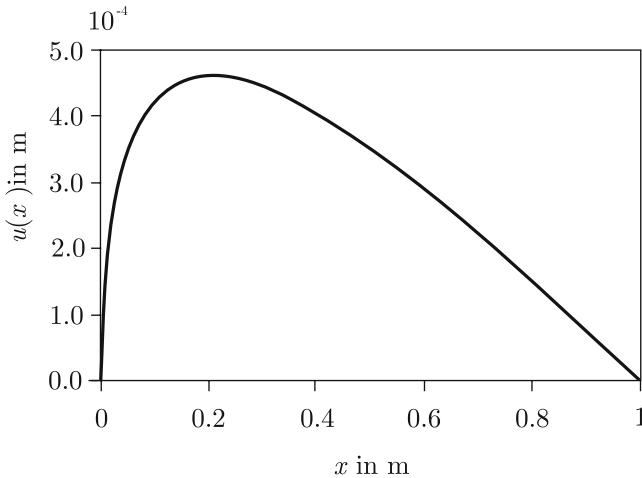


$$E_h = \|u - u_h\|_1.$$

In Figure 6.19 we show the error as the mesh is refined and in Figure 6.20 we show the exact solution together with the finite element solution for our most refined mesh. To use the error estimate given in (6.63) we need first to



**Fig. 6.19.** Convergence diagram.  $N$  is the number of free degrees of freedom



**Fig. 6.20.** Finite element solution for the 1024 element mesh and exact solution. No difference can be seen in the scale of the graph

verify that

$$|u(x)|_2 = \left( \int_0^L \left( \frac{d^2u}{dx^2} \right)^2 dx \right)^{1/2} < \infty$$

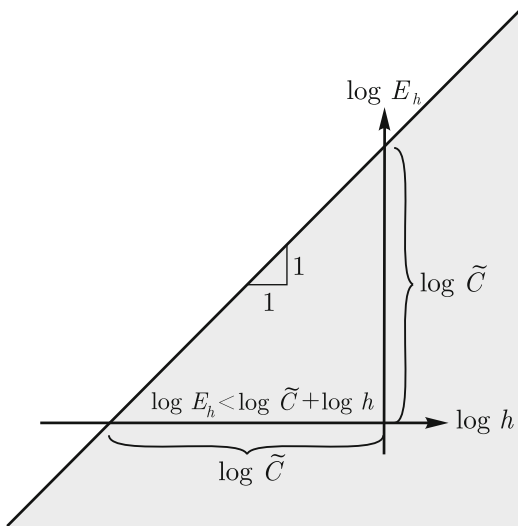
which, indeed is true, and can be evaluated using the exact solution (6.64).

Considering the error estimate (6.63), we have

$$\log \|u - u_h\|_1 \leq \log(\tilde{C}h)$$

$$\log E_h \leq \log \tilde{C} + \log h.$$

Using this inequality we can construct the diagram of Figure 6.21. Therefore, for a given mesh the ordered pair  $(\log E_h, \log h)$  has to lie either on the straight line or in the highlighted region and in practice we find that the numerical results are frequently close to the straight line.



**Fig. 6.21.** Log-log diagram used for convergence study

If the solution is known it is convenient to use the relative error which is defined as

$$E_h^r = \frac{\|u - u_h\|_1}{\|u\|_1} = \frac{E_h}{\|u\|_1}$$

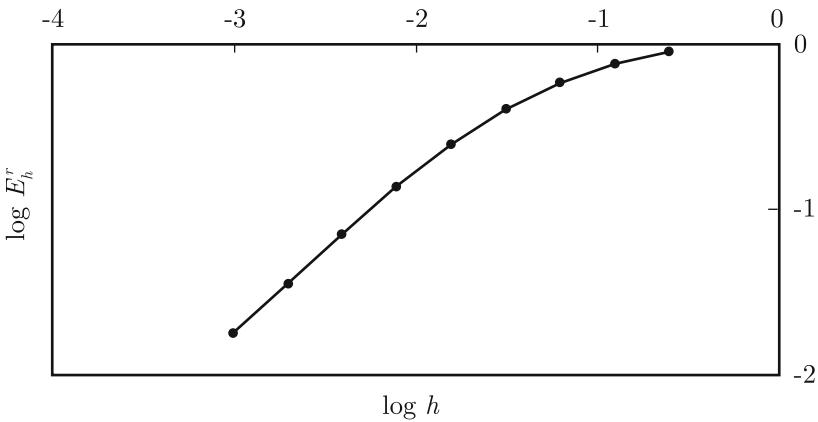
since  $E_h^r$  gives the error measured with respect to the 1-norm value of the exact solution. Also, note that from (6.63), we can write

$$\frac{\|u - u_h\|_1}{\|u\|_1} \leq \frac{\tilde{C}}{\|u\|_1} h$$

leading to

$$\log E_h^r \leq \log \hat{C} + \log h.$$

In Figure 6.22 we show the pairs  $(\log E_h^r, \log h)$  obtained in the solution of the problem described in Figure 6.18. The convergence rate evaluated based on the first two meshes is 0.244 and it increases as we consider pairs of more refined meshes. The convergence rate for the two most refined meshes is 0.9958 which is close to 1.



**Fig. 6.22.** Convergence diagram for problem of Figure 6.18 for uniform meshes

It is usual to measure convergence with respect to the number of degrees of freedom. The number of free degrees of freedom  $N$  corresponding to the 2-node element meshes used to solve the problem of Figure 6.18 is equal to the number of elements, that is,

$$N = n_e = \frac{L}{h} \quad \text{or} \quad h = N^{-1}L$$

and, therefore the error estimate (6.63) can be re-written in terms of  $N$  as

$$\|u - u_h\|_1 \leq \tilde{C}LN^{-1}$$

or

$$\|u - u_h\|_1 \leq C'N^{-1} \tag{6.65}$$

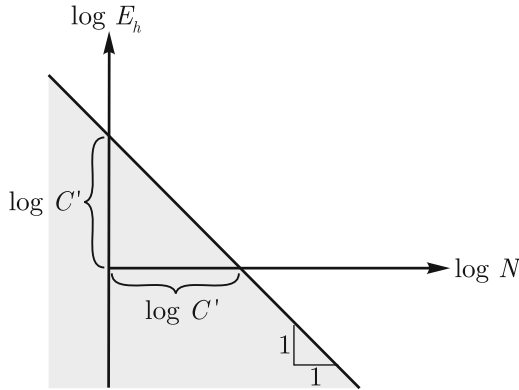
which leads to

$$\log E_h \leq \log C' - \log N$$

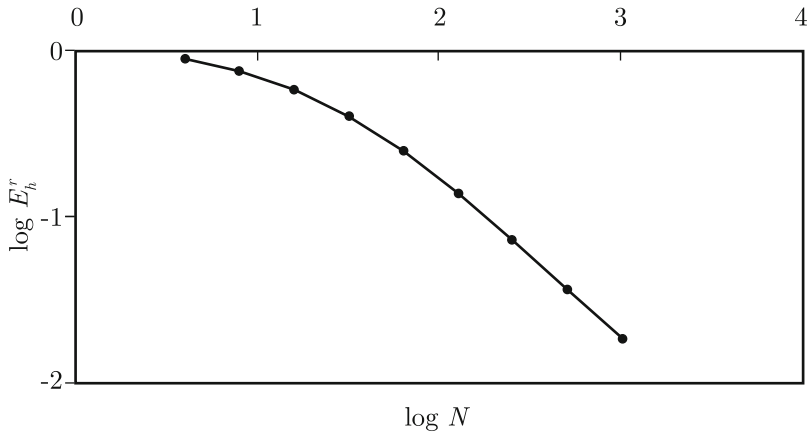
and a diagram, analogous to that shown in Figure 6.21, is reported in Figure 6.23. Of course, we can use  $E_h^r$  instead, which leads to

$$\log E_h^r \leq \log \bar{C} - \log N.$$

The convergence results shown in Figure 6.22 are reported in terms of  $N$  in Figure 6.24.



**Fig. 6.23.** Log-log diagram in terms of  $N$  (number of free degrees of freedom)



**Fig. 6.24.** Convergence diagram for problem of Figure 6.18 for uniform meshes in terms of  $N$

Referring to the exact solution  $u(x)$  of the problem described in Figure 6.18, which is reported in Figure 6.20, we see that in the region near the

support  $u(x)$  varies with highly varying gradients, and that for  $x > 0.5$ , the gradient of  $u(x)$  is almost constant. Therefore, it is quite intuitive that we can potentially improve the finite element predictions with respect to using a uniform mesh if we use smaller elements in the region of highly varying gradients and larger elements in the rest of the region. This kind of refinement strategy is known as *mesh grading* and we exemplify its potential benefits by means of the next example. □

### Example 6.4

For the problem of Figure 6.18, study the convergence behavior of the finite element solutions using a mesh grading strategy.

### Solution

Let us define the mesh grading by specifying the nodal positions as

$$x_i = \left( \frac{i}{n_e} \right)^\beta, \quad i = 0, 1, 2, \dots, n_e \quad ; \quad n_e \geq 2$$

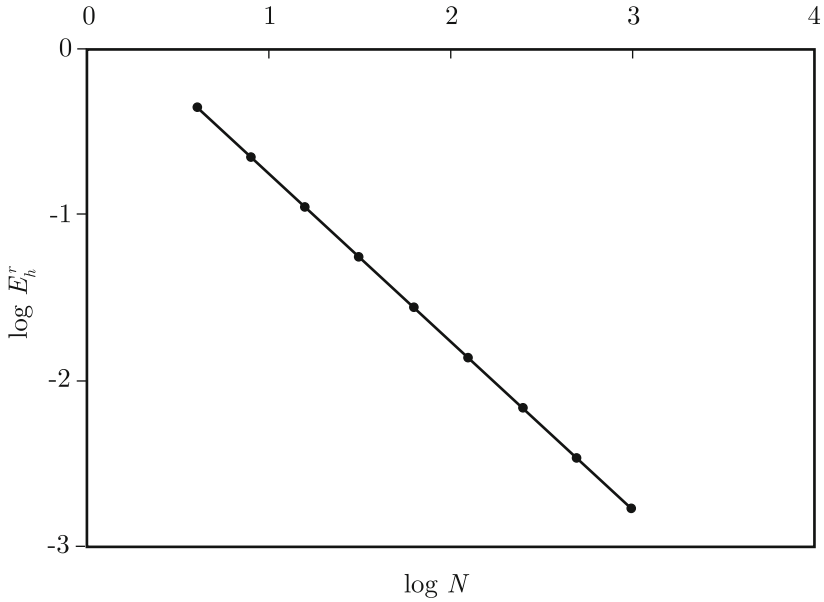
where  $x_0, x_1, \dots, x_{n_e}$  are the nodal coordinates,  $n_e$  is the number of 2-node elements and  $\beta$  is a positive real constant which defines the grading. Note that  $\beta = 1$  gives, as a particular case, the uniform mesh. Since we would like smaller elements as we approach  $x = 0$ , we consider  $\beta > 1.0$ .

In Figure 6.25 we show the convergence behavior of the finite element solutions for  $\beta = 4.0$ . The rate of convergence evaluated using the first two meshes ( $n_e = 4$  and  $n_e = 8$ ) is 0.9928 and using the last two meshes ( $n_e = 512$  and  $n_e = 1024$ ) is 0.9999926.

In Table 6.2 we show some selected results for some  $\beta$  values. We note that any grading refinement strategy leads to superior performance when compared to the uniform refinement ( $\beta = 1$ ) which can be measured by the error of the most refined mesh. Note that a rate of convergence very close to 1 is attained for the last two meshes for all values of  $\beta$ .

We can now revisit the finite element solutions reported in Figure 6.15 for the problem described in Figure 6.14. We note that for the left half of the domain, *i.e.*, for  $0 \leq x \leq 1$ , this problem is identical to the problem discussed in Examples 6.3 and 6.4. Therefore, the discussion presented in these examples is directly applicable and explains why the grading leading to the results shown in Figure 6.15d is efficient.

Regarding the right half of the domain, of course the exact displacements in this region varies linearly and only one element predicts the exact strain. However, the displacements are in error as long as the displacement at  $x = 1$  is not the exact displacement. □



**Fig. 6.25.** Convergence diagram for problem of Figure 6.18 for graded meshes

**Table 6.2.** Selected results for various  $\beta$  values

$\beta$	Length of smallest elem. (1024 elem.)	Length of largest elem (1024 elem.)	Relative error ( $E_h^r$ ) (1024 elem.)
1.0	$0.976 \times 10^{-3}$	$0.976 \times 10^{-3}$	$3.5 \times 10^{-5}$
2.0	$0.954 \times 10^{-3}$	$1.95 \times 10^{-3}$	$5.0 \times 10^{-6}$
3.0	$0.931 \times 10^{-3}$	$2.93 \times 10^{-3}$	$3.6 \times 10^{-6}$
4.0	$0.909 \times 10^{-3}$	$3.90 \times 10^{-3}$	$3.4 \times 10^{-6}$

$\beta$	Convergence rate for first two meshes	Convergence rate for last two meshes
1.0	0.24	0.995486
2.0	0.99	0.999974
3.0	0.76	0.999992
4.0	0.99	0.999999

Finally, we should note that we discussed here only the convergence of displacement-based elements. The behavior of mixed interpolated elements referred to in Section 6.5 can be much more difficult to assess, see *e.g.* Brezzi and Fortin, 1991, Chapelle and Bathe, 2010*a* and Hiller and Bathe, 2003.

#### 6.2.4 Smoothness of the solution

We mentioned earlier that to derive the error estimate (6.63), we must have

$$|u|_2 < \infty \tag{6.66}$$

and if higher-order elements are used even stricter conditions may be applicable, that is the exact solution need be sufficiently smooth.

Hence if (6.66) is not satisfied, the estimate (6.63) can not directly be used and further mathematical analysis is required to obtain valid estimates for specific situations. In fact, it can be shown that the same rate of convergence as for the smooth solution case can still be achieved if the mesh is properly graded (Ciarlet, 1978 and Bathe, 1996 and Chapelle and Bathe, 2010*a*). Considering the full realm of elasticity, solutions with poor smoothness properties are encountered in problems with sharp corners and cracks and special error estimates are then required.

#### 6.2.5 The $h$ , $p$ and $h - p$ finite element methods

The strategy used so far to refine finite element meshes is called the *h method*: the elements of size  $h$  are simply subdivided. In the *p method*, we start with a mesh and obtain larger finite element spaces by increasing the order of the interpolation functions in each element. For example, we start with a mesh of linear elements and then consider quadratic, cubic ... elements. The element interpolations of order  $p$  are constructed in a special way to render the procedure as efficient as possible.

In the  $h - p$  method, elements are subdivided and the polynomial order of the elements is increased. This method combines the advantages of the  $h$  and  $p$  methods.

Of course, there are several issues concerning the implementation, general applicability and efficiency of these methods specially when we consider 2-D, 3-D solids, and plate and shell elements.

In engineering applications of the finite element method mostly linear elements (2-node elements in 1-D, 4-node elements in 2-D and 8-node elements in 3-D) or quadratic elements are used. Then the  $h$  method is employed to refine the meshes. For these analyses computer programs are available to generate and refine the meshes for complex geometries of engineering interest.

### 6.3 Displacement-based finite element formulation for solids

In the previous sections we introduced the fundamental concepts of a finite element formulation and solution considering one-dimensional problems.

In this section, we shall extend the finite element formulation to 3-D elastic bodies. Of course, some complexity is added, since the problem domain is multi-dimensional. However, as seen shortly, the concepts involved are the same as for the one-dimensional case.

In 2-D solutions the finite element interpolation functions can be pictorially well presented and then the generalization for 3-D solutions is apparent and straight forward. Hence, we start with the 2-D formulation and in Section 6.3.5 we discuss the 3-D formulation.

Our starting point is, as for the 1-D case, the principle of virtual work for 3-D

$$\int_V \bar{\varepsilon}^T \tau dV = \int_V \bar{\mathbf{u}}^T \mathbf{f}^B dV + \int_{S_f} \bar{\mathbf{u}}^T \mathbf{f}^S dS. \quad (6.67)$$

This equation is applicable for plane stress, plane strain and axisymmetric solids (see Section 5.2.1). We shall consider the plane stress case (see Section 5.2.2) but all concepts are also directly applicable to the other 2-D cases.

We consider (5.40) which gives the principle of virtual work for plane stress conditions when the thickness  $t$  (here assumed constant) is kept in the equation. For the finite element solution we express this principle in terms of displacements only. Therefore, we introduce the constitutive equation  $\tau = \mathbf{C}\varepsilon$  and the compatibility relations, *i.e.*, the strain-displacement relations  $\varepsilon = \partial_\varepsilon \mathbf{u}$  given in Table 4.3. Substituting, we obtain:

Find  $\mathbf{u}$  such that

$$t \int_A (\partial_\varepsilon \bar{\mathbf{u}})^T \mathbf{C} \partial_\varepsilon \mathbf{u} dA = t \int_A \bar{\mathbf{u}}^T \mathbf{f}^B dA + t \int_{L_f} \bar{\mathbf{u}}^T \mathbf{f}^S dL$$

$$\forall \bar{\mathbf{u}}, \bar{\mathbf{u}} = \mathbf{0} \quad \text{in } L_u \quad (6.68)$$

In the finite element analysis we assume  $\mathbf{u}$  and  $\bar{\mathbf{u}}$  to have a particular functional form given by the interpolation functions and we proceed as discussed below.

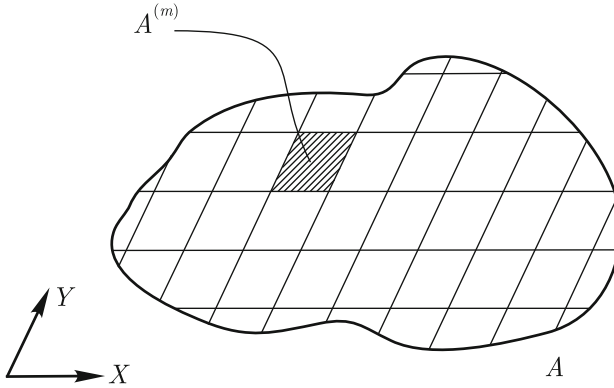
#### 6.3.1 Discretization methodology

Consider a typical finite element discretization as shown in Figure 6.26 where a generic element ( $m$ ) is highlighted. For each element in the discretization a set of nodal points is defined, see Figures 6.27 and 6.28. We are taking four nodes per element, *i.e.*, we are considering 4-node elements, and note that a nodal point is usually shared by several elements. For instance, we can see in Figure 6.28 that node  $k$  belongs to elements  $p, l, m$  and  $q$ . In order to define a

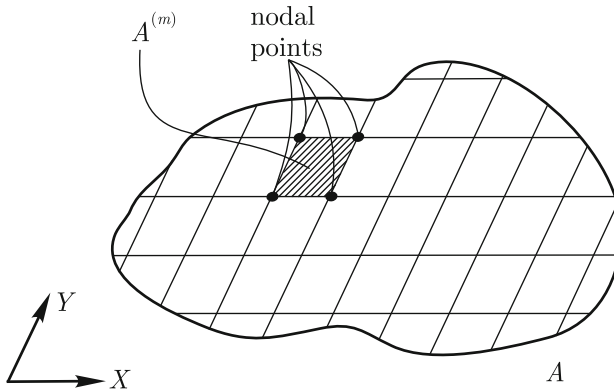


typical finite element approximation for the exact unknown displacements, we assume all element displacements to vary according to interpolation functions. As in the 1-D case, the displacements inside an element depend only on the displacement values at the element nodal points.

Consider the rectangular element ( $m$ ) as shown in Figure 6.29 with the global nodal degrees of freedom. It is effective to use a local coordinate



**Fig. 6.26.** Partition of the 2-D domain into subdomains, *i.e.*, elements. Only part of the domain is shown



**Fig. 6.27.** Nodal points for element ( $m$ )

system and a local node numbering as shown in Figure 6.30 to define the interpolation functions. Then, the interpolation function associated with node 1 is given by

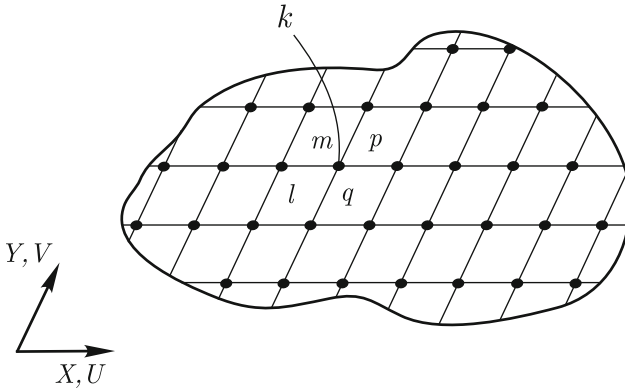


Fig. 6.28. Nodal points considering all elements in the part of the domain shown

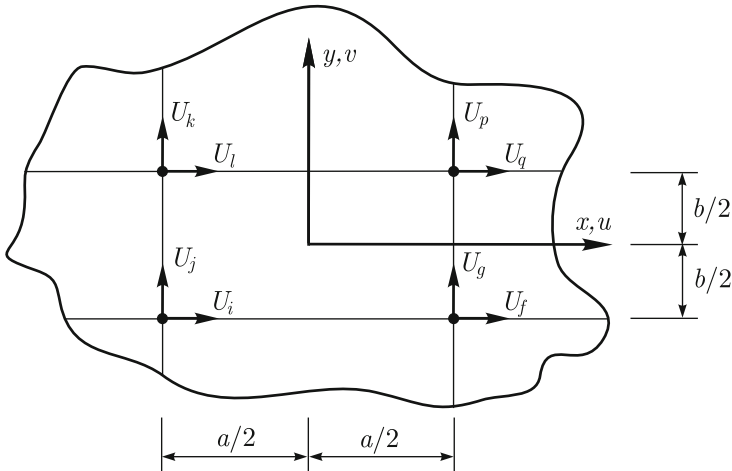


Fig. 6.29. Detail of a generic element ( $m$ ) indicating the global nodal degrees of freedom

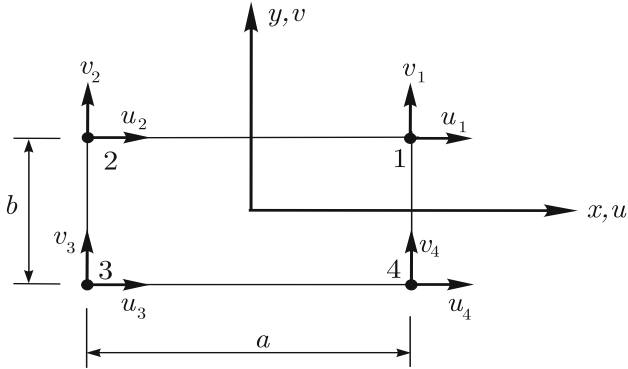
$$h_1(x, y) = \frac{1}{4ab} (a + 2x)(b + 2y). \quad (6.69)$$

This function is pictorially shown in Figure 6.31. Note that  $h_1(x, y)$  is equal to 1 for the nodal coordinates of node 1, *i.e.*, at  $x = a/2, y = b/2$ , and is equal to 0 for the nodal coordinates of nodes 2, 3 and 4. The function  $h_1(x, y)$  is linear in  $x$  for a fixed  $y$  and linear in  $y$  for a fixed  $x$ . We can define  $h_i(x, y), i = 2, 3, 4$  with analogous properties to  $h_1$ , *i.e.*, being 1 for the coordinates of node  $i$  and 0 for the coordinates of node  $j, j \neq i$ , by

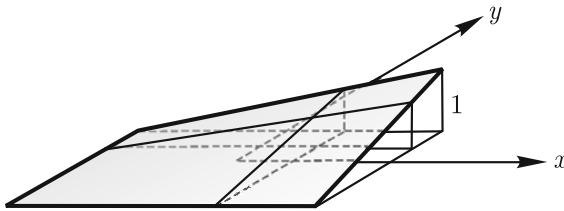
$$h_2(x, y) = \frac{1}{4ab} (a - 2x)(b + 2y) \quad (6.70)$$

$$h_3(x, y) = \frac{1}{4ab} (a - 2x) (b - 2y) \tag{6.71}$$

$$h_4(x, y) = \frac{1}{4ab} (a + 2x) (b - 2y) . \tag{6.72}$$



**Fig. 6.30.** Local degrees of freedom; the local degrees of freedom act into the same directions as the global degrees of freedom



**Fig. 6.31.** Schematic description of function  $h_1(x, y)$

Using these interpolation functions we can define the assumed displacements within element ( $m$ ) at any point  $(x, y)$  from their values at the nodal points by

$$u^{(m)}(x, y) = \sum_{i=1}^4 h_i(x, y) u_i$$

and

$$v^{(m)}(x, y) = \sum_{i=1}^4 h_i(x, y) v_i.$$

Denoting the coordinate of node  $i$  by  $(x_i, y_i)$ , it is easy to verify that

$$u^{(m)}(x_i, y_i) = u_i$$

$$v^{(m)}(x_i, y_i) = v_i.$$

Using matrix notation, we have

$$\mathbf{u}^{(m)} = \begin{bmatrix} u^{(m)}(x, y) \\ v^{(m)}(x, y) \end{bmatrix} = \mathbf{H} \hat{\mathbf{u}} \tag{6.73}$$

where

$$\mathbf{H} = \begin{bmatrix} h_1 & 0 & h_2 & 0 & h_3 & 0 & h_4 & 0 \\ 0 & h_1 & 0 & h_2 & 0 & h_3 & 0 & h_4 \end{bmatrix}. \tag{6.74}$$

and

$$\hat{\mathbf{u}}^T = \begin{bmatrix} u_1 & v_1 & u_2 & v_2 & u_3 & v_3 & u_4 & v_4 \end{bmatrix}$$

We shall use the hat symbol ( $\hat{\phantom{x}}$ ) to denote nodal quantities, such as nodal displacements in equation (6.73), whenever the distinction between nodal and continuum quantities is not obviously implied.

For the derivation below, it is convenient to define a column matrix which collects all  $N$  global nodal displacement degrees of freedom

$$\mathbf{U}^T = [U_1 \ U_2 \ \dots \ U_N]$$

and also define  $\mathbf{H}^{(m)}$  by

$$\mathbf{u}^{(m)} = \mathbf{H}^{(m)} \mathbf{U} \tag{6.75}$$

In equations (6.73) and (6.75)  $\mathbf{H}$  corresponds to the local nodal displacement degrees of freedom ( $(m)$  being implied), whereas  $\mathbf{H}^{(m)}$  corresponds to the global nodal displacement degrees of freedom. We assume that the local degrees of freedom act into the same directions as the global degrees of freedom, in which case the columns in  $\mathbf{H}^{(m)}$  are either zero or given by the columns defined in  $\mathbf{H}$ . For example, considering the element in Figure 6.29, we have

$$\mathbf{u}^{(m)} = \begin{bmatrix} & f & g & & i & j & k & l & & p & q \\ \dots & h_4 & 0 & \cdot & h_3 & 0 & 0 & h_2 & \dots & 0 & h_1 & \dots \\ \dots & 0 & h_4 & \cdot & 0 & h_3 & h_2 & 0 & \dots & h_1 & 0 & \dots \end{bmatrix} \mathbf{U}. \tag{6.76}$$

Only the columns of  $\mathbf{H}^{(m)}$  with non-zero entries are shown.

We can now evaluate the strains from  $\mathbf{u}^{(m)}$  using the strain-displacement relations

$$\varepsilon^{(m)} = \mathbf{B}^{(m)}\mathbf{U} \tag{6.77}$$

where

$$\mathbf{B}^{(m)} = \partial_\varepsilon \mathbf{H}^{(m)} \tag{6.78}$$

and the stresses are obtained using the constitutive equation for element ( $m$ )

$$\tau^{(m)} = \mathbf{C}^{(m)} \varepsilon^{(m)}. \tag{6.79}$$

Since the virtual displacements are interpolated in the same way as the real displacements we have

$$\bar{\mathbf{u}}^{(m)} = \mathbf{H}^{(m)}\bar{\mathbf{U}} \tag{6.80}$$

and

$$\bar{\varepsilon}^{(m)} = \mathbf{B}^{(m)}\bar{\mathbf{U}}. \tag{6.81}$$

Therefore all quantities involved in the principle of virtual displacements are defined elementwise. Since we can write the integral over the domain  $A$  as a sum of integrals performed over the elements, we obtain

$$\begin{aligned} \sum_{m=1}^{n_e} t \int_{A^{(m)}} \bar{\varepsilon}^T \tau^{(m)} dA^{(m)} &= \sum_{m=1}^{n_e} t \int_{A^{(m)}} \bar{\mathbf{u}}^{(m)T} \mathbf{f}^{B^{(m)}} dA^{(m)} + \\ &\sum_{m=1}^{n_e} t \int_{L_1^{(m)} \dots L_q^{(m)}} \bar{\mathbf{u}}^{(m)T} \mathbf{f}^{S^{(m)}} dL^{(m)} \end{aligned} \tag{6.82}$$

where  $n_e$  is the number of elements in the mesh and  $L_1^{(m)} \dots L_q^{(m)}$  represent the sides of element ( $m$ ) that belong to the boundary  $L_f$ . Note that an element in the interior of the domain does not have any sides that are on  $L_f$ , and therefore there is no contribution from such an element to the last term in (6.82).

Substituting from (6.75) to (6.81) into (6.82) we arrive at

$$\begin{aligned} \bar{\mathbf{U}}^T \left[ \sum_{m=1}^{n_e} t \int_{A^{(m)}} \mathbf{B}^{(m)T} \mathbf{C}^{(m)} \mathbf{B}^{(m)} dA^{(m)} \right] \mathbf{U} = \\ \bar{\mathbf{U}}^T \left[ \sum_{m=1}^{n_e} t \left( \int_{A^{(m)}} \mathbf{H}^{(m)T} \mathbf{f}^{B^{(m)}} dA^{(m)} \right) \right. \\ \left. + \sum_{m=1}^{n_e} t \left( \int_{L_1^{(m)}, \dots, L_q^{(m)}} \mathbf{H}^{(m)T} \mathbf{f}^{S^{(m)}} dL^{(m)} \right) \right] \end{aligned} \tag{6.83}$$

Note that  $\bar{\mathbf{U}}$  and  $\mathbf{U}$  were taken out of the sums and integrals since they are independent of  $(m)$ . Defining

$$\mathbf{K}^{(m)} = t \int_{A^{(m)}} \mathbf{B}^{(m)T} \mathbf{C}^{(m)} \mathbf{B}^{(m)} dA^{(m)} \quad (6.84)$$

$$\mathbf{R}_B^{(m)} = t \int_{A^{(m)}} \mathbf{H}^{(m)T} \mathbf{f}^{B^{(m)}} dA^{(m)} \quad (6.85)$$

$$\mathbf{R}_S^{(m)} = t \int_{L_1^{(m)}, \dots, L_q^{(m)}} \mathbf{H}^{(m)T} \mathbf{f}^{S^{(m)}} dL^{(m)} \quad (6.86)$$

and

$$\mathbf{K} = \sum_{m=1}^{n_e} \mathbf{K}^{(m)} \quad (6.87)$$

$$\mathbf{R}_B = \sum_{m=1}^{n_e} \mathbf{R}_B^{(m)} \quad (6.88)$$

$$\mathbf{R}_S = \sum_{m=1}^{n_e} \mathbf{R}_S^{(m)} \quad (6.89)$$

$$\mathbf{R} = \mathbf{R}_B + \mathbf{R}_S$$

we can write (6.83) as

$$\bar{\mathbf{U}}^T (\mathbf{K}\mathbf{U} - \mathbf{R}) = 0.$$

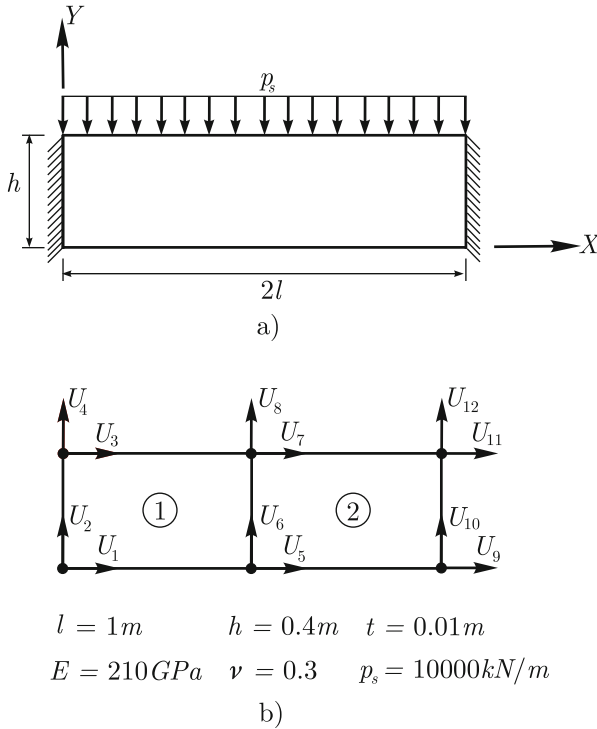
Since the virtual displacements are arbitrary,  $\bar{\mathbf{U}}$  should be made arbitrary leading to

$$\mathbf{K}\mathbf{U} = \mathbf{R}. \quad (6.90)$$

### Example 6.5

Consider the problem shown in Figure 6.32. For the given finite element discretization calculate:

- (i) The nodal displacements.
- (ii) The displacements and stresses at the material point P which has coordinates  $X = l/2, Y = h$ .



**Fig. 6.32.** Two-dimensional plane stress problem

**Solution**

We can write (6.90) as

$$\begin{bmatrix} \mathbf{K}_{aa} & \mathbf{K}_{ab} \\ \mathbf{K}_{ba} & \mathbf{K}_{bb} \end{bmatrix} \begin{bmatrix} \mathbf{U}_a \\ \mathbf{U}_b \end{bmatrix} = \begin{bmatrix} \mathbf{R}_a \\ \mathbf{R}_b \end{bmatrix}$$

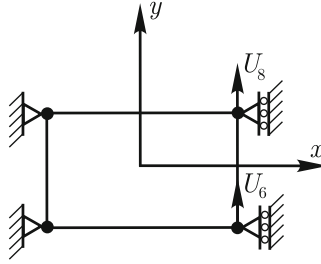
where  $\mathbf{U}_a$  and  $\mathbf{U}_b$  list respectively the unknown and known nodal point displacements (see also (2.53) and (2.54)). The equations to be solved are

$$\mathbf{K}_{aa}\mathbf{U}_a = \mathbf{R}_a - \mathbf{K}_{ab}\mathbf{U}_b \tag{6.91}$$

where then

$$\mathbf{R}_b = \mathbf{K}_{ba}\mathbf{U}_a + \mathbf{K}_{bb}\mathbf{U}_b.$$

Considering the problem in Figure 6.32, we recognize that due to symmetry we only need to solve the problem given in Figure 6.33 with only  $U_6$  and  $U_8$  as unknowns. Therefore, using equation (6.91)



**Fig. 6.33.** Finite element problem to be solved considering symmetry

$$\begin{bmatrix} K_{66} & K_{68} \\ K_{86} & K_{88} \end{bmatrix} \begin{bmatrix} U_6 \\ U_8 \end{bmatrix} = \begin{bmatrix} R_6 \\ R_8 \end{bmatrix}. \tag{6.92}$$

Let us evaluate the required terms. Denoting by  $\mathbf{B}_j^{(m)}$  the column matrix corresponding to the  $j$ th column of  $\mathbf{B}^{(m)}$  and considering equation (6.84), we have

$$K_{ij}^{(m)} = t \int_{A^{(m)}} \mathbf{B}_i^{(m)T} \mathbf{C}^{(m)} \mathbf{B}_j^{(m)} dA^{(m)}.$$

The evaluation of  $\mathbf{B}_6^{(1)}$  and  $\mathbf{B}_8^{(1)}$  is therefore required. Since in the local element numbering  $U_6$  corresponds to  $v_4$  and  $U_8$  to  $v_1$

$$\mathbf{B}_6^{(1)T} = \left[ 0 \quad \frac{\partial h_4}{\partial y} \quad \frac{\partial h_4}{\partial x} \right], \quad \mathbf{B}_8^{(1)T} = \left[ 0 \quad \frac{\partial h_1}{\partial y} \quad \frac{\partial h_1}{\partial x} \right].$$

From equations (6.69) to (6.72), with  $a = l, b = h$

$$\begin{aligned} \frac{\partial h_1}{\partial x} &= \frac{1}{2lh} (h + 2y), & \frac{\partial h_1}{\partial y} &= \frac{1}{2lh} (l + 2x) \\ \frac{\partial h_4}{\partial x} &= \frac{1}{2lh} (h - 2y), & \frac{\partial h_4}{\partial y} &= -\frac{1}{2lh} (l + 2x). \end{aligned}$$

Hence,



$$\begin{aligned}
 K_{66} &= K_{66}^{(1)} = \frac{Et}{(1-\nu^2)} \int_{-l/2}^{l/2} \int_{-h/2}^{h/2} \left[ 0 \quad -\frac{1}{2lh} (l+2x) \quad \frac{1}{2lh} (h-2y) \right] \\
 &\quad \begin{bmatrix} 1 & \nu & 0 \\ \nu & 1 & 0 \\ 0 & 0 & \frac{1-\nu}{2} \end{bmatrix} \begin{bmatrix} 0 \\ -\frac{1}{2lh} (l+2x) \\ \frac{1}{2lh} (h-2y) \end{bmatrix} dydx = \\
 &= \frac{Et}{(1-\nu^2)} \frac{h^2(1-\nu) + 2l^2}{6hl}
 \end{aligned}$$

Analogously, we obtain

$$\begin{aligned}
 K_{88} &= K_{88}^{(1)} = \frac{Et}{(1-\nu^2)} \int_{-l/2}^{l/2} \int_{-h/2}^{h/2} \left[ 0 \quad \frac{1}{2lh} (l+2x) \quad \frac{1}{2lh} (h+2y) \right] \\
 &\quad \begin{bmatrix} 1 & \nu & 0 \\ \nu & 1 & 0 \\ 0 & 0 & \frac{1-\nu}{2} \end{bmatrix} \begin{bmatrix} 0 \\ \frac{1}{2lh} (l+2x) \\ \frac{1}{2lh} (h+2y) \end{bmatrix} dydx = \\
 &= \frac{Et}{(1-\nu^2)} \frac{h^2(1-\nu) + 2l^2}{6hl}
 \end{aligned}$$

$$\begin{aligned}
 K_{68} &= K_{86} = \frac{Et}{(1-\nu^2)} \int_{-l/2}^{l/2} \int_{-h/2}^{h/2} \left[ 0 \quad \frac{1}{2lh} (l+2x) \quad \frac{1}{2lh} (h+2y) \right] \\
 &\quad \begin{bmatrix} 1 & \nu & 0 \\ \nu & 1 & 0 \\ 0 & 0 & \frac{1-\nu}{2} \end{bmatrix} \begin{bmatrix} 0 \\ -\frac{1}{2lh} (l+2x) \\ \frac{1}{2lh} (h-2y) \end{bmatrix} dydx = \\
 &= \frac{Et}{(1-\nu^2)} \frac{h^2(1-\nu) - 4l^2}{12hl}.
 \end{aligned}$$

For the load vector, denoting the  $j$ th column of  $\mathbf{H}^{(m)}$  by  $\mathbf{H}_j^{(m)}$  and the  $j$ th line of the column matrix  $\mathbf{R}_S^{(m)}$  by  $R_{S_j}^{(m)}$ , we can write

$$R_{S_j}^{(m)} = t \int_{L_1^{(m)}, \dots, L_q^{(m)}} \mathbf{H}_j^{(m)T} \mathbf{f}^S dL^{(m)}.$$

Hence

$$\begin{aligned}
 R_{S_6} &= R_{S_6}^{(1)} = 0 \\
 R_{S_8} &= R_{S_8}^{(1)} = t \int_{-l/2}^{l/2} \begin{bmatrix} 0 & h_1(x, y = h/2) \end{bmatrix} \begin{bmatrix} 0 \\ -p_s/t \end{bmatrix} dx = \quad (6.93) \\
 &= \int_{-l/2}^{l/2} \frac{1}{2l} (l + 2x) (-p_s) dx = -\frac{p_s l}{2}.
 \end{aligned}$$

Since  $p_s$  is a line load, we divided by  $t$  to obtain the equivalent pressure load corresponding to  $\mathbf{f}^S$ . Of course, if we bring  $t$  inside the integral in equation (6.93) we can use  $p_s$  directly. Note that in the evaluation of  $\mathbf{R}_S^{(1)}$  the only element sides that are in  $L_f$  are those given by  $y = h/2, y = -h/2$ . Since  $h_4$  which enters in the evaluation of  $\mathbf{R}_{S_6}^{(1)}$  is zero for  $y = +h/2$  and  $\mathbf{f}^S$  is zero for  $y = -h/2$ , it is immediate to conclude that  $\mathbf{R}_{S_6}^{(1)} = 0$ . Also the integral for the evaluation of  $\mathbf{R}_{S_8}^{(1)}$  is performed only for  $y = +h/2$  since  $\mathbf{f}^S = \mathbf{0}$  for  $y = -h/2$ . Therefore

$$\frac{Et}{(1 - \nu^2)} \begin{bmatrix} \frac{h^2(1-\nu)+2l^2}{6hl} & \frac{h^2(1-\nu)-4l^2}{12hl} \\ \frac{h^2(1-\nu)-4l^2}{12hl} & \frac{h^2(1-\nu)+2l^2}{6hl} \end{bmatrix} \begin{bmatrix} U_6 \\ U_8 \end{bmatrix} = \begin{bmatrix} 0 \\ -\frac{p_s l}{2} \end{bmatrix}. \quad (6.94)$$

Substituting the numerical values and solving

$$U_6 = -0.0148352 \text{ m}$$

$$U_8 = -0.0161172 \text{ m}.$$

In order to evaluate the stresses at  $P$  we use

$$\tau|_P = \mathbf{C}^{(1)} \mathbf{B}^{(1)}|_P \mathbf{U}.$$

The local coordinates of  $P$  are  $x = 0, y = h/2$  which are used in the evaluation of  $\mathbf{B}^{(1)}|_P$ . Therefore

$$\tau|_P = \frac{E}{1 - \nu^2} \begin{bmatrix} 1 & \nu & 0 \\ \nu & 1 & 0 \\ 0 & 0 & \frac{1-\nu}{2} \end{bmatrix} \begin{bmatrix} 0 \\ \frac{\partial h_4}{\partial y} U_6 + \frac{\partial h_1}{\partial y} U_8 \\ \frac{\partial h_4}{\partial x} U_6 + \frac{\partial h_1}{\partial x} U_8 \end{bmatrix}_{x=0, y=h/2}$$

resulting in

$$\tau|_P = \begin{bmatrix} \tau_{xx} \\ \tau_{yy} \\ \tau_{xy} \end{bmatrix} = \begin{bmatrix} -0.11094 \text{ GPa} \\ -0.36981 \text{ GPa} \\ -1.30177 \text{ GPa} \end{bmatrix}.$$

□

Of course, this example was chosen to merely demonstrate the finite element analysis process. A much finer mesh (of many more elements) would be needed to solve the problem in Figure 6.32a accurately.

We showed in (6.74) to (6.76) how the matrices  $\mathbf{H}$  and  $\mathbf{H}^{(m)}$  are related.

Analogously, we can define the matrices  $\mathbf{B}$  and  $\mathbf{k}^{(m)}$  which would correspond to  $\mathbf{B}^{(m)}$  and  $\mathbf{K}^{(m)}$  when we consider only the entries associated with the local element degrees of freedom. Then  $\mathbf{B}$  is defined by

$$\varepsilon^{(m)} = \mathbf{B}\hat{\mathbf{u}}. \quad (6.95)$$

For instance, for the four-node element in Figure 6.30

$$\mathbf{B} = \begin{bmatrix} \frac{\partial h_1}{\partial x} & 0 & \frac{\partial h_2}{\partial x} & 0 & \frac{\partial h_3}{\partial x} & 0 & \frac{\partial h_4}{\partial x} & 0 \\ 0 & \frac{\partial h_1}{\partial y} & 0 & \frac{\partial h_2}{\partial y} & 0 & \frac{\partial h_3}{\partial y} & 0 & \frac{\partial h_4}{\partial y} \\ \frac{\partial h_1}{\partial y} & \frac{\partial h_1}{\partial x} & \frac{\partial h_2}{\partial y} & \frac{\partial h_2}{\partial x} & \frac{\partial h_3}{\partial y} & \frac{\partial h_3}{\partial x} & \frac{\partial h_4}{\partial y} & \frac{\partial h_4}{\partial x} \end{bmatrix}. \quad (6.96)$$

The matrix  $\mathbf{k}^{(m)}$  can be defined by

$$\mathbf{k}^{(m)} = t \int_A \mathbf{B}^T \mathbf{C} \mathbf{B} \, dA \quad (6.97)$$

where the domain  $A$ , and the matrices  $\mathbf{B}$  and  $\mathbf{C}$  correspond to the element considered.

A generic entry in the matrix  $\mathbf{K}^{(m)}$  is given by (see also Example 6.5)

$$K_{ij}^{(m)} = t \int_{A^{(m)}} \mathbf{B}_i^{(m)T} \mathbf{C} \mathbf{B}_j^{(m)} \, dA^{(m)} \quad (6.98)$$

where  $K_{ij}^{(m)}$  is different from zero only when  $\mathbf{B}_i^{(m)}$  and  $\mathbf{B}_j^{(m)}$  have entries that are non-zero. This happens only when the degrees of freedom  $U_i$  and  $U_j$  belong to element  $(m)$ . Therefore all entries of  $\mathbf{K}^{(m)}$  are also in  $\mathbf{k}^{(m)}$  since all columns of  $\mathbf{B}^{(m)}$  which have non-zero entries are in  $\mathbf{B}$ . Hence, we can obtain  $\mathbf{K}^{(m)}$  from  $\mathbf{k}^{(m)}$  by properly assigning the entries in  $\mathbf{k}^{(m)}$  to entries in  $\mathbf{K}^{(m)}$ . This is achieved by using the element connectivity array  $\mathbf{LM}^{(m)}$  which lists the global degrees of freedom numbers ordered according to the local numbering. As already detailed for matrix structural analysis (see Sections 2.3 and 4.2.4), considering the element described in Figure 6.29, we would have

$$\mathbf{LM}^{(m)T} = \begin{bmatrix} & u_1 & v_1 & u_2 & v_2 & u_3 & v_3 & u_4 & v_4 \\ q & p & l & k & i & j & f & g & \end{bmatrix}. \quad (6.99)$$

The contributions of element ( $m$ ) to the global stiffness matrix  $\mathbf{K}$  can be obtained by summing

$$\begin{aligned} &k_{11}^{(m)} \text{ to the entry } qq \text{ of the array;} \\ &k_{12}^{(m)} \text{ to the entry } qp; \\ &\quad \vdots \\ &k_{18}^{(m)} \text{ to the entry } qg; \\ &k_{22}^{(m)} \text{ to the entry } pp; \\ &\quad \vdots \\ &k_{28}^{(m)} \text{ to the entry } pg; \end{aligned}$$

and so on.

Here by taking advantage of the symmetry of  $\mathbf{K}$  we assemble only the upper part of  $\mathbf{K}$  including the diagonal entries. This is why in the above procedure after adding the contribution of  $k_{18}$  we did not start from  $k_{21}$ . The complete process for all finite elements corresponds to the summation of stiffness values in (6.87), where we start with a global stiffness matrix containing only zero entries and successively add the element stiffness matrices. If a degree of freedom is restrained to a zero value, a zero is placed in the corresponding position of  $\mathbf{LM}$  for each element, and the stiffness contribution is not added to the stiffness matrix. In other words, we are only constructing the stiffness matrix corresponding to the unknown degrees of freedom ( $\mathbf{K}_{aa}$  in (2.57)).

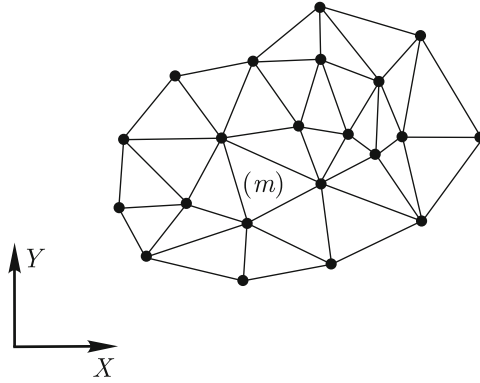
We used the rectangular element to introduce the basic ideas of the finite element procedure for 2-D analysis. The formulation of other types of elements follows the same approach and rests on the definition of the interpolation functions. The evaluation of the stiffness matrix and load vectors follows the same steps as described for rectangular elements.

### Example 6.6

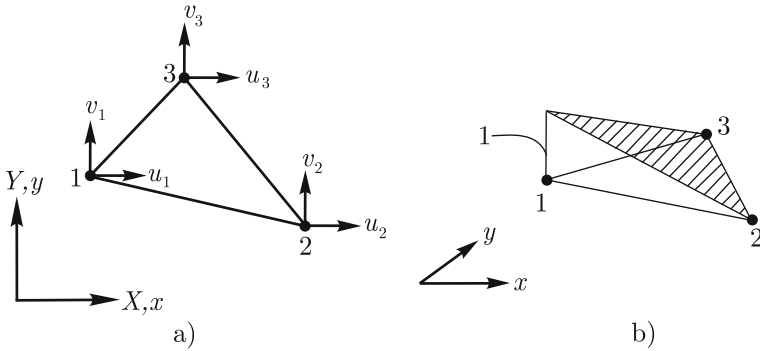
Consider the mesh of triangular elements shown in Figure 6.34. Define the interpolation functions for a generic element of the mesh. Indicate how to obtain the stiffness matrix of this element.

### Solution

The interpolation functions can be constructed obeying the same property used in the formulation of the rectangular elements, *i.e.*, the interpolation functions  $h_i$  assumes the value of one at node  $i$  and zero at node  $j$ ,  $j \neq i$ .



**Fig. 6.34.** Mesh of three-node triangular elements



**Fig. 6.35.** a) Generic three-node triangular element; b) Interpolation function  $h_1$  geometrically defined

Therefore, using the property that three non-colinear points determine a unique plane, we construct the interpolation functions. For instance,  $h_1$  is given by the unique plane which passes through the point that has out-of-plane value of one at the coordinates of node 1 and through nodes 2 and 3. This is pictorially shown in Figure 6.35b. The analytical expression of  $h_1$  is

$$h_1(x, y) = \frac{1}{2A_t} (a_1 + b_1x + c_1y) \tag{6.100}$$

where  $A_t$  is the area of the triangular element which can be calculated by

$$2A_t = x_1y_2 + x_2y_3 + x_3y_1 - y_1x_2 - y_2x_3 - y_3x_1$$

where  $(x_1, y_1)$ ,  $(x_2, y_2)$  and  $(x_3, y_3)$  are the coordinates of nodes 1, 2 and 3 respectively. The remaining constants are

$$a_1 = x_2y_3 - x_3y_2$$

$$b_1 = y_2 - y_3$$

$$c_1 = x_3 - x_2.$$

It is immediate to verify that equation (6.100) is, in fact, the analytical form of the interpolation function sought since, by substitution,

$$h_1(x_1, y_1) = 1, \quad h_1(x_2, y_2) = 0, \quad h_1(x_3, y_3) = 0$$

and since the functional form of  $h_1(x, y)$  corresponds to a plane, all requirements are satisfied. Analogously,

$$h_2(x, y) = \frac{1}{2A_t} (a_2 + b_2x + c_2y)$$

and

$$h_3(x, y) = \frac{1}{2A_t} (a_3 + b_3x + c_3y)$$

with

$$a_2 = x_3y_1 - x_1y_3, \quad a_3 = x_1y_2 - x_2y_1$$

$$b_2 = y_3 - y_1, \quad b_3 = y_1 - y_2$$

$$c_2 = x_1 - x_3, \quad c_3 = x_2 - x_1.$$

Having the interpolation functions defined, we can evaluate the matrices  $\mathbf{H}$ ,  $\mathbf{B}$  and  $\mathbf{k}^{(m)}$ . We note that from the functional form of the interpolation functions  $h_i(x, y)$ , the strains  $\varepsilon_{xx}$ ,  $\varepsilon_{yy}$  and  $\gamma_{xy}$ , and consequently the stresses  $\tau_{xx}$ ,  $\tau_{yy}$  and  $\tau_{xy}$  are constant over the element. This element is usually referred to as the constant strain triangle. □

### 6.3.2 Equilibrium properties of the finite element solutions for 2-D

As discussed for the 1-D finite element formulation, when we introduce the finite element formulation assumptions into the principle of virtual work statement expressed only in terms of displacements, we are satisfying exactly compatibility and the stress-strain law. However, equilibrium is satisfied only in an approximate manner. We also showed that there are two equilibrium properties that are satisfied for any finite element discretization, no matter how coarse the mesh might be (see also Bathe, 1996). Namely:

1. *Nodal equilibrium.* The external applied nodal forces are equilibrated by the element nodal point forces.

2. *Element equilibrium.* The element nodal point forces are always in equilibrium for any given element.

These same properties can be generalized for the 2-D finite element discretization.

We define the element nodal point forces for a generic element ( $m$ ) by

$$\mathbf{F}^{(m)} = \int_{A^{(m)}} \mathbf{B}^{(m)T} \boldsymbol{\tau}^{(m)} dA^{(m)} = \mathbf{K}^{(m)} \mathbf{U} \tag{6.101}$$

where  $\mathbf{U}$  is the finite element nodal displacement solution<sup>3</sup>. Hence, these nodal point forces give the forces acting onto the element at the element nodal points.

To show Property 1, part of a generic mesh of triangular elements (actually, the results that are demonstrated do not depend on the mesh being of triangular elements) and the nodal point forces of each element are shown in Figure 6.36.

For every node, the element nodal forces are in equilibrium with the externally applied nodal forces. In fact

$$\sum_{m=1}^{n_e} \mathbf{F}^{(m)} = \sum_{m=1}^{n_e} \mathbf{K}^{(m)} \mathbf{U} = \mathbf{K} \mathbf{U} = \mathbf{R}.$$

In Figure 6.36 we give a pictorial representation of this property for node  $k$ .

To illustrate Property 2 consider the nodal point forces of a generic element ( $m$ ) as shown in Figure 6.37 which are given by

$$\mathbf{F}^{(m)T} = \{0 \cdots \overset{e}{F_e} \cdots \overset{f}{F_f} \cdots \overset{g}{F_g} \cdots \overset{h}{F_h} \cdots \\ \overset{k}{F_k} \cdots \overset{\ell}{F_\ell} \cdots 0\}$$

where only the non-zero entries are shown and consider a vector of nodal displacements corresponding to a rigid translation of intensity  $\Delta$  in the  $x$  direction, *i.e.*,

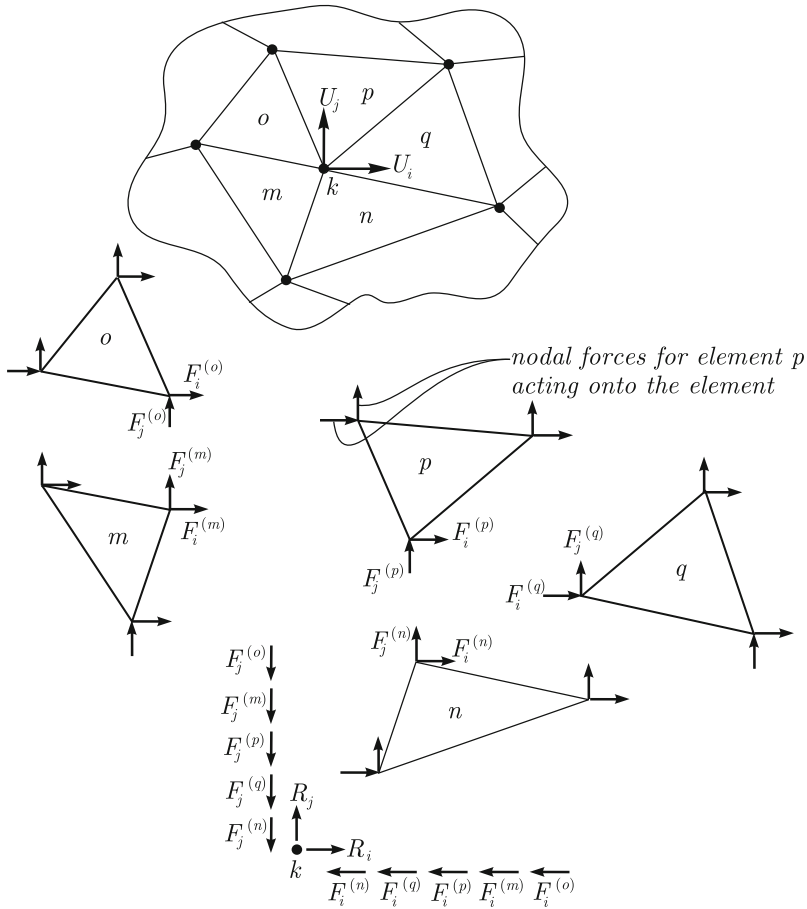
$$\bar{\mathbf{U}}^T = \{0 \cdots \overset{e}{\Delta} \cdots \overset{g}{\Delta} \cdots \overset{k}{\Delta} \cdots 0\}.$$

We can write

$$\bar{\mathbf{U}}^T \mathbf{F}^{(m)} = \Delta.F_e + \Delta.F_g + \Delta.F_k \tag{6.102}$$

and using the definition of  $\mathbf{F}^{(m)}$  given in (6.101), we obtain

<sup>3</sup> The equations in this section are presented for the plane strain model of unit thickness. For the plane stress and axisymmetric models the integrations would have to be performed accordingly (see Sections 5.2.2 and 5.2.4)



**Fig. 6.36.** Nodal forces for some elements in a mesh

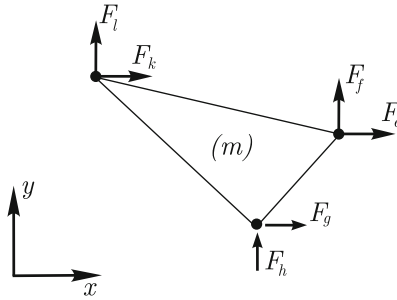
$$\begin{aligned}
 \bar{\mathbf{U}}^T \mathbf{F}^{(m)} &= \bar{\mathbf{U}}^T \mathbf{K}^{(m)} \mathbf{U} \\
 &= \bar{\mathbf{U}}^T \int_{A^{(m)}} \mathbf{B}^{(m)T} \mathbf{C} \mathbf{B}^{(m)} dA^{(m)} \mathbf{U} \\
 &= \int_{A^{(m)}} \bar{\mathbf{U}}^T \mathbf{B}^{(m)T} \mathbf{C} \mathbf{B}^{(m)} dA^{(m)} \mathbf{U}
 \end{aligned}$$

Note that

$$\bar{\mathbf{U}}^T \mathbf{B}^{(m)T} = \bar{\boldsymbol{\epsilon}}^{(m)T}$$

are the strains associated with the displacements  $\bar{\mathbf{u}}^{(m)} = \mathbf{H}^{(m)} \bar{\mathbf{U}}$ . As mentioned already, it is a fundamental requirement that the element displacement interpolations must contain the rigid body mode displacements (see Bathe, 1996). Since, of course, this element represents exactly rigid body





**Fig. 6.37.** Nodal forces for a generic element  $(m)$ .

modes – that is, for nodal displacements corresponding to a rigid body mode, the interpolated displacements inside the element correspond to the same rigid body mode – we have  $\bar{\varepsilon}^{(m)} = 0$ . Therefore

$$\bar{\mathbf{U}}^T \mathbf{F}^{(m)} = 0. \quad (6.103)$$

Then, from equations (6.102) and (6.103), we obtain

$$F_e + F_g + F_k = 0$$

which is the equilibrium condition in the  $x$  direction. Following an analogous derivation, considering a rigid translation in the  $y$  direction, we arrive at the equilibrium condition in the  $y$  direction, *i.e.*,

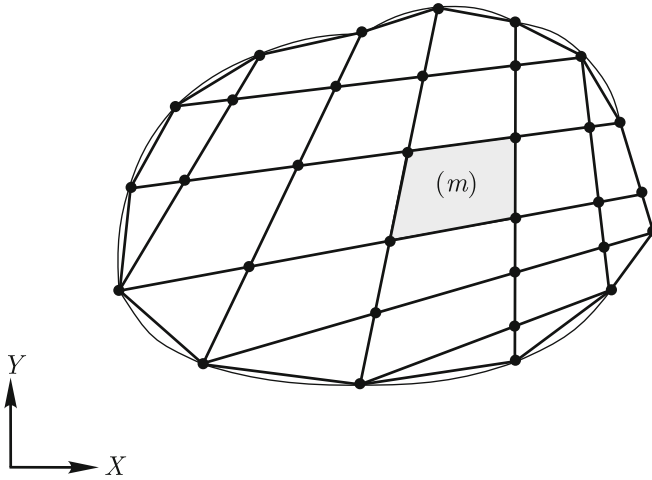
$$F_f + F_h + F_l = 0.$$

Finally, if we consider a rigid body rotation we arrive at the moment equilibrium condition for the element  $(m)$  nodal forces.

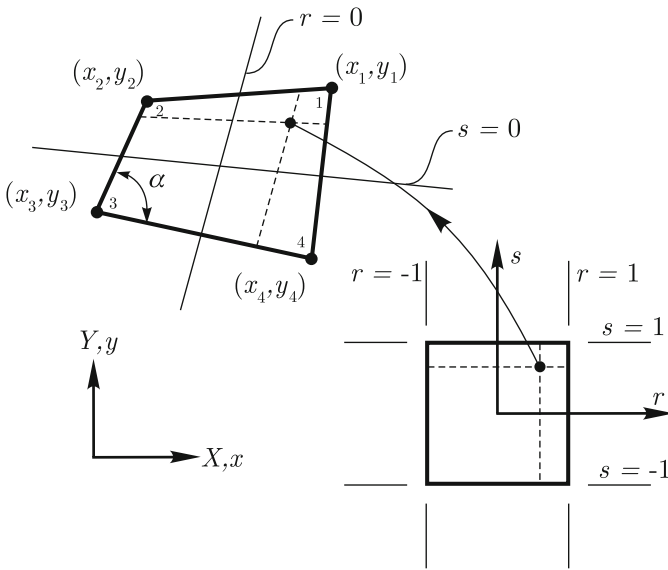
### 6.3.3 Isoparametric finite elements

In engineering practice we need to discretize, in general, very complex geometric domains requiring general quadrilateral and triangular elements. The isoparametric element concept provides a very powerful methodology to construct such general elements. In particular, also elements with more than 3 or 4 nodes can be constructed allowing curved element sides.

Consider the finite element mesh shown in Figure 6.38 in which we have 4-node quadrilateral and 3-node triangular elements. In order to introduce the concept of isoparametric element formulations consider the generic quadrilateral element  $(m)$  shown in Figure 6.38. To formulate the element matrices, we have to define the interpolation of the displacements inside the element from its nodal point displacements. For this purpose we now use an auxiliary reference domain of coordinates  $r$  and  $s$  as shown in Figure 6.39.



**Fig. 6.38.** Mesh with quadrilateral and triangular elements



**Fig. 6.39.** Schematic representation of the domain and the mapping; interior angle  $\alpha < 180^\circ$

The mapping we use, which relates every point  $(r, s)$  of the reference domain to a point  $(x, y)$  in the physical element domain, is

$$x(r, s) = \sum_{i=1}^4 h_i(r, s) x_i \tag{6.104}$$

$$y(r, s) = \sum_{i=1}^4 h_i(r, s) y_i \quad (6.105)$$

where the  $(x_i, y_i)$  are the nodal point coordinates of element ( $m$ ), see Figure 6.39. We assume that this mapping is defined uniquely for every  $(r, s)$  and  $(x, y)$  and hence invertible at all points. This requires that all interior angles  $\alpha$ , see Figure 6.39, be smaller than  $180^\circ$ , see Bathe, 1996. The interpolation functions  $h_i(r, s)$  are given by

$$\begin{aligned} h_1 &= \frac{1}{4}(1+r)(1+s) \\ h_2 &= \frac{1}{4}(1-r)(1+s) \\ h_3 &= \frac{1}{4}(1-r)(1-s) \\ h_4 &= \frac{1}{4}(1+r)(1-s) \end{aligned} \quad (6.106)$$

Of course, these functions are the interpolation functions of a 2 by 2 square element, defined in the local coordinates  $r$  and  $s$ . A straight line given in the reference domain by a constant  $r$  is mapped to a straight line in the element physical domain, and the same holds for a straight line given by a constant  $s$ . Therefore, the sides of the reference domain are mapped to the sides of the actual physical element and the vertices of the reference domain are mapped to the element nodes.

In Figure 6.40 we show the element nodal point displacements following the local node numbering. The element displacement interpolation can now be defined by

$$u(r, s) = \sum_{i=1}^4 h_i(r, s) u_i \quad (6.107)$$

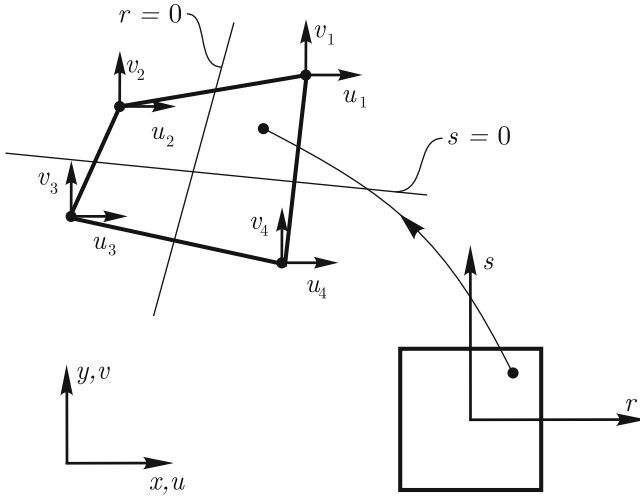
and

$$v(r, s) = \sum_{i=1}^4 h_i(r, s) v_i. \quad (6.108)$$

The term “isoparametric” refers to the fact that the same interpolations are used for the geometry and for the displacements.

Note that, since the  $h_i$  are defined as functions of  $r$  and  $s$ , the displacements  $(u, v)$  for an interior point of the element in the directions of  $x$  and  $y$ , respectively, are given in terms of  $r$  and  $s$  by equations (6.107) and (6.108). However, considering that the mapping defined in (6.104) and (6.105) is invertible, we can write

$$r = r(x, y) \quad (6.109)$$



**Fig. 6.40.** Nodal displacements of element in local numbering

$$s = s(x, y). \tag{6.110}$$

Hence, given  $(x, y)$  in the physical element, (6.109) and (6.110) give the corresponding  $(r, s)$  in the reference domain. Therefore, using equations (6.109) and (6.110), we can re-write (6.107) and (6.108) as

$$\begin{aligned} u(r(x, y), s(x, y)) &= \sum_{i=1}^4 h_i(r(x, y), s(x, y)) u_i \\ &= \sum_{i=1}^4 \tilde{h}_i(x, y) u_i \end{aligned} \tag{6.111}$$

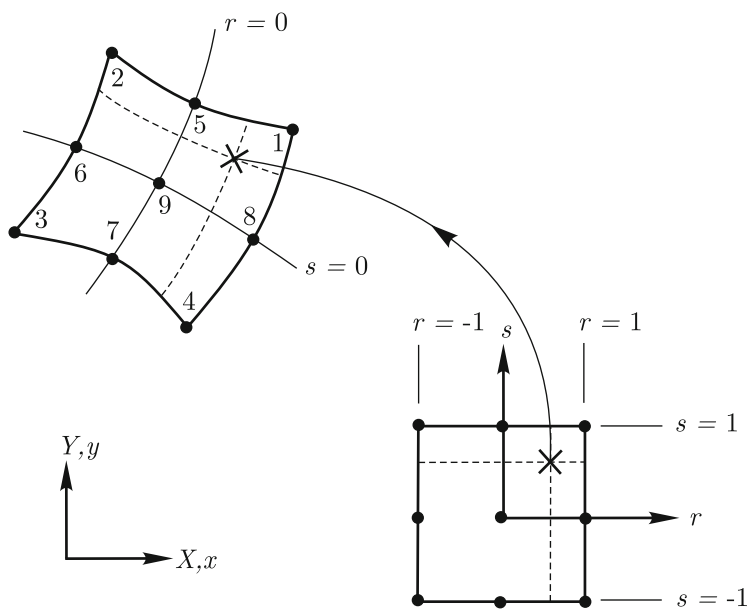
$$\begin{aligned} v(r(x, y), s(x, y)) &= \sum_{i=1}^4 h_i(r(x, y), s(x, y)) v_i \\ &= \sum_{i=1}^4 \tilde{h}_i(x, y) v_i. \end{aligned} \tag{6.112}$$

Hence, the displacement interpolation is well defined which allows the evaluation of  $\mathbf{H}$ ,  $\mathbf{B}$  and  $\mathbf{k}^{(m)}$ . In practice, the inversion used in equations (6.109) and (6.110) is not explicitly performed, because the evaluation of the matrices  $\mathbf{H}$ ,  $\mathbf{B}$  and  $\mathbf{k}^{(m)}$  do not require such an inversion. However, it is important to realize that in theory, such an inversion must be possible. The Jacobian  $\mathbf{J}$  of the isoparametric mapping defined in equations (6.104) and (6.105) is given by

$$\mathbf{J} = \begin{bmatrix} \frac{\partial x}{\partial r} & \frac{\partial y}{\partial r} \\ \frac{\partial x}{\partial s} & \frac{\partial y}{\partial s} \end{bmatrix} \quad (6.113)$$

with  $dxdy = \det\mathbf{J} drds$ , see Bathe, 1996. Hence the condition for uniqueness between  $(x, y)$  and  $(r, s)$  and a proper formulation is that  $\det\mathbf{J} > 0$  for  $-1 \leq r \leq 1$ , and  $-1 \leq s \leq 1$ . Hence, when constructing the mesh, the nodal points should be placed in such way that  $\det\mathbf{J} > 0$ . This is achieved when all interior angles are smaller than 180 degrees, see Figure 6.39.

The procedures given above are directly applicable to higher-order elements. Figure 6.41 shows a generic 9-node element, which is much used in practice. The interpolation function  $h_i$  should be 1 at  $(x_i, y_i)$  and zero at every other node. Of course, the interpolation functions will now involve quadratic monomials. Then, the mapping is given by



**Fig. 6.41.** Generic 9-node element and associated mapping

$$x = \sum_{i=1}^9 h_i(r, s) x_i \quad (6.114)$$

$$y = \sum_{i=1}^9 h_i(r, s) y_i \quad (6.115)$$

and the interpolation of the displacement is given by

$$u = \sum_{i=1}^9 h_i(r, s) u_i \quad (6.116)$$

$$v = \sum_{i=1}^9 h_i(r, s) v_i. \quad (6.117)$$

The objective of our discussion on isoparametric finite elements was only to present basic equations of this class of elements which are used in virtually all general purpose finite programs due to their versatility and good approximation properties. Of course, there are many details regarding these element formulations and we refer to Bathe, 1996 for a more complete discussion on isoparametric finite elements.

### 6.3.4 Numerical integration

In order to complete our presentation of finite element formulations, we want to briefly introduce the numerical integration procedures which are widely used to evaluate finite element matrices.

In finite element analysis, we are required to obtain the numerical value of

$$\int_V g(x, y, z) dV, \quad \int_S w(x, y) dS, \quad \int_L f(x) dL$$

where the real valued functions  $g(x, y, z)$ ,  $w(x, y)$  and  $f(x)$  are known. Since the integral over 2-D and 3-D domains can be obtained as successive integrations in 1-D, we want a procedure to evaluate

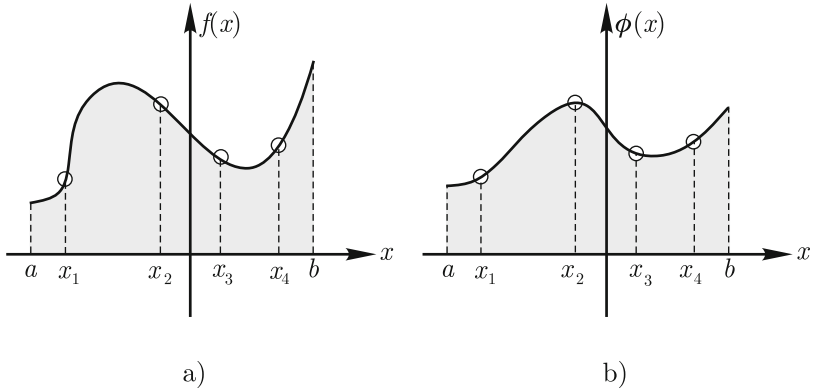
$$\int_a^b f(x) dx \quad \text{for } f(x) \text{ known.}$$

Since  $f(x)$  may be a complicated function, which is problem dependent, it is not effective and general (and may not be possible) to perform an analytical integration. Instead, we integrate a function  $\phi(x)$  for which  $\phi(x_i) = f(x_i)$  at selected points  $x_i$  of the function domain – sampling points – and take

$$\int_a^b f(x) dx \doteq \int_a^b \phi(x) dx.$$

Of course, the evaluation of the integral of  $\phi(x)$  should be systematic, computationally effective and, if sufficient points  $x_i$  are used, should lead to an accurate approximation of the integral of  $f(x)$ .

Consider the function  $f(x)$  shown in Figure 6.42a and the selected points  $x_i$ ,  $i = 1, \dots, 4$ . In Figure 6.42b we show  $\phi(x)$  which is defined as the polynomial function for which  $\phi(x_i) = f(x_i)$ ,  $i = 1, \dots, 4$ . The integral of  $\phi(x)$



**Fig. 6.42.** a) Function  $f(x)$  to be integrated and sampling points; b) Polynomial function that assumes the values of  $f(x)$  at given points

which is given by the shaded area in Figure 6.42b is an approximation of the integral of  $f(x)$  given by the shaded area in Figure 6.42a.

There are two main integration schemes used in finite element analysis. In the Newton-Cotes integration scheme the evaluation points are defined by subdividing the domain into equal parts and also include the end points. In this case, if  $f(x)$  is a polynomial of order  $n$ , we need  $n + 1$  points to exactly integrate  $f(x)$ , since the unique polynomial  $\phi(x)$  of order  $n$  passes through the  $n + 1$  points and  $\phi(x) \equiv f(x)$ . On the other hand, in the Gauss integration scheme, specific locations of the evaluation points are used in order to maximize the precision of the numerical integration procedure and these do not include the end points. As shown in Bathe, 1996, using the Gauss scheme only  $n$  points are required to integrate exactly a polynomial function of order  $2n - 1$ .

Let us consider, without loss of generality, our domain of integration to be  $[-1, 1]$ . We can write

$$\int_{-1}^{+1} f(r)dr \doteq \int_{-1}^{+1} \phi(r)dr$$

where  $\phi(r)$  is the polynomial function which assumes the values of  $f(r)$  at the  $n$  sampling points, *i.e.*,  $\phi(r_i) = f(r_i)$   $i = 1, 2, \dots, n$ . It can be shown that

$$\int_{-1}^{+1} \phi(r)dr = \sum_{i=1}^n \alpha_i f(r_i)$$

where  $\alpha_i, r_i, i = 1, \dots, n$  are available for a given numerical integration order. The  $\alpha_i$  are called the weights,  $r_i$  the sampling points and  $n$  the integration order. In Table 6.3 we show these data for Gauss integration up to order 3.

The procedures used in 1-D integrations can directly be applied in 2-D and 3-D integrations. Consider the two 2-D domains shown in Figure 6.43

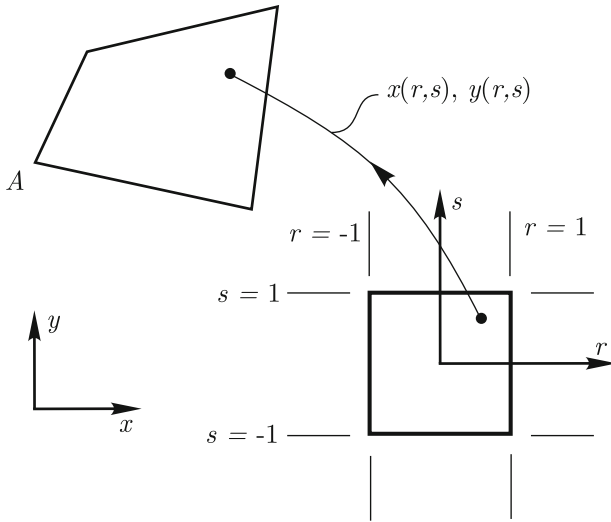
**Table 6.3.** Coordinates and weights for the Gauss points in one-dimension

Integration order	Gauss sampling points ( $r$ coordinate)	Weights
1	0.0000000000000000	2.0000000000000000
2	$\pm 0.577350269189626$	1.0000000000000000
3	$\pm 0.774596669241483$ 0.0000000000000000	0.5555555555555556 0.8888888888888889

which are related by the mapping  $x(r, s), y(r, s)$ . Let  $f(x, y)$  be a function defined in the domain  $A$ . We have

$$\int_A f(x, y) dx dy = \int_{-1}^{+1} \int_{-1}^{+1} f(x(r, s), y(r, s)) \det \mathbf{J} dr ds \tag{6.118}$$

where  $\mathbf{J}$  is the Jacobian of the mapping. For example, the stiffness matrix of



**Fig. 6.43.** Two-dimensional domains related by the isoparametric mapping

a 2-D isoparametric element is, for a unit thickness,

$$\mathbf{k} = \int_{-1}^{+1} \int_{-1}^{+1} \mathbf{B}^T \mathbf{C} \mathbf{B} \det \mathbf{J} dr ds \tag{6.119}$$

where, for a 4-node element,  $x(r, s)$  and  $y(r, s)$  are given by (6.107) and (6.108). Here each entry  $k_{ij}$  is of the form (6.118).

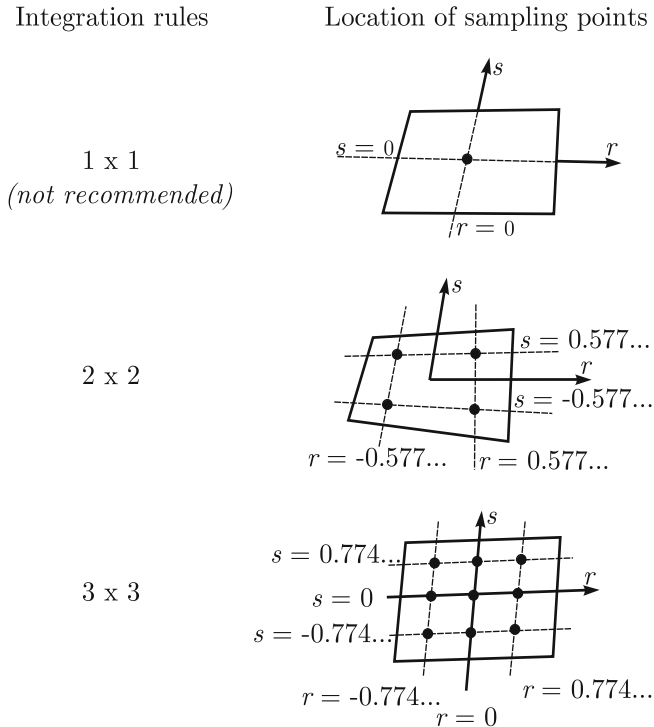


The rule of numerical integration is given by

$$\int_{-1}^{+1} \int_{-1}^{+1} g(r, s) dr ds \cong \sum_{i=1}^{n_{intr}} \sum_{j=1}^{n_{ints}} \alpha_i \alpha_j g(r_i, s_j) \tag{6.120}$$

where  $g(r, s) = f(x(r, s), y(r, s)) \det \mathbf{J}$ . In (6.120)  $n_{intr}$  and  $n_{ints}$  represent the number of integration points in the  $r$  and  $s$  directions, respectively,  $\alpha_i$  and  $\alpha_j$  are the weights and  $r_i$  and  $s_j$  the sampling points, each corresponding to one-dimensional integration, see Table 6.3. In Figure 6.44 we show the locations of the sampling points of the most common integration rules used for 2-D isoparametric elements.

An important question is “What order of numerical integration should be used for a specific element?” This question and other considerations are discussed in Bathe, 1996.

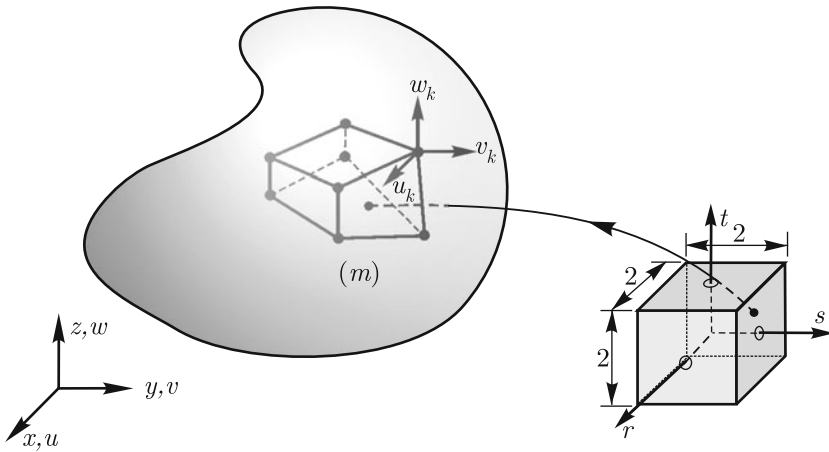


**Fig. 6.44.** Location of the sampling points for quadrilateral elements

### 6.3.5 Displacement-based finite element formulations for 3-D solids

The starting point is the principle of virtual work for 3-D elasticity written in terms of displacements given in (6.67).

We need to define the displacement interpolations. In Figure 6.45, we show a typical 3-D element inside the solid being discretized. Our task is to define  $u^{(m)}$ ,  $v^{(m)}$  and  $w^{(m)}$ , *i.e.*, the displacements for element ( $m$ ) from those at the nodes. A typical node  $k$  and its nodal degrees of freedom are also shown in Figure 6.45. A convenient way to define the interpolation is to use the isoparametric formulation. In the 3-D case the reference domain is a cube (see Figure 6.45).



**Fig. 6.45.** A generic 3-D element

The isoparametric mapping can be defined by

$$x = \sum_{i=1}^q h_i x_i, \quad y = \sum_{i=1}^q h_i y_i, \quad z = \sum_{i=1}^q h_i z_i$$

where the  $x_i$ ,  $y_i$ ,  $z_i$  are the element nodal coordinates and the  $h_i(r, s, t)$  are the interpolation functions defined in the reference domain as for the 2-D case. The number of nodes, which is 8 for the element shown in Figure 6.45, is generically given by  $q$ . The displacement interpolations are given by

$$u = \sum_{i=1}^q h_i u_i, \quad v = \sum_{i=1}^q h_i v_i, \quad w = \sum_{i=1}^q h_i w_i$$

where  $u_i$ ,  $v_i$ ,  $w_i$  are the nodal displacements of node  $i$ . Therefore

$$\mathbf{H} = \left[ \begin{array}{ccc|ccc|ccc} h_1 & 0 & 0 & \cdots & h_i & 0 & 0 & \cdots & h_q & 0 & 0 \\ 0 & h_1 & 0 & \cdots & 0 & h_i & 0 & \cdots & 0 & h_q & 0 \\ 0 & 0 & h_1 & \cdots & 0 & 0 & h_i & \cdots & 0 & 0 & h_q \end{array} \right].$$

Of course, when  $\mathbf{H}$  is defined we can evaluate  $\mathbf{B}$  and  $\mathbf{k}^{(m)}$  (see equations (6.122) and (6.123) below). The interpolation functions are given, for example, in Bathe, 1996.

### 6.3.6 Framework to formulate displacement-based finite elements

In Chapter 5 we presented a generalized form of the principle of virtual work which is applicable to the mathematical models of Chapter 4 and to the 3-D elasticity model presented in Chapter 3. Finite element formulations can then be obtained defining finite element interpolations for the kinematic variables. In fact, to arrive at a specific element formulation we would define the nodal points and the displacement interpolation, that is,

$$\mathbf{u} = \mathbf{H}\hat{\mathbf{u}} \quad (6.121)$$

where  $\mathbf{u}$  is the generalized displacement column matrix (see Section 4.5) and  $\hat{\mathbf{u}}$  is the specific element nodal displacement column matrix. The generalized strain is given by

$$\varepsilon = \partial_\varepsilon \mathbf{u} = \partial_\varepsilon \mathbf{H}\hat{\mathbf{u}} = \mathbf{B}\hat{\mathbf{u}}. \quad (6.122)$$

Then, the element stiffness matrix can be obtained by

$$\mathbf{k}^{(m)} = \int_V \mathbf{B}^T \mathbf{C} \mathbf{B} \, dV. \quad (6.123)$$

In the above expression  $\mathbf{C}$  is the generalized constitutive matrix. We presented above the definitions of the matrices  $\mathbf{H}$ ,  $\mathbf{B}$  and  $\mathbf{k}^{(m)}$  at the element level. Of course, it is implied that  $\mathbf{H}^{(m)}$ ,  $\mathbf{B}^{(m)}$  can be defined and the finite element equations would then be established, in principle, as above (see Section 6.3.1).

## 6.4 Finite elements for beams, plates and shells

In this section we will discuss finite elements which together with those for 2-D and 3-D solids can be used to undertake comprehensive modeling of engineering structures. Of course, the mathematical models of Chapter 4 are the basis for the formulations to be presented.

In Section 6.3.6, we presented a framework to formulate displacement-based finite elements which is applicable to all mathematical models discussed in this book. However, we will not detail the finite element formulation for all these models. Instead, we concentrate on fewer models which capture the relevant structural behaviors rendering the associated finite elements widely applicable and very attractive for engineering structural analysis.

In Section 6.4.1, we present the Bernoulli-Euler beam finite element, in Section 6.4.2 we compare the finite element and matrix structural analysis formulations in the modeling of frame structures, in Section 6.4.3 we briefly introduce plate and shell finite elements, and in Section 6.4.4 we present more general beam elements.

### 6.4.1 Bernoulli-Euler beam finite element

Let us consider first the Bernoulli-Euler model for transverse loading only as detailed in Section 4.2.2.

Following the framework of Section 6.3.6, we recall that

$$\begin{aligned}\boldsymbol{\tau} &= [M(x)], \quad \boldsymbol{\varepsilon} = [\kappa(x)], \quad \mathbf{C} = [EI], \\ \mathbf{u} &= [w(x)], \quad \partial_\varepsilon = \left[ \frac{d^2}{dx^2} \right].\end{aligned}$$

We note that we need to interpolate the transverse displacement  $w(x)$ . The curvature (the generalized strain)

$$\kappa = \frac{d^2 w}{dx^2}$$

involves the second derivative of  $w(x)$ . So far, we detailed finite element formulations for which the strains involved only the first derivatives of the displacement functions.

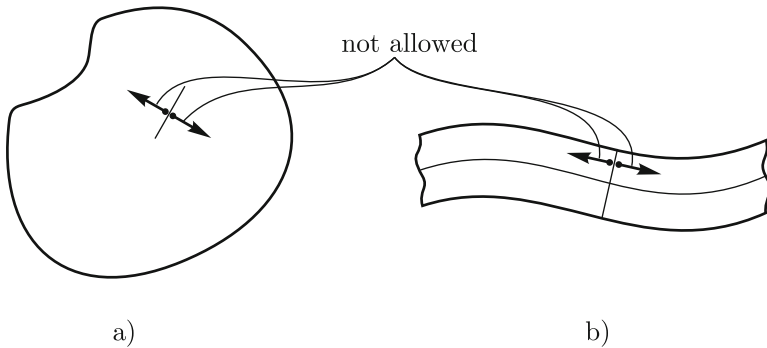
As discussed in Section 6.2, for the principle of virtual work formulation to be well defined both the displacement solution and the virtual displacement should belong to a given space of functions  $V$ . This space should be such that the strain energy is finite for every displacement function in  $V$ . We recall that the strain energy for the Bernoulli-Euler beam model is given by

$$a(w, w) = \frac{1}{2} \int_0^L \boldsymbol{\varepsilon}^T \mathbf{C} \boldsymbol{\varepsilon} \, dV = \frac{1}{2} \int_0^L \kappa EI \kappa \, dx = \frac{1}{2} \int_0^L EI \left( \frac{d^2 w}{dx^2} \right)^2 \, dx.$$

It can be shown that for  $w(x)$  and  $\frac{dw}{dx}(x)$  piecewise continuous the strain energy is finite. Hence, when we choose a finite element mesh, both  $w_h(x)$  and  $\frac{dw_h(x)}{dx}$  should be continuous at the element interfaces, *i.e.*, at the nodes. To have this property, we use the so-called Hermitian interpolation functions, which we have already used. In fact, we can refer to Table 4.1 where these interpolation functions are defined.

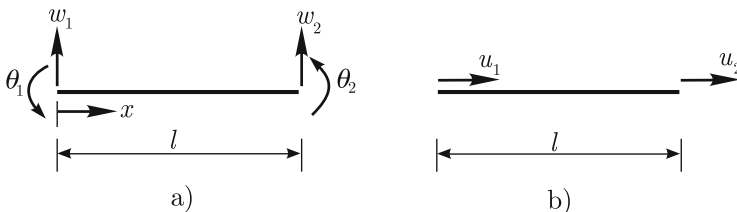
Elements for which continuity of the kinematic variables and of their first derivatives is satisfied are referred to as  $C^1$  elements since a  $C^1$  function is continuous with continuous first derivatives. The elements for which only the continuity of the kinematic variables is satisfied are referred to as  $C^0$  elements since a  $C^0$  function is continuous.

To obtain physical insight regarding these mathematical conditions, we note that for elastic solids the displacements should be continuous throughout the domain since the material particles should not separate from each other, that is, the solid should not “break”. This same restriction physically justifies why  $\frac{dw}{dx}$  should also be continuous. Namely, since  $\theta = \frac{dw}{dx}$  gives the beam section rotation, a discontinuity would lead to a section “breakage” (a hinge). Figure 6.46 summarizes these considerations.



**Fig. 6.46.** Requirements for kinematic variables

Let  $(m)$  be a generic element of length  $l$  as summarized in Figure 6.47a, in which the local coordinate system given by the  $x$  axis and the element nodal displacement and rotation degrees of freedom  $w_1, \theta_1 = \frac{dw}{dx}|_{x=0}, w_2, \theta_2 = \frac{dw}{dx}|_{x=l}$  are shown. Then, we can write



**Fig. 6.47.** a) Two-node beam element; b) Axial degrees of freedom for two-node beam element

$$w_h(x) = h_2(x)w_1 + h_5(x)w_2 + h_3(x)\theta_1 + h_6(x)\theta_2$$

where the interpolation functions are those given in Table 4.1 when we take  $L = l$ . Continuity of the derivatives is assured as long as we take the same nodal rotation degrees of freedom at element interfaces. The matrix  $\mathbf{B}$  is implicitly given by

$$\boldsymbol{\kappa} = \mathbf{B}\mathbf{u} = \begin{bmatrix} \frac{d^2 h_2}{dx^2} & \frac{d^2 h_3}{dx^2} & \frac{d^2 h_5}{dx^2} & \frac{d^2 h_6}{dx^2} \end{bmatrix} \begin{bmatrix} w_1 \\ \theta_1 \\ w_2 \\ \theta_2 \end{bmatrix}$$

and the stiffness matrix is given by

$$\mathbf{k} = \int_0^l \mathbf{B}^T E I \mathbf{B} \, dx = \begin{bmatrix} \frac{12EI}{l^3} & \frac{6EI}{l^2} & -\frac{12EI}{l^3} & \frac{6EI}{l^2} \\ \frac{6EI}{l^2} & \frac{4EI}{l} & -\frac{6EI}{l^2} & \frac{2EI}{l} \\ -\frac{12EI}{l^3} & -\frac{6EI}{l^2} & \frac{12EI}{l^3} & -\frac{6EI}{l^2} \\ \frac{6EI}{l^2} & \frac{2EI}{l} & -\frac{6EI}{l^2} & \frac{4EI}{l} \end{bmatrix}.$$

Note that we can also consider the axial deformation introducing the degrees of freedom shown in Figure 6.47b. The interpolation of the axial displacements is linear in each element as detailed before, and if we define

$$\mathbf{u}^T = \left[ u_1 \quad w_1 \quad \theta_1 \quad u_2 \quad w_2 \quad \theta_2 \right]$$

we obtain exactly the stiffness matrix associated with the matrix formulation of the Bernoulli-Euler beam theory given in (4.176).

### 6.4.2 Matrix and finite element structural analysis for frames

We would like to briefly comment on the similarities and differences between the matrix and the finite element formulation for bars.

We recall that the matrix formulation for a single bar gives the exact solution as long as the bar is subjected to end forces only. When deriving the matrix formulation for an assemblage of bars, equilibrium and compatibility were enforced at every node and, therefore, the exact solution is also obtained as long as the loads are applied to the nodes. When there are distributed forces along the members, we can still obtain the exact solution if we use superposition of effects as detailed in Section 4.2.4.

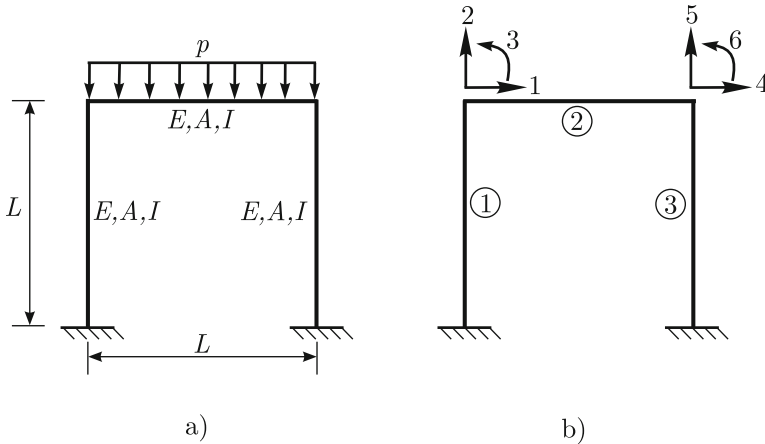
We note that the finite element formulation for the Bernoulli-Euler beam detailed in the previous section gives the exact solution of the mathematical model whenever the loads are applied to the nodes. The reason is that the

interpolations used for the transverse displacements are those of the exact solution when there is no distributed loading applied to the bars, and, as discussed in Section 6.2, when the exact solution is contained in the finite element space, the finite element solution is the exact solution. Hence, of course, the same stiffness matrix is obtained for both formulations.

In the finite element formulation when there are distributed loads applied to the bars, they are transferred to the nodes as consistent nodal forces. Differential equilibrium is no longer satisfied since the interpolation functions correspond to the exact solution when there is no distributed loading. Therefore, in the finite element formulation we need to refine the mesh to improve the solution for such case or – of course – correct the internal element forces as in the matrix formulation.

**Example 6.7**

Consider the simple frame structure shown in Figure 6.48a. The problem is to be solved both by matrix and finite element analysis. Considering the definitions shown in 6.48b which apply for both formulations:



**Fig. 6.48.** Problem definition:  $p = 400 \text{ kN/m}$ ,  $L = 2 \text{ m}$ ,  $E = 20 \times 10^6 \text{ kN/m}^2$ ,  $A = 0.12 \text{ m}^2$ ,  $I = 36 \times 10^{-4} \text{ m}^4$

- (i) Calculate the load column matrix associated with the free degrees of freedom.
- (ii) Find the nodal displacements.
- (iii) Find the bending moment diagram for bar 2.
- (iv) Consider bar 2 discretized with 10 finite elements. Find the solution for the degrees of freedom of the original discretization. Show the bending moment diagram for the domain of bar 2.

**Solution**

(i) For the finite element analysis

$$\mathbf{R}_a = \mathbf{R}_{B,a}$$

and for this case  $\mathbf{R} = \mathbf{R}_B = \mathbf{R}_B^{(2)}$

$$\mathbf{R}_B^{(2)} = \int_0^L \mathbf{H}^{(2)T} (-p) dx = -p \int_0^L \mathbf{H}^{(2)T} dx.$$

Considering the free degrees of freedom

$$\mathbf{R}_a = -p \begin{bmatrix} 0 \\ \int_0^L h_2(x) dx \\ \int_0^L h_3(x) dx \\ 0 \\ \int_0^L h_5(x) dx \\ \int_0^L h_6(x) dx \end{bmatrix} = \begin{bmatrix} 0 \\ -\frac{pL}{2} \\ -\frac{pL^2}{12} \\ 0 \\ -\frac{pL}{2} \\ \frac{pL^2}{12} \end{bmatrix}. \tag{6.124}$$

For the matrix analysis, referring to Section 4.2.4, we need to evaluate  $\mathbf{R}_a - \mathbf{R}_{0,a}$ . Since there are no loads applied to the nodes  $\mathbf{R}_a = \mathbf{0}$ . Referring to Figure 4.45

$$\mathbf{f}_0^{(2)T} = \left[ 0 \quad \frac{pL}{2} \quad \frac{pL^2}{12} \quad 0 \quad \frac{pL}{2} \quad -\frac{pL^2}{12} \right]$$

and for this case

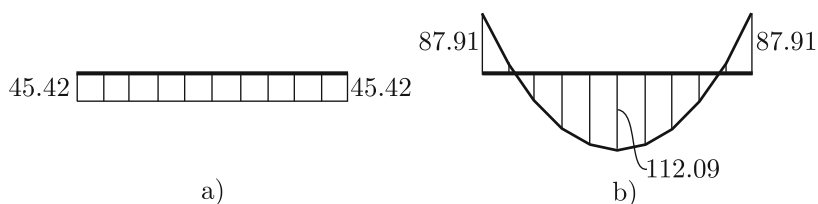
$$-\mathbf{R}_{0,a}^T = -\mathbf{f}_0^{(2)T} = \left[ 0 \quad -\frac{pL}{2} \quad -\frac{pL^2}{12} \quad 0 \quad -\frac{pL}{2} \quad \frac{pL^2}{12} \right]. \tag{6.125}$$

Hence, we obtained the same load column matrix for both approaches.

(ii) Since the load column matrix for the free degrees of freedom are the same for both formulations, the nodal displacements will also be the same. Solving the matrix equation we obtain the predictions for  $\mathbf{U}_a$  for both approaches

$$\mathbf{U}_a^T = \begin{bmatrix} 2.717 \times 10^{-5} & -3.333 \times 10^{-4} & -6.309 \times 10^{-4} \\ -2.717 \times 10^{-5} & -3.333 \times 10^{-4} & 6.309 \times 10^{-4} \end{bmatrix}.$$





**Fig. 6.49.** Moment diagram for bar 2. a) Finite element analysis; b) Matrix structural analysis (moments are given in kN.m)

(iii) In Figure 6.49 we show the moment diagram for bar 2 using the finite element approach and structural matrix analysis.

We note that the matrix structural analysis gives the exact moment distribution as detailed in Section 4.2.4. Since in the finite element solution the distributed load is lumped to the nodes, we do not obtain the exact moment distribution and the differential equilibrium along the bar is violated. We also note that the moment distribution is always linear in the finite element approach since the loads are lumped to the nodes.

We recall that in matrix structural analysis to obtain the exact nodal solution when part of the external loads is applied to the bars, we used the superposition as illustrated in Example 4.14. We can proceed in the same way in the finite element solution. We first clamp each bar, calculate the fixed-end forces and moments, apply the reverse to the structure free to move, and then superimpose the two solutions.

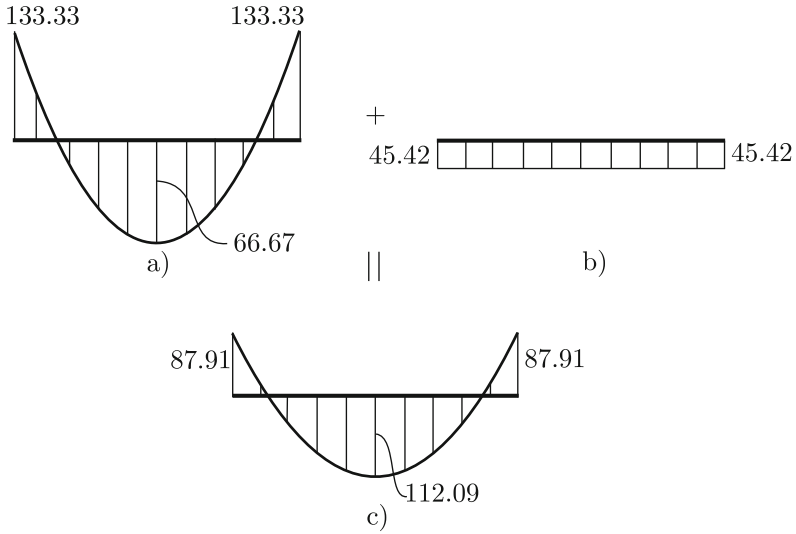
In the present analysis, we have for bar 2, the situation summarized in Figure 6.50.

(iv) In Figure 6.51 we show the bending moment diagram for the domain corresponding to bar 2 obtained with the finite element approach without any correction when the bar is discretized with 10 elements.

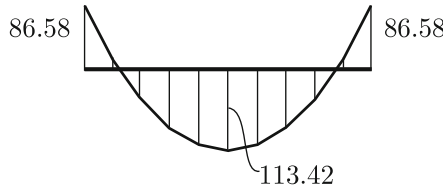
Here, despite the fact the moment diagram is linear in each element, we obtain a reasonable approximation of the moment distribution directly from the finite element solution without taking recourse to the superposition described above.

□

A very important observation is that there is no matrix analysis approach that leads to the exact solution for 2-D, 3-D solids, plates and shells. One reason is that for these models we can not solve the governing differential equations defined in an element domain for the nodal displacements since these are defined only at discrete locations, not representing the complete element boundary which is a line for 2-D, plate and shell models, and a surface for 3-D models.



**Fig. 6.50.** Superposition for bar 2. a) Solution for clamped bar at both ends; b) Finite element solution (moments are given in kN.m); c) Solution obtained by superposition



**Fig. 6.51.** Moment distribution for bar 2 (moments are given in kN.m)

### 6.4.3 Plate and shell finite elements

Referring to the brief description of the shell models presented in Section 4.4.2, a number of mathematical models could lead to shell finite element formulations. Setting as a requirement that we would like the elements to be *general*, *i.e.*, representing as many behaviors as possible, the choice is the *basic shell model*.

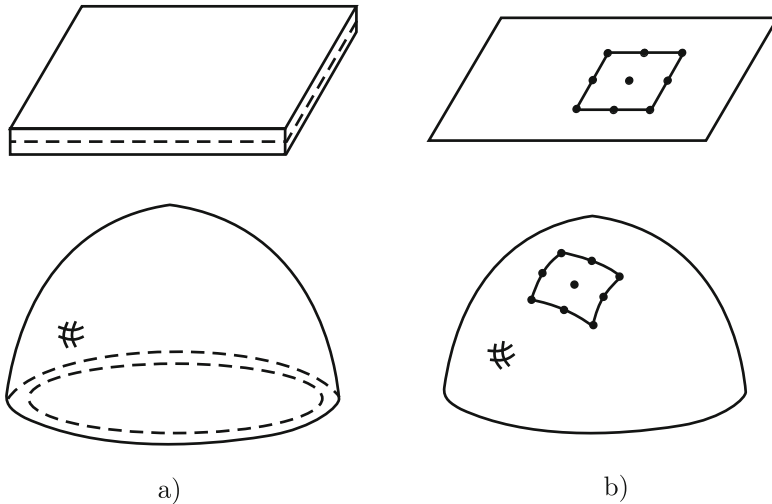
Due to the kinematic hypothesis, the basic shell model represents transverse shear deformations, therefore the model can be used to analyze moderately thick as well as thin shells. The fundamental idea of the shell finite element formulation is to introduce the kinematic and stress hypotheses of the basic shell model through the discretization process into a 3-D description of the shell. This discretization strategy involves the interpolation of the geometry and the displacements and leads to the so-called degenerated solid approach which was proposed by Ahmad, Irons and Zienkiewicz, 1970.

Later, Chapelle and Bathe, 2000 formulated the basic shell mathematical model whose discretization leads to the degenerated solid approach, see also Lee and Bathe, 2005.

We also note that when the midsurface of the shell is flat and the shell (plate) is subjected to transverse loading only, the degenerated solid approach corresponds to the displacement-based finite element formulation for the Reissner-Mindlin plate bending model.

When a flat shell (plate) is also subjected to in-plane loading, the solution can be obtained by superposition of the Reissner-Mindlin plate model and the plane stress model since, in this case, the in-plane and bending responses are decoupled. The degenerated solid approach implicitly models both, the in-plane and bending behaviors. In summary, the shell finite element formulation based on the basic shell model contains an effective plate bending element formulation and the plane stress element formulation as special cases.

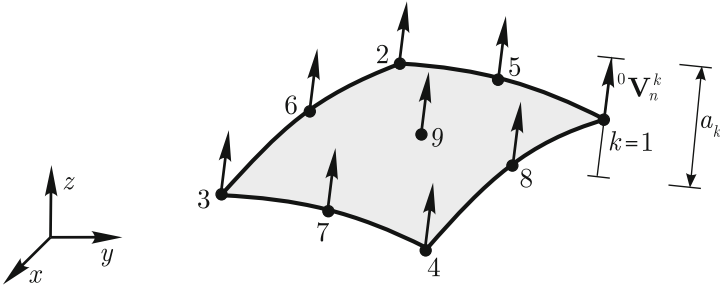
Consider typical plate and shell structures as shown in Figure 6.52a. In Figure 6.52b we show the plate and shell midsurfaces and typical elements defined on the midsurfaces. The shell element is also shown in Figure 6.53 where we define for any generic node  $k$  a unit vector  ${}^0\mathbf{V}_n^k$ , called director vector, and a shell thickness denoted by  $a_k$ .



**Fig. 6.52.** Generic representation of a shell, its midsurface and a shell finite element

We define the interpolation of the geometry corresponding to a generic element by

$${}^0\mathbf{x}(r, s, t) = \sum_{k=1}^q h_k(r, s) {}^0\mathbf{x}_k + \frac{t}{2} \sum_{k=1}^q a_k h_k(r, s) {}^0\mathbf{V}_n^k. \quad (6.126)$$



**Fig. 6.53.** Director vector and thickness definitions

Here we are using the isoparametric mapping and the interpolation functions  $h_k(r, s)$  are the usual two-dimensional interpolation functions of a  $q$ -node element. We can identify two terms in equation (6.126). The first term gives the interpolation of the midsurface, where  ${}^0\mathbf{x}_k$  represents the position vector of node  $k$  in the undeformed configuration. Of course, when the isoparametric coordinates  $r$  and  $s$  span the intervals  $-1 \leq r \leq 1$  and  $-1 \leq s \leq 1$ , the first term gives the position vector of all points on the interpolated shell element midsurface. The second term is needed to obtain the geometry interpolation for the points out of the midsurface. In fact, considering a fixed  $r, s$ , say  $r^*, s^*$ , the second term gives the points on a straight line which crosses the midsurface at the point defined by the first term when evaluated at  $r^*$  and  $s^*$ . For  $t = -1$  we have the point of this straight line located at the lower outer surface, point  $A$ , and when  $t = +1$  at the upper outer surface, *i.e.*, point  $B$ . In Figure 6.54 we summarize the definitions given above.

We note that the left superscript 0 which was used in expression (6.126) indicates that these quantities are referred to the undeformed configuration of the shell and, therefore, (6.126) gives the interpolation of the undeformed configuration.

Now, if we denote by  ${}^1\mathbf{x}_k, {}^1\mathbf{V}_k^n$  the analogous quantities for the deformed configuration, we can define this configuration for a generic element by

$${}^1\mathbf{x}(r, s, t) = \sum_{k=1}^q h_k(r, s) {}^1\mathbf{x}_k + \frac{t}{2} \sum_{k=1}^q a_k h_k(r, s) {}^1\mathbf{V}_n^k \tag{6.127}$$

which complies with the kinematic hypothesis of the basic shell model. Indeed, equations (6.126) and (6.127) synthesize what we meant by introducing the kinematic hypothesis of the basic shell model through the discretization process. The displacements can be written as

$$\mathbf{u} = {}^1\mathbf{x} - {}^0\mathbf{x} = \sum_{k=1}^q h_k(r, s) \mathbf{u}_k + \frac{t}{2} \sum_{k=1}^q a_k h_k(r, s) ({}^1\mathbf{V}_n^k - {}^0\mathbf{V}_n^k) \tag{6.128}$$

where  $\mathbf{u}_k$  are the nodal point displacements. The director vector  ${}^1\mathbf{V}_n^k$  is actually  ${}^0\mathbf{V}_n^k$  after a rigid rotation. Let us define an orthonormal coordinate

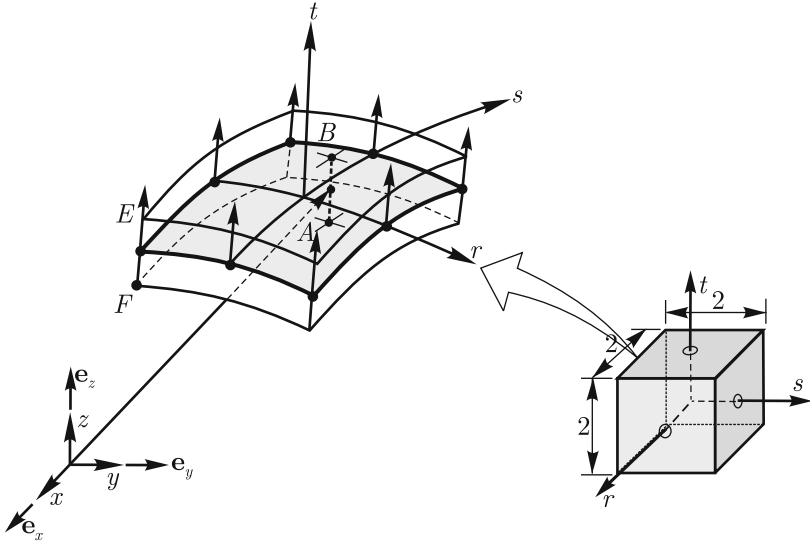


Fig. 6.54. Interpolation of shell geometry

system whose base vectors are  $(\mathbf{V}_1^k, \mathbf{V}_2^k, \mathbf{V}_n^k)$  as shown in Figure 6.55a which are characterized by

$${}^0\mathbf{V}_1^k = \frac{\mathbf{e}_y \times {}^0\mathbf{V}_n^k}{\|\mathbf{e}_y \times {}^0\mathbf{V}_n^k\|} \tag{6.129}$$

where  $\mathbf{e}_y$  is a unit vector in the direction of the  $y$  axis (when  ${}^0\mathbf{V}_n^k$  is parallel to  $\mathbf{e}_y$ , we can use  ${}^0\mathbf{V}_1^k = \mathbf{e}_z$ ), and

$${}^0\mathbf{V}_2^k = {}^0\mathbf{V}_n^k \times {}^0\mathbf{V}_1^k. \tag{6.130}$$

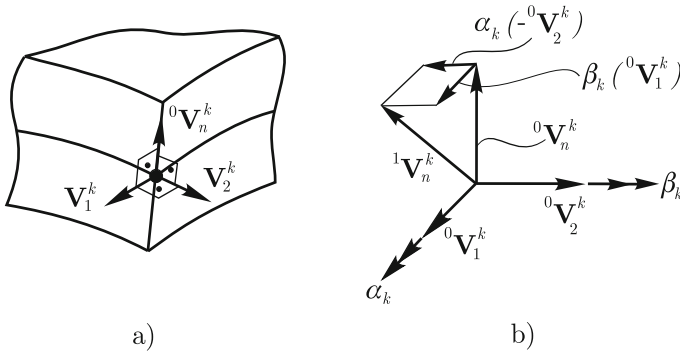
Of course, equations (6.129) and (6.130) are not the only possibility of defining an orthonormal basis for which  $\mathbf{V}_n^k$  is the third base vector. But, it is certainly a valid way. Since the rotation of  ${}^0\mathbf{V}_n^k$  is assumed to be infinitesimally small, we have

$${}^1\mathbf{V}_n^k - {}^0\mathbf{V}_n^k = \beta_k \mathbf{V}_1^k - \alpha_k \mathbf{V}_2^k \tag{6.131}$$

where  $\alpha_k$  and  $\beta_k$  are the rotation components as summarized in Figure 6.55b. Equation (6.128) can now be re-written using (6.131) as

$$\mathbf{u} = \sum_{k=1}^q h_k \mathbf{u}_k + \frac{t}{2} \sum_{k=1}^q a_k h_k (\beta_k \mathbf{V}_1^k - \alpha_k \mathbf{V}_2^k)$$

which implicitly defines the element displacement interpolation. The element nodal displacement column matrix is given by



**Fig. 6.55.** a) A local orthonormal basis; b) Kinematics for the director vector at node  $k$

$$\hat{\mathbf{u}}^T = \left[ u_1 \quad v_1 \quad w_1 \quad \alpha_1 \quad \beta_1 \quad \left| \cdots \cdots \cdots \right. \quad u_q \quad v_q \quad w_q \quad \alpha_q \quad \beta_q \right]$$

and therefore the interpolation matrix  $\mathbf{H}$  is

$$\mathbf{H} = \left[ \begin{array}{ccccc} h_1 & 0 & 0 & -\frac{t}{2}a_1h_1V_{2x}^1 & \frac{t}{2}a_1h_1V_{1x}^1 \\ 0 & h_1 & 0 & -\frac{t}{2}a_1h_1V_{2y}^1 & \frac{t}{2}a_1h_1V_{1y}^1 \\ 0 & 0 & h_1 & -\frac{t}{2}a_1h_1V_{2z}^1 & \frac{t}{2}a_1h_1V_{1z}^1 \end{array} \right] \cdots \cdots$$

$$\cdots \cdots \left[ \begin{array}{ccccc} h_q & 0 & 0 & -\frac{t}{2}a_qh_qV_{2x}^q & \frac{t}{2}a_qh_qV_{1x}^q \\ 0 & h_q & 0 & -\frac{t}{2}a_qh_qV_{2y}^q & \frac{t}{2}a_qh_qV_{1y}^q \\ 0 & & h_q & -\frac{t}{2}a_qh_qV_{2z}^q & \frac{t}{2}a_qh_qV_{1z}^q \end{array} \right]$$

where  $V_{1x}^k, V_{1y}^k$  and  $V_{1z}^k$  are respectively the  $x, y$  and  $z$  components of  $\mathbf{V}_1^k$ , and analogous definitions hold for  $\mathbf{V}_2^k$ . Since the displacement interpolation has been fully characterized, the stiffness matrix can be derived following the steps detailed before. We remark that the second hypothesis of the basic shell model, that the normal stress in planes parallel to the midsurface is zero, is imposed when defining the matrix  $\mathbf{C}$  much like it was done for the plate and shell models in Chapter 4. Of course, in route to the stiffness matrix there are several details that need to be established. We refer the interested reader to Bathe, 1996.

We list below the main reasons that make this shell element formulation attractive:

- Since the element is based on the basic shell model it can be used to describe thin and moderately thick shells.
- When the midsurface of the shell is flat it becomes a plate element. Actually, due to the kinematic and mechanical hypotheses it corresponds to the plate element of the Reissner-Mindlin mathematical model.

- Since the midsurface is interpolated it can be used to model shells of an arbitrary geometry even those for which an analytical equation of its midsurface is not known. For example, the coordinates of the midsurface may only be given at discrete locations from the output of a geometric modeling program.
- The formulation does not contain the assumption that the ratio of thickness to radius of curvature  $\ll 1.0$ .
- In geometric nonlinear analysis – as introduced in Chapter 8 – the solution is obtained incrementally in load steps and for each load level a new configuration is established. Therefore, to be used in general nonlinear analysis, an element should be able to represent these incremental configurations. For example, a plate subjected to a transverse load deforms and becomes a shell as the load is increased. Considering the kinematic description of the element given in equations (6.126) and (6.127), we see that this element can be used to characterize any configuration; hence the formulation can be directly extended to general nonlinear analysis, see Bathe, 1996.
- The nodal degrees of freedom are only displacements and rotations.

Although the element formulation has all the desirable properties mentioned above, the elements are not reliable and effective, because they suffer from a difficult and detrimental numerical deficiency called locking, which will be addressed in Section 6.5. Fortunately, these elements were successfully modified to largely overcome locking while preserving the desirable characteristics outlined above.

#### 6.4.4 Beam finite elements

If we set for beams the same requirements of generality as for shell elements, we would promptly recognize that no beam mathematical model of Chapter 4 provides this desired level of generality which could be outlined as:

- The beam axis can be straight, a planar curve or a three-dimensional curve. The axis could even be described only by a set of discrete locations.
- The beam should model transverse shear deformations.
- The beam should model cross-sectional variations along its axis.
- The beam should not contain the assumption that the ratio of thickness to radius of curvature  $\ll 1.0$ , as used in Section 4.2.7.

As for shells, we can identify basic hypotheses of beam behavior characterizing a basic beam model and reflect these hypotheses in the beam finite element formulation through the discretization process. The hypotheses are:

*Kinematic hypothesis:* Plane sections remain plane during deformations.

*Mechanical hypothesis:* Normal stresses acting on planes normal to the cross-sectional plane are zero. Also, the in-plane shear stresses at the cross-section are zero.

We next present the formulation of a beam element which complies with the above requirements. To characterize the beam element, we define the cross-section of the beam at the nodal locations. In Figure 6.56 we show these definitions for a 3-node beam element of rectangular cross-section; of course different cross-sections could be used. Note that at each nodal point

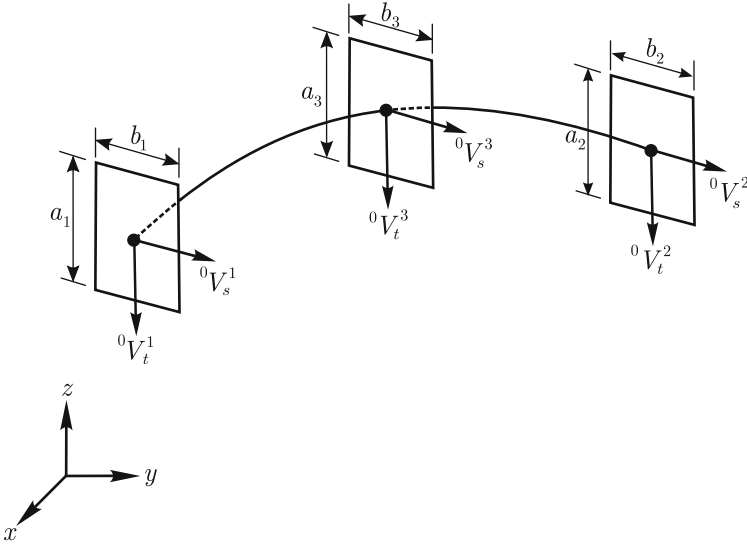


Fig. 6.56. Definition of beam geometric properties at nodal locations

the unit vectors  ${}^0\mathbf{V}_s^k, {}^0\mathbf{V}_t^k$  position the cross-section in 3-D space. The beam axis is implicitly defined by the interpolation of the geometry given by

$${}^0\mathbf{x}(r, s, t) = \sum_{k=1}^q h_k(r) {}^0\mathbf{x}^k + \frac{t}{2} \sum_{k=1}^q a_k h_k(r) {}^0\mathbf{V}_t^k + \frac{s}{2} \sum_{k=1}^q b_k h_k(r) {}^0\mathbf{V}_s^k \quad (6.132)$$

which is written for the  $q$ -node element. The nodal points are given by  ${}^0\mathbf{x}^k$ ,  $h_k(r)$  are the 1-D interpolation functions for the  $q$ -node element and the reference cube with the isoparametric coordinates  $(r, s, t)$  (see for example Figures 6.45 and 6.54) is mapped to the beam element geometry by equation (6.132). The deformed configuration can be written in analogous form

$${}^1\mathbf{x}(r, s, t) = \sum_{k=1}^q h_k(r) {}^1\mathbf{x}^k + \frac{t}{2} \sum_{k=1}^q a_k h_k(r) {}^1\mathbf{V}_t^k + \frac{s}{2} \sum_{k=1}^q b_k h_k(r) {}^1\mathbf{V}_s^k$$

where the left superscript 1 identifies  $\mathbf{x}_k, \mathbf{V}_t^k, \mathbf{V}_s^k$  for the deformed configuration.

The displacements are obtained by



$$\mathbf{u} = {}^1\mathbf{x} - {}^0\mathbf{x} = \sum_{k=1}^q h_k(r) \mathbf{u}^k + \frac{t}{2} \sum_{k=1}^q a_k h_k(r) \mathbf{V}_t^k + \frac{s}{2} \sum_{k=1}^q b_k h_k(r) \mathbf{V}_s^k \quad (6.133)$$

where  $\mathbf{u}^k$  are the nodal displacements and

$$\mathbf{V}_t^k = {}^1\mathbf{V}_t^k - {}^0\mathbf{V}_t^k, \quad \mathbf{V}_s^k = {}^1\mathbf{V}_s^k - {}^0\mathbf{V}_s^k.$$

Since the displacements are assumed to be infinitesimally small, we can write

$$\mathbf{V}_t^k = \theta_k \times {}^0\mathbf{V}_t^k \quad (6.134)$$

$$\mathbf{V}_s^k = \theta_k \times {}^0\mathbf{V}_s^k \quad (6.135)$$

where  $\theta_k$  is the rotation vector of the section located at node  $k$  which can be written in the global reference system as

$$\theta_k = \begin{bmatrix} \theta_x^k \\ \theta_y^k \\ \theta_z^k \end{bmatrix}.$$

Therefore, there are six degrees of freedom per node and the nodal displacement column matrix can be written as

$$\hat{\mathbf{u}}^T = \left[ u_1 \quad v_1 \quad w_1 \quad \theta_x^1 \quad \theta_y^1 \quad \theta_z^1 \mid \cdots \mid u_q \quad v_q \quad w_q \quad \theta_x^q \quad \theta_y^q \quad \theta_z^q \right].$$

The  $\mathbf{H}$  matrix can be obtained from (6.133), (6.134) and (6.135). The constitutive equation is given by

$$\begin{bmatrix} \tau_{\eta\eta} \\ \tau_{\eta\xi} \\ \tau_{\eta\zeta} \end{bmatrix} = \begin{bmatrix} E & 0 & 0 \\ 0 & Gk & 0 \\ 0 & 0 & Gk \end{bmatrix} \begin{bmatrix} \varepsilon_{\eta\eta} \\ \gamma_{\eta\xi} \\ \gamma_{\eta\zeta} \end{bmatrix}$$

where  $(\eta, \xi, \zeta)$  is a convected coordinate system such that at a cross-section  $\tau_{\eta\eta}$  is the normal stress and  $\tau_{\eta\xi}, \tau_{\eta\zeta}$  are the transverse shear stresses with  $\xi$  and  $\zeta$  parallel to the sides of the rectangular cross-section, and  $k$  is the shear correction factor. With these definitions  $\mathbf{B}$  and  $\mathbf{k}^{(m)}$  can be evaluated. We refer to Bathe, 1996 for the details of these matrices and their derivations. Here warping displacements were not considered, but can also be introduced (see Bathe and Chaudhary, 1982).

These elements, as the shell elements in Section 6.4.3 are not yet effective – they are prone to locking – and need to be modified to arrive at reliable and hence useful elements (see Section 6.5).

## 6.5 Effective finite elements

In the previous sections we introduced a displacement-based finite element formulation for beams, plates and shells. The associated elements seem attractive due to their simple formulations and, apparently, general applicability. However, these elements<sup>4</sup> suffer from a detrimental numerical deficiency in that they can be much too stiff when bending situations are modeled – for which these elements are to be used extensively! This deficiency has been termed “locking” since the “numerical stiffening” can lead to very small displacements – and in the limit to zero deformations.

A similar locking phenomenon is also seen when the 2-D (plane strain and axisymmetric) and 3-D solid displacement-based elements presented above are used to model incompressible or almost incompressible behavior.

A tremendous research effort has been directed to overcome the locking deficiency in order to arrive at finite elements which are general and at the same time reliable and efficient. Nowadays, some such elements are known and we call them effective elements.

In the following sections, we first present the basic convergence properties of displacement-based finite element formulations and introduce the deleterious effects of locking. Then, in the simple setting of the 2-node Timoshenko beam element, we examine the source of locking and how to overcome it. Finally, the main characteristics of locking for the remaining mathematical models earlier discussed are summarized and a list of effective elements is given with references to their formulations.

### 6.5.1 Convergence of displacement-based finite element formulations and the effects of locking

We considered in Section 6.2 the convergence of 1-D finite element solutions and much of that discussion is also applicable to 2-D and 3-D solutions of solids. Let us summarize below the convergence results for the displacement-based formulations for the analysis of a solid.

Let<sup>5</sup>  $\mathbf{V}$  be the admissible displacement space defined by

$$\mathbf{V} = \{ \mathbf{v}, \mathbf{v} : Vol \rightarrow \mathbb{R}^n \mid a(\mathbf{v}, \mathbf{v}) < \infty, \mathbf{v}|_{S_u} = 0 \}$$

where  $a(\mathbf{v}, \mathbf{v})$  as defined in (5.43) is twice the strain energy corresponding to  $\mathbf{v}$ ,  $Vol$  represents the domain of the undeformed configuration and  $n = 2$  for a 2-D formulation and  $n = 3$  for a 3-D formulation. Merely for ease of presentation, we consider that the displacements are zero on  $S_u$ .

<sup>4</sup> Except the Bernoulli-Euler beam element for modeling straight beams. The reason is that shear deformations are not modeled and the beam axis is straight.

<sup>5</sup> Here we use  $\mathbf{V}$  in boldface and soon also  $\mathbf{V}_h$  since these are spaces of vector valued functions

Let  $\mathbf{V}_h$  be a generic finite element space given by a mesh choice of isoparametric elements. Note that a generic element of  $\mathbf{V}_h$  can be characterized elementwise from the nodal displacements using (6.121). The continuity property at element interfaces guarantees that  $\mathbf{V}_h \subset \mathbf{V}$ . We can construct a sequence of finite element spaces which obey (6.50) by subdividing the elements of the initial mesh which defines  $\mathbf{V}_h^1$ .

Let  $\mathbf{u}$  be the exact solution and  $\mathbf{u}_h^i$  the finite element solution obtained using  $\mathbf{V}_h^i$ . It can be shown that

$$\|\mathbf{u} - \mathbf{u}_h^i\|_1 \leq Ch^k \quad (6.136)$$

when  $\mathbf{u}$  is smooth enough. Note the similarity between (6.136) and (6.63). Here  $C$  is a positive constant and  $h$  is the size of the largest element (see Bathe, 1996 for a precise definition of element sizes in 2-D and 3-D situations). The 1-norm for a function  $\mathbf{f} : Vol \rightarrow \mathbb{R}^3$

$$\mathbf{f} = \begin{bmatrix} f_x(x, y, z) \\ f_y(x, y, z) \\ f_z(x, y, z) \end{bmatrix} \quad (6.137)$$

is given by

$$\begin{aligned} \|\mathbf{f}\|_1 = & \left\{ \int_{Vol} \left[ \left( \frac{\partial f_x}{\partial x} \right)^2 + \left( \frac{\partial f_x}{\partial y} \right)^2 + \left( \frac{\partial f_x}{\partial z} \right)^2 + \left( \frac{\partial f_y}{\partial x} \right)^2 + \left( \frac{\partial f_y}{\partial y} \right)^2 \right. \right. \\ & + \left. \left( \frac{\partial f_y}{\partial z} \right)^2 + \left( \frac{\partial f_z}{\partial x} \right)^2 + \left( \frac{\partial f_z}{\partial y} \right)^2 + \left( \frac{\partial f_z}{\partial z} \right)^2 \right. \\ & \left. \left. + (f_x)^2 + (f_y)^2 + (f_z)^2 \right] dVol \right\}^{1/2}. \end{aligned} \quad (6.138)$$

For  $\mathbf{f} : Vol \rightarrow \mathbb{R}^2$  it suffices to suppress  $f_z$  in (6.137) and (6.138). Note that (6.138) is a generalization of (6.55) since now we have to account for all the function components and their partial derivatives.

To define  $k$ , we consider the Pascal triangle for 2-D shown in Figure 6.57, and note that  $k$  is given by the order of the complete polynomial which is exactly represented in each element. For example,  $k = 2$  when  $P_2$  is represented, *i.e.*, each monomial  $1, x, y, x^2, xy, y^2$  can be exactly and independently represented. Note that to guarantee convergence  $k$  should be at least 1. In Bathe, 1996 it is shown that every isoparametric element, even if distorted and/or curved, represents  $P_1$  and hence the convergence of displacement-based isoparametric elements is assured. For the finite element formulation to satisfy compatibility and contain  $P_1$  is equivalent to representing exactly the rigid body modes and the constant strain states for any patch of finite elements. This is sometimes referred to as the convergence condition for continuum elements.

1	Degree of complete polynomial	corresponding space
$x \quad y$ .....	1 .....	$P_1$
$x^2 \quad xy \quad y^2$ .....	2 .....	$P_2$
$x^3 \quad x^2y \quad xy^2 \quad y^3$ .....	3 .....	$P_3$
$x^4 \quad x^3y \quad x^2y^2 \quad xy^3 \quad y^4$ .....	4 .....	$P_4$
$x^5 \quad x^4y \quad x^3y^2 \quad x^2y^3 \quad xy^4 \quad y^5$ .....	5 .....	$P_5$

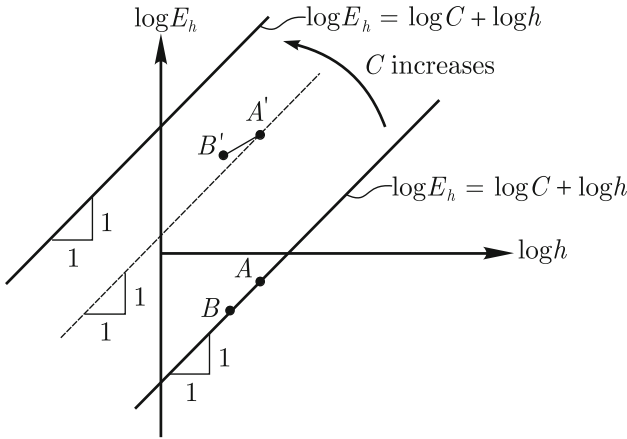
**Fig. 6.57.** Pascal triangle

For the displacement-based beam, plate and shell elements it is possible to show that error estimates such as (6.136) also hold (but the value of  $k$  may be linear than given by the Pascal triangle) and therefore their convergence properties are also guaranteed, see Chapelle and Bathe, 2010*a*.

Since it is possible to obtain error estimates like (6.136) for every displacement-based formulation studied so far, the reader might ask: “What can possibly be the deficiency of displacement-based finite element formulations which leads to locking?”

To address this question, we refer to Figure 6.21 in which the error estimate (6.136) is graphically given for  $k = 1$ . In problems prone to locking, the constant  $C$  in (6.136) depends on a problem parameter such as the thickness (beam, plates and shells) or  $\nu$  (for the elasticity problems) and this constant may become very large. Therefore, as this parameter changes and  $C$  becomes larger the straight line in Figure 6.21 shifts position as schematically shown in Figure 6.58.

To understand the consequences of this shift, we show the pairs  $(\log h, \log E_h)$  represented by  $A$  and  $B$  for two meshes before the locking parameter was changed. We assume that these two meshes are fine enough such that accurate predictions were obtained ( $E_h$  is small enough) and that the full convergence rate has already been achieved for these meshes. If we further refine the mesh the convergence rate will not diminish. However, as the parameter is changed and the straight line shifts due to the increase of the constant  $C$  as shown in Figure 6.58 the same meshes yield points  $A'$  and  $B'$  shown in the diagram. That is, the errors increased ( $A$  compared to  $A'$ ) and the convergence rate decreased ( $A'$  to  $B'$  compared to  $A$  to  $B$ ) since the condition now for the pairs  $(\log h, \log E_h)$  is to be below or on the upper solid line. The shift may be so large that accurate predictions may be obtained only for extremely fine meshes that are of no practical interest.



**Fig. 6.58.** Possible change in convergence diagram due to locking

Note that for a given problem with the applicable parameter fixed, the finite element solution converges if we sufficiently refine the mesh due to (6.136). However, due to locking and consequently a very large  $C$ , the fact that convergence is eventually achieved has no value for engineering applications since we obtain very inaccurate predictions for meshes of practical interest.

Therefore, a formulation is free of locking if the constant  $C$  in (6.136) and the order of convergence are independent of the parameter which governs locking. Then, convergence curves do not shift due to changes of the parameter and convergence rates are not affected.

Although we introduced the effects of locking, we did not address its source which is discussed in the next section by means of the Timoshenko beam element.

### 6.5.2 Locking for the 2-node Timoshenko beam element

The general beam formulation discussed in Section 6.4.4 degenerates to the Timoshenko beam element formulation when the axis is straight. We can use this simple beam formulation to exemplify the phenomenon of locking, see also Bathe, 1996 and Chapelle and Bathe, 2010*a*. For this purpose we rewrite the formulation as the minimization of the total potential energy

$$\begin{aligned} \Pi(w(x), \beta(x)) = & \frac{EI}{2} \int_0^L \left( \frac{d\beta}{dx} \right)^2 dx + \frac{GAk}{2} \int_0^L \left( \frac{dw}{dx} - \beta \right)^2 dx \\ & - \int_0^L wp dx \end{aligned} \tag{6.139}$$

and refer to Section 4.2.8 for the definition of the quantities appearing in this expression. Of course,  $I = \frac{bt^3}{12}$ ,  $A = bt$  with  $b$  the width and  $t$  the thickness

of the rectangular cross-section. The solution is given by the functions  $w(x)$  and  $\beta(x)$  which minimize the potential. The phenomenon of locking is seen as the beam becomes thin and to study it, we consider a sequence of problems. Each problem in the sequence is associated with a different thickness which is made smaller and smaller. Clearly, if (6.139) is simply used with the same load  $p$ , we must expect the displacement  $w(x)$  to become infinitely large as  $t \rightarrow 0$ . To seek well-behaved solutions, we consider for each problem of the sequence a load given by

$$p(x) = t^3 g(x)$$

and the scaled potential

$$\begin{aligned} \tilde{\Pi} &= \frac{\Pi}{t^3} = \frac{bE}{24} \int_0^L \left( \frac{d\beta}{dx} \right)^2 dx + \frac{Gbk}{t^2} \int_0^L \left( \frac{dw}{dx} - \beta \right)^2 dx \\ &\quad - \int_0^L wg \, dx. \end{aligned} \quad (6.140)$$

Note that the functions  $w(x)$  and  $\beta(x)$  which minimize  $\Pi$  are the same functions that minimize  $\tilde{\Pi}$ .

Considering the minimization of  $\tilde{\Pi}$  as  $t \rightarrow 0$  we have that

$$\int_0^L \left( \frac{dw}{dx} - \beta \right)^2 dx \rightarrow 0 \quad \text{as} \quad t \rightarrow 0.$$

Otherwise, the term of  $\tilde{\Pi}$  associated with the shear strain energy would go to infinity as  $t \rightarrow 0$ . Therefore, for a very thin beam we need to have

$$\frac{dw}{dx} - \beta \cong 0 \quad \Rightarrow \quad \frac{dw}{dx} \cong \beta \quad (6.141)$$

and of course (6.141) illustrates the reasonableness of the kinematic assumption of the Bernoulli-Euler beam model, where we assume  $\frac{dw}{dx} = \beta$ . The result given in (6.141) indicates that the Timoshenko beam solution tends to the Bernoulli-Euler beam solution as the beam thickness tends to zero.

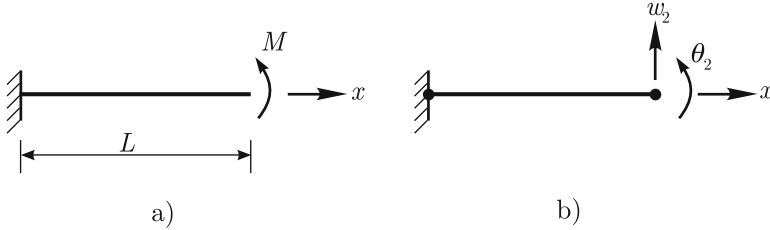
Now, considering the finite element solution we need to have

$$\frac{dw_h(x)}{dx} - \beta_h(x) \cong 0 \quad \text{as} \quad t \text{ becomes small} \quad (6.142)$$

where  $w_h(x)$  and  $\beta_h(x)$  need to be in the finite element spaces for displacements,  $W_h$ , and rotations,  $B_h$ , corresponding to the mesh, *i.e.*,  $w_h \in W_h$  and  $\beta_h \in B_h$ . The condition (6.142) represents a constraint for the finite element solutions  $w_h(x)$  and  $\beta_h(x)$ . Hence, we need that  $W_h$  and  $B_h$  be such that the constraint  $\frac{dw_h}{dx} = \beta_h$  can be satisfied for a sufficient number of functions in  $W_h$  and  $B_h$ . By a sufficient number of functions, we mean that these functions should be able to give a reasonable approximation of the exact solution of the mathematical model. If this is not the case, the finite element discretization will lock. We illustrate the source of the difficulty in the next example.

**Example 6.8**

Consider a cantilever Timoshenko beam of rectangular cross-section subjected to a tip moment as shown in Figure 6.59a and the discretization with a single two-node Timoshenko beam element as shown in Figure 6.59b. Examine the behavior of the solution as the beam thickness tends to zero.



**Fig. 6.59.** Problem definition discretized with one Timoshenko beam element

This problem is also considered in Bathe, 1996.

**Solution**

Since the interpolation is linear for, both, displacement and section rotations and the displacement and section rotation are zero at the clamped end, we have

$$w_h(x) = \frac{x}{L}w_2, \quad \beta_h(x) = \frac{x}{L}\theta_2$$

and the shear strain is given by

$$\gamma_h(x) = \frac{dw_h}{dx} - \beta_h = \frac{1}{L}(w_2 - x\theta_2). \quad (6.143)$$

The above discussion shows that as  $t$  becomes small, the constraint  $\gamma_h \rightarrow 0$  is increasingly enforced and for  $t$  small enough we have

$$w_h(x) \cong 0 \quad \text{and} \quad \beta_h(x) \cong 0. \quad (6.144)$$

This illustrates the phenomenon of solution locking. In Table 6.4 we provide some values of  $w_2$  and  $\theta_2$  normalized with respect to the exact solution for different ratios  $t/L$ . We can see that, indeed  $w_2$  and  $\theta_2$  tend to zero, and even for  $t/L = 1/10$  the solution is already much too stiff.

□

We have used the coarsest discretization possible in the example above, but the locking behavior is of course also seen for any fine mesh of 2-node

**Table 6.4.** Normalized values for tip displacements and rotations obtained with the model of Figure 6.59 using the displacement-based element

$t/L$	Calculated transverse displacement /exact transverse displacement	Calculated section rotation /exact section rotation
1/10	$2.03 \times 10^{-2}$	$2.00 \times 10^{-2}$
1/100	$2.03 \times 10^{-4}$	$2.00 \times 10^{-4}$
1/1000	$2.03 \times 10^{-6}$	$2.00 \times 10^{-4}$

Timoshenko beam elements. Since each element in the fine mesh then behaves as does the single element in the example, the locking phenomenon simply propagates through the mesh.

Mathematically, locking in general beam, plate and shell analyses means that uniform convergence of the finite element solution with respect to the thickness  $t$  of the beam (plate or shell) is not seen. That is, we do not have the desirable property

$$\frac{\|u - u_h\|}{\|u\|} \leq Ch^p \tag{6.145}$$

where  $\tilde{C}$  and  $p$  are independent of  $t$ , see Chapelle and Bathe, 2010a.

The most successful approach to overcome locking is the use of a mixed method based on a variational formulation analogous to the principle of virtual work. A mixed formulation for the Timoshenko beam model considered in (6.140) can be constructed by introducing a shear strain type variable in the formulation, see Bathe, 1996.

Find  $w(x) \in W$ ,  $\beta(x) \in B$  and  $\zeta(x) \in Q$  such that

$$\begin{aligned} \frac{Eb}{12} \int_0^L \frac{d\bar{\beta}}{dx} \frac{d\beta}{dx} dx + Gbk \int_0^L \zeta \left( \bar{\beta} - \frac{d\bar{w}}{dx} \right) dx \\ = \int_0^L g\bar{w} dx \quad \text{for all } \bar{\beta}(x) \in B, \bar{w}(x) \in W \tag{6.146} \\ Gb \int_0^L \bar{\zeta} \left( \beta - \frac{dw}{dx} \right) dx - t^2 \int_0^L \bar{\zeta} \zeta dx = 0 \quad \text{for all } \bar{\zeta} \in Q. \end{aligned}$$

The additional function  $\zeta(x)$  can be interpreted as a shear strain field. The functions  $\bar{\beta}(x)$ ,  $\bar{w}(x)$  and  $\bar{\zeta}(x)$  are virtual fields and the analogy to the principle of virtual work is immediate. The functional spaces  $W, B$  and  $Q$  can be precisely defined and their choices should guarantee that the integrals above are finite.

It can be shown that the solution for  $w(x)$  and  $\beta(x)$  of problem (6.146) and of the minimization problem defined by (6.140) are the same. Therefore,



in the continuum setting, problem (6.146) is an alternative formulation – yet more complex – to formulate the Timoshenko beam problem.

A finite element formulation of (6.146) can be obtained by choosing finite element spaces  $W_h \in W$ ,  $B_h \in B$  and  $Q_h \in Q$ . Consider the choice where  $W_h$  and  $B_h$  are continuous piecewise linear functions and  $Q_h$  piecewise constant functions. To see whether this choice makes sense, we consider the case  $t = 0$  in (6.146) and obtain the problem.

Find  $w_h(x) \in W_h$ ,  $\beta_h(x) \in B_h$  and  $\zeta_h(x) \in Q_h$  such that

$$\begin{aligned} \frac{Eb}{12} \int_0^L \frac{d\bar{\beta}_h}{dx} \frac{d\beta_h}{dx} dx + Gbk \int_0^L \zeta_h \left( \bar{\beta}_h - \frac{dw_h}{dx} \right) dx \\ = \int_0^L g\bar{w}_h dx \text{ for all } \bar{w}_h(x) \in W_h, \bar{\beta}_h(x) \in B_h \\ \int_0^L \bar{\zeta}_h \left( \beta_h - \frac{dw_h}{dx} \right) dx = 0 \text{ for all } \bar{\zeta}_h \in Q_h. \end{aligned}$$

The second equation above plays the role of the constraint  $\int_0^L \left( \frac{dw_h}{dx} - \beta_h \right)^2 dx = 0$ . However, taking into account that  $\beta_h(x) - \frac{dw_h(x)}{dx}$  is linear in each element, the condition that

$$\int_0^L \bar{\zeta}_h \left( \beta_h - \frac{dw_h}{dx} \right) dx = 0$$

where  $\bar{\zeta}_h$  can assume an arbitrary constant value in each element is satisfied only if

$$\left( \beta_h - \frac{dw_h}{dx} \right) \Big|_{\text{mid point of element } (m)} = 0 \text{ for each element } (m). \quad (6.147)$$

The equation (6.147) is the constraint associated with the mixed formulation. This constraint is much less restrictive than that associated with the displacement-based formulation.

It is possible to show that this formulation leads to optimal error estimates for the transverse displacements and section rotations independent of the beam thickness. Such result guarantees uniform optimal convergence with respect to the beam thickness, therefore, no shear locking. For the problem of Figure 6.59a we report in Table 6.5 the solutions obtained with the 2-node mixed Timoshenko beam element.

The finite element formulation of the mixed problem given in (6.146) for any thickness  $t$  and for certain choices of  $W_h$ ,  $B_h$  and  $Q_h$  can be obtained from a much simpler mathematical statement given by:

Find  $w_h(x) \in W_h$ ,  $\beta_h(x) \in B_h$  such that

**Table 6.5.** Normalized values for tip displacements and rotations obtained with the model of Figure 6.59 using a single mixed-formulated element

$t/L$	Calculated transverse displacement /exact transverse displacement	Calculated section rotation /exact section rotation
1/10	1.00	1.00
1/100	1.00	1.00
1/1000	1.00	1.00

$$\frac{Ebt^3}{12} \int_0^L \frac{d\bar{\beta}_h}{dx} \frac{d\beta_h}{dx} dx + GAk \int_0^L \bar{\gamma}_h^{AS} \gamma_h^{AS} dx = \tag{6.148}$$

$$\int_0^L p\bar{w} dx \text{ for all } \bar{\beta}_h(x) \in B_h, \bar{w}_h(x) \in W_h$$

where  $\gamma_h^{AS}$  is an assumed (ASsumed) shear strain field. We note that (6.148) is actually the principle of virtual work when we use  $\gamma_h^{AS}$  for the shear strain.

However, we still need to define  $\gamma_h^{AS}$  to fully characterize the formulation given in (6.148). It is possible to show that the choices of  $W_h$  and  $B_h$  of continuous piecewise linear functions, and  $Q_h$  of piecewise constant functions for (6.146) lead to an identical formulation as that obtained with (6.148) when we choose

$$\gamma_h^{AS} = \left( \frac{dw_h}{dx} - \beta_h \right) \Big|_{\text{mid point of the element}} \tag{6.149}$$

which is then, of course, constant in each element.

We can use

$$\gamma_h^{DI} = \gamma_h = \frac{dw_h}{dx} - \beta_h$$


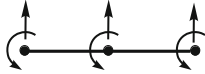
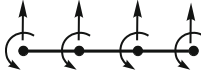
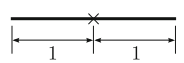
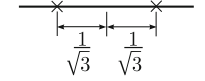
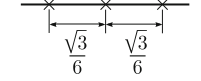
where *DI* (Direct Interpolation) emphasizes that the  $\gamma_h^{DI}$  gives the strains obtained from the interpolated kinematic variables  $\beta_h$  and  $w_h$ . Then (6.149) can be re-written as

$$\gamma_h^{AS} = \gamma_h^{DI} \Big|_{\text{mid point of the element}}$$

Since  $\gamma_h^{AS}$  is obtained from the kinematic variables  $w_h$  and  $\beta_h$ , the element stiffness matrix will correspond to nodal transverse displacement and section rotation degrees of freedom only. Therefore, the fact that the element is derived from a mixed formulation is not apparent when using the element since it has only the usual degrees of freedom.

The points where we impose  $\gamma_h^{AS} = \gamma_h^{DI}$  are referred to as tying points. Higher-order mixed elements which have optimal convergence properties, *i.e.*,

**Table 6.6.** Mixed interpolated Timoshenko beam elements

	2-node	3-node	4-node
$w, \theta$			
Tying			

which are independent of the beam thickness, can be derived. Table 6.6 summarizes the elements, see Bathe, 1996 and Chapelle and Bathe, 2010a.

The tying points shown in Table 6.6 are actually Gauss points and an efficient implementation of these elements is obtained by using these Gauss points to perform the integrations. Since these points lead to integration rules which are of lower order than those usually required, their usage might be referred to as reduced integration. However, in general, we can not obtain the implementation of a mixed element formulation by means of a reduced integration rule. In fact, there are no reduced integration rules which lead to the mixed plate and shell elements we recommend.

### 6.5.3 Locking in a general setting

There are several mathematical models for which the displacement-based finite element formulations are prone to locking. In all such cases the potential energy of the model can, in principle, be written as

$$\Pi(\mathbf{v}) = \frac{1}{2} (\varepsilon^3 E_1(\mathbf{v}) + \varepsilon E_2(\mathbf{v})) - \varepsilon^3 P(\mathbf{v}) \tag{6.150}$$

where

$$\mathcal{U}(\mathbf{v}) = \frac{1}{2} (\varepsilon^3 E_1(\mathbf{v}) + \varepsilon E_2(\mathbf{v}))$$

is the strain energy,  $P(\mathbf{v})$  the potential of the external loads,  $\mathbf{v}$  the kinematic field of the model and  $\varepsilon$  is a parameter which may become very small.

Since we are interested in situations in which  $\varepsilon$  is very small, we consider a sequence of problems, each problem in the sequence associated with a value of  $\varepsilon$ . We can define for a particular problem in the sequence the normalized potential

$$\Pi_\varepsilon(\mathbf{v}) = \frac{\Pi(\mathbf{v})}{\varepsilon^3} = \frac{1}{2} \left( E_1(\mathbf{v}) + \frac{1}{\varepsilon^2} E_2(\mathbf{v}) \right) - P(\mathbf{v}).$$

**Table 6.7.** Locking characterization for mathematical models

Mathematical model	$\frac{\varepsilon^3}{2} E_1$	$\frac{\varepsilon}{2} E_2$	$\varepsilon$
Timoshenko beam model	Bending strain energy	Shear strain energy	$t$ : section height
3-D elasticity Plane strain Axisymmetric	Distortional strain energy $\times (\sqrt{1 - 2\nu})^3$	Volumetric strain energy $\times (\sqrt{1 - 2\nu})^3$	$\sqrt{1 - 2\nu}$ $\nu$ : Poisson's ratio
Reissner-Mindlin Plate	Bending strain energy	Shear strain energy	$t$ : plate thickness
Membrane-bending shell model	Bending strain energy	Membrane strain energy	$t$ : shell thickness
Shear-membrane-bending shell model	Bending strain energy	Membrane and shear strain energy	$t$ : shell thickness
Basic shell model	Bending strain energy	Membrane and shear strain energy	$t$ : shell thickness

The solution for a problem in the sequence is given by that  $\mathbf{u}$  which minimizes the potential  $\Pi$  or equivalently  $\Pi_\varepsilon$ . For the limit problem  $\varepsilon \rightarrow 0$  the solution  $\mathbf{u}$  has to satisfy

$$E_2(\mathbf{u}) = 0 \tag{6.151}$$

otherwise the term  $\frac{1}{\varepsilon^2} E_2(\mathbf{u})$  would become unbounded. Therefore, when  $\varepsilon$  approaches zero (6.151) is a constraint for the mathematical model whose potential is given by (6.150). Of course, for the Timoshenko beam model this constraint is  $\frac{dw}{dx} - \beta = 0$  as discussed above.

When we introduce a finite element formulation by the choice of a finite element space  $\mathbf{V}_h$ , the solution is given, for a problem in the sequence, by that  $\mathbf{u}_h$  which minimizes the normalized potential  $\Pi_\varepsilon$  among all functions in  $\mathbf{V}_h$ . Therefore, by the same argument, when  $\varepsilon \rightarrow 0$  the solution for the finite element problem should satisfy

$$E_2(\mathbf{u}_h) = 0$$

which depending on the choice of  $\mathbf{V}_h$  may lead to locking.

In Table 6.7, we summarize the mathematical models which are potentially prone to locking and how they fit into the framework described above.

The overcoming of locking for these models has represented a great challenge to the finite element community which motivated a tremendous research effort. The use of mixed finite element formulations has proven to be the most

successful approach to arrive at finite elements that are free of locking, reliable and, therefore, effective. There are now mixed elements which can be recommended for engineering analysis for all mathematical models listed in Table 6.7. For practical purposes, finite elements with optimal convergence properties, *i.e.*, which are independent of the value of the parameter  $\varepsilon$ , have been obtained using mixed formulations for all the mathematical models of Table 6.7 except for shell models. The reliable analysis of complex shells – considering also nonlinear analysis – represents one of the greatest challenges in all of mechanics. However, numerical experimentations, guided by deep mathematical analysis, have shown that there are also some mixed shell elements which are quite reliable for many analyses and the range of shell thickness of engineering interest, Bucleam and Bathe, 1997, Bathe and Lee, 2011.

As detailed for the Timoshenko beam model, a mixed formulation has additional unknown fields besides the displacement fields. Its finite element formulation requires the choice of finite element spaces for the kinematic fields, generically represented by  $\mathbf{V}_h$ , and also for the additional fields described by  $\mathbf{Q}_h$ . In Table 6.8 we summarize the fields of the mixed formulations which are interpolated by the choices of  $\mathbf{V}_h$  and  $\mathbf{Q}_h$ . We also introduce the terminology for the formulations of the most effective elements. For the 2-D and 3-D incompressible or almost incompressible analyses, we refer to the displacement-pressure formulation – u/p formulation. For plates and shells we mention the MITC (Mixed Interpolation of the Tensorial Components) formulation.

For a given mixed formulation, the choices of pairs of finite element spaces  $\mathbf{V}_h, \mathbf{Q}_h$  which lead to optimal convergence properties, independent of the parameter  $\varepsilon$ , is not trivial. Mathematically, the choice is governed by the ellipticity and inf-sup conditions ( Brezzi and Bathe, 1990, Brezzi and Fortin, 1991, Bathe, 2001, Chapelle and Bathe, 2010*b*). We refer to Bathe, 1996 for a discussion of the inf-sup condition where the inf-sup condition is presented in various forms. One form of the inf-sup condition, based on our earlier discussion, see 6.2.3, is for displacement-based formulations given by

$$\|\mathbf{u} - \mathbf{u}_h\|_V \leq c d(\mathbf{u}, \mathbf{V}_h)_V$$

with  $c$  independent of the parameter  $\varepsilon$ . This result is, in essence, (6.136) with  $C$  independent of the parameter  $\varepsilon$  since

$$d(\mathbf{u}, \mathbf{V}_h)_V \leq \tilde{c} h^k \tag{6.152}$$

for  $\mathbf{u}$  sufficiently smooth. Of course,  $\tilde{c}$  does not depend on the parameter  $\varepsilon$  since (6.152) is only a functional approximation result and does not depend on the finite element solution. Therefore, the satisfaction of the inf-sup condition would render the displacement-based formulation free of locking. However, this is very difficult to achieve for the problems of interest in practical analyses, and the use of mixed formulations and elements is much more effective.

**Table 6.8.** Effective elements for incompressible materials and plates/shells

Mathematical model	Effective elements
Timoshenko beam model	<ul style="list-style-type: none"> <li>• 2, 3 and 4-node mixed elements</li> </ul> ref. Bathe, 1996
2-D elasticity <ul style="list-style-type: none"> <li>• Plane strain</li> <li>• Axisymmetric</li> </ul>	<ul style="list-style-type: none"> <li>• Quadrilateral: 9-3 u/p element</li> <li>• Triangular: 7-3 u/p element</li> </ul> ref. Crouzeix and Raviart, 1973, Brezzi and Bathe, 1986, Sussman and Bathe, 1987
3-D elasticity	<ul style="list-style-type: none"> <li>• Hexahedral: 27-4 u/p element</li> <li>• Tetrahedral: 11-4 u/p element</li> </ul> ref. Crouzeix and Raviart, 1973, Brezzi and Bathe, 1986, Sussman and Bathe, 1987
Reissner-Mindlin plate model	<ul style="list-style-type: none"> <li>• Quadrilateral: MITC4, MITC9, MITC16</li> <li>• Triangular: MITC7, MITC12</li> </ul> ref. Bathe, Bucalem and Brezzi, 1990
Basic Shell model	<ul style="list-style-type: none"> <li>• Quadrilateral: MITC4, MITC9, MITC16</li> <li>• Triangular: MITC3, MITC6</li> </ul> ref. Dvorkin and Bathe, 1984, Bathe and Dvorkin, 1986, Bucalem and Bathe, 1993, Bathe and Hiller, 2003 ref. Lee and Bathe, 2004, Kim and Bathe, 2009

In Table 6.8 we summarize the mixed elements that we recommend to be used in engineering practice<sup>6</sup>, see also Bathe, 1996. We note that the nodal degrees of freedom of the elements listed in Table 6.8 are the same as those of their displacement-based counterparts. Therefore, these elements are in use as simple as the displacement-based elements. For beam, plate and shell elements the interpolation of the strains is achieved with the aid of tying points and the computational effort to obtain the stiffness matrix is similar to that of the displacement-based elements. For the u/p elements listed in Table 6.8, the pressure fields are discontinuous at element interfaces allowing the static condensation of the pressure degrees of freedom.

We listed in Table 6.8 only the Timoshenko beam elements free of locking. Of course, the two-node Bernoulli-Euler beam model is very effective in the

<sup>6</sup> Note that for plane stress analysis, the displacement-based elements can be used since the stress-strain law (in Table 4.3) enforces automatically that the thickness is adjusted to satisfy the incompressibility condition (volumetric strain is zero) when Poisson's ratio = 0.5

analysis of straight thin beams, and it is by far most frequently used in engineering analysis.

Plate bending elements for the Kirchhoff model can also be proposed. However, the Reissner-Mindlin elements are preferred due to several reasons. The Reissner-Mindlin model is hierarchically a higher-order model with respect to the Kirchhoff theory and better represents the physical behavior of plates, specially near the edges where boundary layers may develop which are well captured by the Reissner-Mindlin model (see Häggblad and Bathe, 1990). Also, the Reissner-Mindlin model predicts transverse shear deformations and can be used to model moderately thick plates. However, most importantly, the interpolations for the Kirchhoff elements should have  $C^1$  continuity leading to relatively complex and inefficient elements that are also difficult (indeed almost impossible) to further develop for the effective analysis of shells and general nonlinear analysis.

We also recall that the elements for the basic shell model degenerate to Reissner-Mindlin plate bending elements when the shell midsurface is flat. The Reissner-Mindlin elements, which are listed in Table 6.8, have been directly derived for plate analysis and have a complete mathematical convergence analysis. However, in practice it is more efficient to use the elements of the basic shell model for, both, the analysis of plate and shell situations, to unify the analysis approach and since in nonlinear analysis the plate becomes a shell, see Lee and Bathe, 2010. These shell elements can also be hierarchically extended to 3-D shell elements to represent additional 3-D effects, see Kim and Bathe, 2008.

## 6.6 Finite element modeling tools

We discussed in the preceding sections how to formulate reliable finite elements for the mathematical models presented in this book. However, to take advantage of the full potential of these formulations for engineering structural analysis we still need to discuss how to efficiently construct finite element models deemed to solve practical engineering problems.

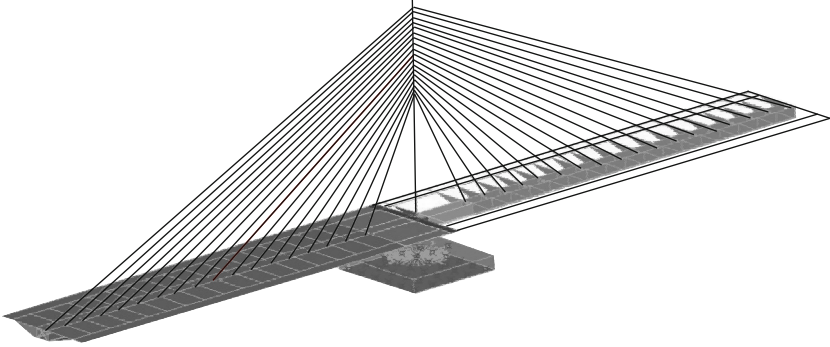
In this section we discuss several issues and techniques related to the construction of such finite element models.

### 6.6.1 Combining different type of elements in the same model

For an engineering problem, an efficient model is usually only obtained when different types of elements are combined. The reasons are many. For example, we may have different structural behaviors for different parts or regions of the model. Sometimes, even for the same region of the model the structural behavior may be more efficiently captured by combining elements.

As an example, we show the model of a cable-stayed bridge in a construction phase.

The bridge has two 127-meter-long spans symmetrically disposed with respect to the pylon, a 28-meter-wide deck carrying six traffic lanes, a 54-meter-tall pylon and a central stay plane with 36 cables.



**Fig. 6.60.** Finite element model of cable stayed bridge

In Figure 6.60 we show the finite element model representing only the mesh outline and in Figure 6.61 a close-up region of the model. The pylon is modeled with Bernoulli-Euler beam elements whose axes are represented in Figure 6.60. The cables are modeled with pre-stressed truss elements, the foundation block with 3-D solid elements, the soil with spring elements and the bridge deck with shell elements. In Figure 6.60 we can see in the first span, the deck exterior and, in the second, its interior which gives an idea of the cellular section used.

We can appreciate that many element types are combined. Otherwise, we would not obtain an efficient model. Of course, depending on the objective of the analysis the deck could be modeled with beam elements, instead.

### 6.6.2 Constraint equations

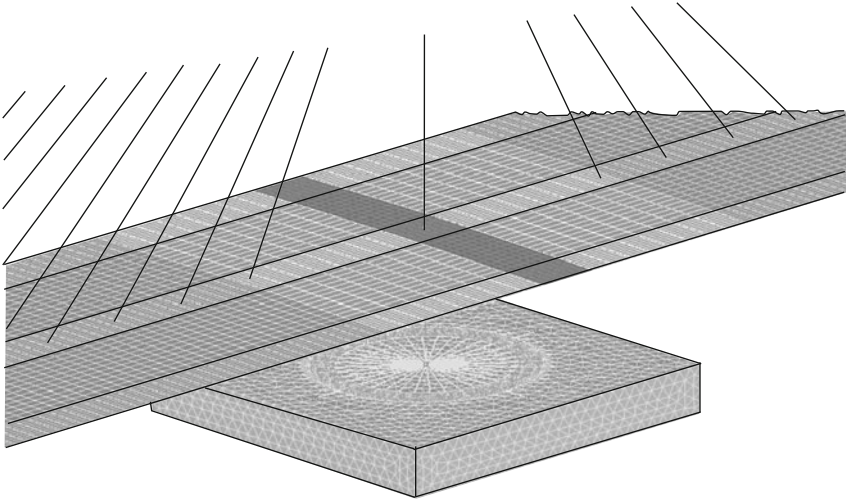
In constructing a finite element model, it is sometimes effective, or even necessary, to establish a relation between the nodal degrees of freedom of the model.

A general form of this linear relation which is referred to as *constraint equation* is

$$U_i = \sum_{j=1}^{r_i} \alpha_{qj} U_{qj}$$

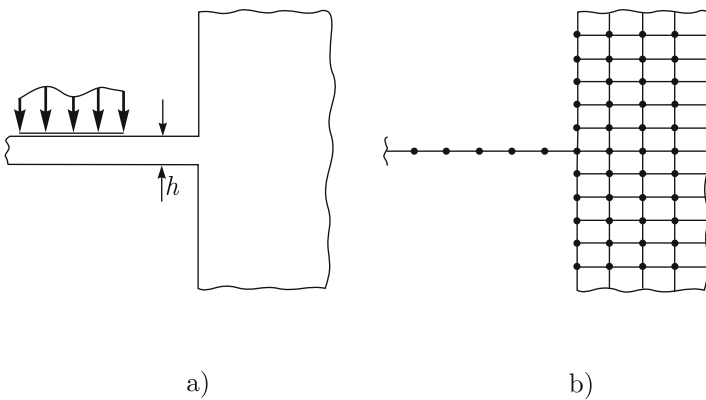
where  $U_i$  is a generic degree of freedom which is constrained or dependent. The degrees of freedom  $U_{q1}, U_{q2}, \dots, U_{qr_i}$  are independent degrees of freedom. As an example, consider the part of a model described in Figure 6.62a, where





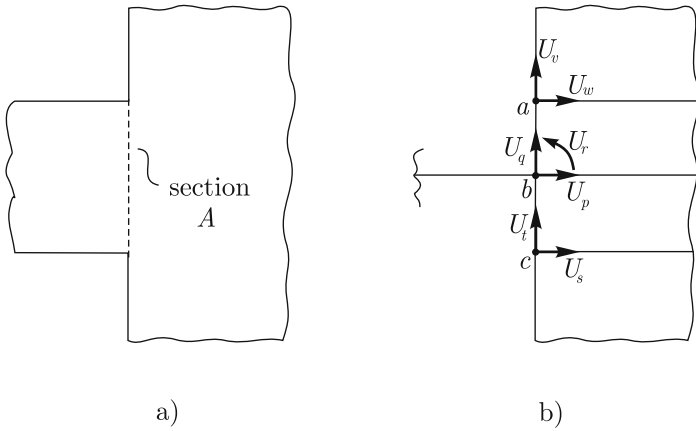
**Fig. 6.61.** Finite element model close-up of pylon deck intersection region

a thin structure working in bending connects to a deformable block. An appropriate modeling choice is to model the thin part with beam elements and the block with 2-D plane stress elements (here  $h$  is small). A mesh choice is shown in Figure 6.62b.



**Fig. 6.62.** a) Part of a structure; b) Mesh choice

In Figure 6.63a, we show a close-up view of the intersection region and in Figure 6.63b the corresponding mesh. Note that for the beam we have three degrees of freedom per node while for the 2-D elements we have only two. For the node which is common to the beam and the 2-D elements we should use three degrees of freedom, where  $U_r$  is the nodal rotation degree of freedom of



**Fig. 6.63.** a) Close up of the intersection region; b) Mesh choice for intersection region

the beam. However, the degree of freedom choices shown in Figure 6.63b do not yet correctly represent the behavior of the structure at the intersection region since the beam would behave as if it were pinned at node *b* neglecting the stiffness contribution of the block to the rotation of the Section *A* of the beam. The constraint equations

$$U_w = -\frac{h}{2}U_r + U_p \tag{6.153}$$

$$U_s = \frac{h}{2}U_r + U_p \tag{6.154}$$

model such stiffness contribution, and couple the rotation of the beam to the block.

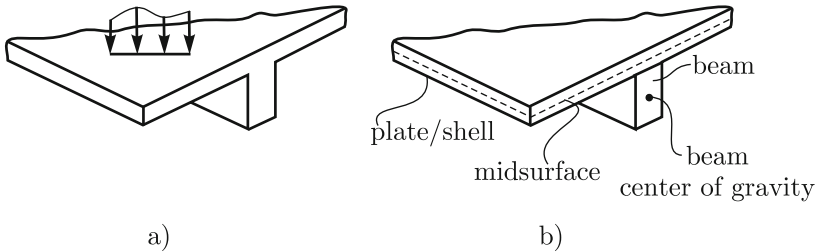
### 6.6.3 Rigid links

A rigid link establishes constraint equations between the degrees of freedom of two nodes. One of the nodes is called the *master* node and the other the *slave* node. The degrees of freedom of the master node are independent while those of the slave node are dependent reflecting the constraint equations associated with the rigid link.

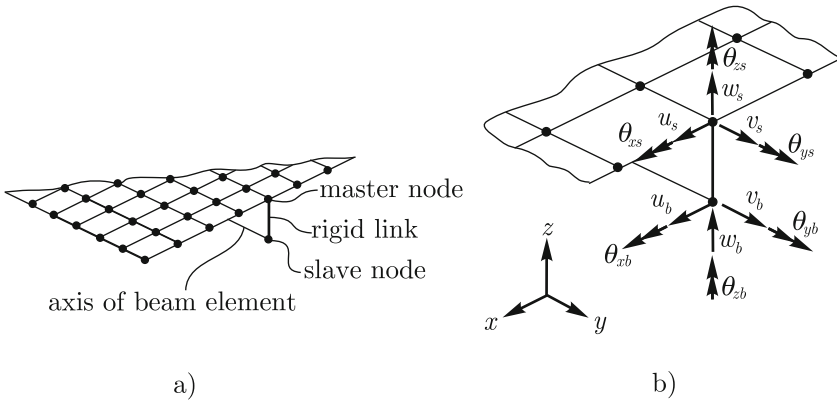
The constraint equations established by the rigid link are such that the distance between the two nodes does not change with deformation and the rotations are the same.

Rigid links are a very useful modeling tool and we exemplify their usage below. In Figure 6.64a we show part of the structure to be modeled. It is representative of a very common arrangement in structural engineering like a concrete slab and beam or a stiffened shell. An efficient modeling is obtained

by using plate/shell and beam models as shown in Figure 6.64b. Of course, the beam should correspond to the geometric region below the bottom surface of the plate/shell.



**Fig. 6.64.** Part of the structure to be modeled

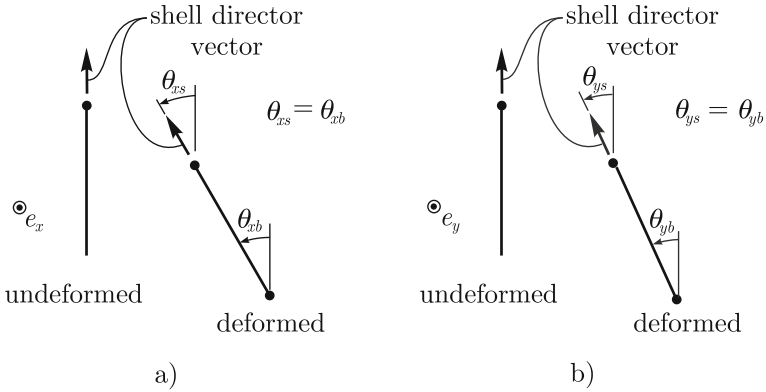


**Fig. 6.65.** Discretization for part of structure of Figure 6.64

In Figure 6.65a we show a typical discretization. One of the rigid links is seen connecting the master node, belonging to a shell element, and the slave node, belonging to a beam element (here, the choice of which node is to be the master node is arbitrary). In Figure 6.65b a detail is shown where we can see the degrees of freedom of the master and slave nodes.

Since the structure is assumed to be working in bending and membrane actions, the constraint is enforcing that the distance between the nodes does not change with deformation.

The constraints for the rotations deserve some detailed comments. In Figure 6.66a, we show the deformation associated with the rotation  $\theta_x$ . The equality  $\theta_{xb} = \theta_{xs}$  enforces that the rotation of the beam is the same as that of the director vector of the shell. These rotations induce bending deforma-



**Fig. 6.66.** Rotations of master and slave node around the  $x$  and  $y$  axes

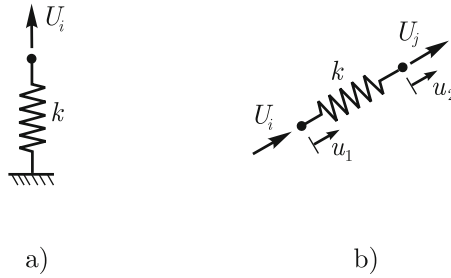
tions both in the shell and in the beam. A similar behavior occurs for the rotation around the  $y$  axis which is summarized in Figure 6.66b. Note that  $\theta_{yb}$  induces torsion in the beam while  $\theta_{ys}$  induces bending in the shell. Finally, the rotation around  $z$  does not induce any deformation in the shell due to the kinematics of the shell element (see Section 6.4) but it induces bending in the beam. Note that the total stiffness associated with the rotation around  $z$  is only coming from the beam. Hence, this shell node should be assigned six degrees of freedom, *i.e.*, we should have  $\theta_z$  as a degree of freedom for the shell node. Otherwise, we would be artificially preventing the rotation of the beam section around  $z$ .

### 6.6.4 Spring elements

Spring elements are very useful for modeling. Sometimes a spring element may be used to represent a whole structure when we are interested in capturing only the stiffness contribution of such structure to the current model. In another instance, it may be used to connect parts of a structure representing the stiffness of the connection. In the modeling of civil engineering structures, springs are also often used to represent the soil supporting the structure foundation.

In Figure 6.67a the most used spring arrangement is shown where the spring links a given degree of freedom  $U_i$  to the “ground” with spring constant  $k$ . Its contribution is accounted for by adding the spring constant  $k$  to the diagonal of the global stiffness matrix corresponding to degree of freedom  $U_i$ .

In Figure 6.67b, we generically represent a spring linking degrees of freedom  $U_i$  and  $U_j$ . The stiffness matrix of this spring in the local system  $u_1, u_2$  is given by



**Fig. 6.67.** Examples of spring arrangements

$$\mathbf{k} = \begin{bmatrix} k & -k \\ -k & k \end{bmatrix}.$$

### 6.6.5 Model symmetries

The use of symmetries can substantially decrease the model size, consequently, the solution and result interpretation efforts.

#### Plane symmetry

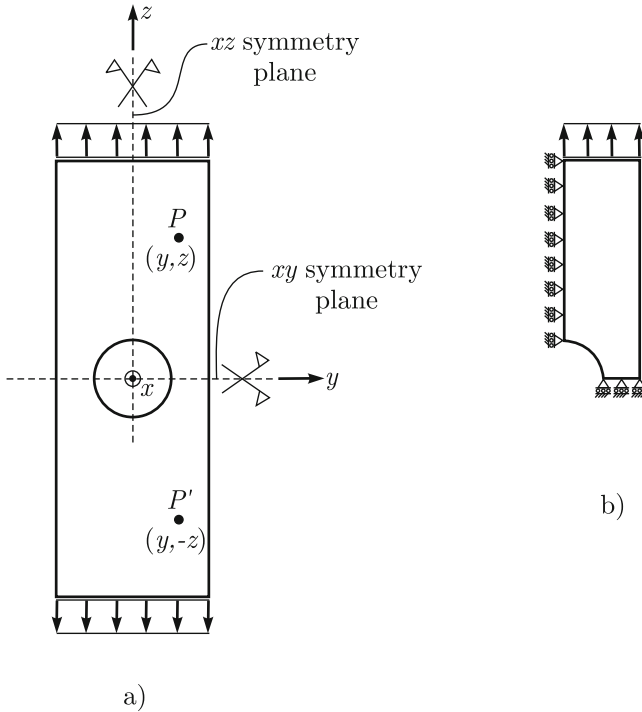
To exemplify the symmetry that occurs at a plane, consider the plate with a hole described in Figure 6.68a, we show the complete model and identify the planes of symmetry. The simplest way to understand symmetry is to recognize that at the plane of symmetry we may keep only one of the symmetric parts of the structure and represent all effects of the other part by means of prescribed boundary conditions. In fact, consider generic points  $P$  and  $P'$  of coordinates  $(y, z)$  and  $(y, -z)$ , respectively. Due to the symmetry conditions, *i.e.*, symmetric geometry and loading, we have

$$v(y, z) = v(y, -z)$$

$$w(y, z) = -w(y, -z)$$

which lead, at the plane of symmetry  $xy$ , to zero displacements in the  $z$  direction and unconstrained displacements in the  $y$  direction, *i.e.*, zero tractions in the  $y$  direction. Of course, at the plane of symmetry there can not be either a positive or negative  $w$  justifying the conclusion of  $w$  being zero. Since the displacements  $v$  are the same for symmetric points located at infinitesimally small distances from the plane of symmetry there is no tendency of relative motion between the parts in the  $y$  direction leading to zero shear stress at the symmetry plane. Hence, as we extract one part, we should impose a zero traction condition in the  $y$  direction.

In Figure 6.68b, we show the boundary conditions which take into account the planes of symmetry  $xy$  and  $xz$ . Note that the boundary conditions associated to the plane of symmetry  $xz$  are justified by an analogous reasoning.



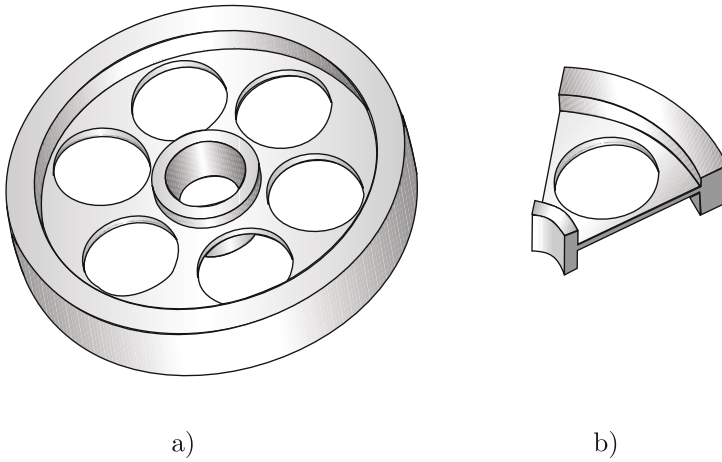
**Fig. 6.68.** a) Complete model; b) Model taking advantage of the symmetry

**Cyclic symmetry**

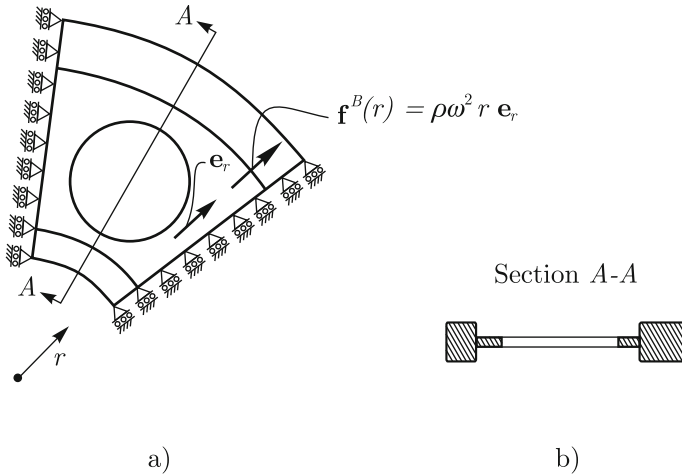
Consider the flywheel shown in Figure 6.69a. The flywheel can be geometrically obtained as a repetition and rotation of the part shown in Figure 6.69b. Suppose that the flywheel is rotating at constant angular velocity. Then, the deformations and stresses can be obtained by solving a static problem with the structure subjected to the inertia forces. These are body forces which act in the radial direction and also repeat themselves for a generic part such as that of 6.69b. We can establish a plane stress model of the flywheel considering the different thicknesses of its parts. Due to cyclic symmetry of the geometry and loading, we only need to model the part of Figure 6.69b with appropriate boundary conditions to take into account the cyclic symmetry as described in Figure 6.70. The justifications for these boundary conditions are as for planes of symmetry (see above).

Of course, although we presented the cyclic symmetry modeling for a specific problem, it can be used for any structure which complies with the cyclic symmetry conditions for the geometry and loading.

In case the geometry is cyclic symmetric but not the loading, we can still use solution procedures which take advantage of the cyclic symmetry of the



**Fig. 6.69.** a) Complete flywheel; b) Cyclic symmetric part

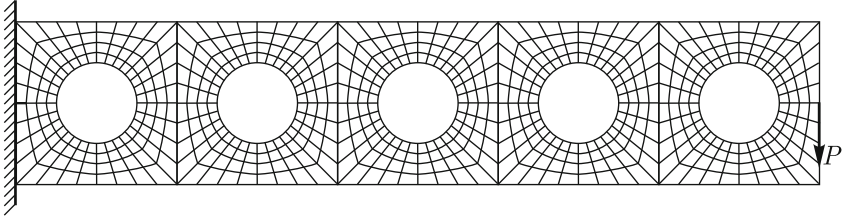


**Fig. 6.70.** Plane stress model of the flywheel. Only a part needs to be modeled

geometry. These solution procedures can result into major advantages since only one cyclic part needs to be meshed and the solution times can be much smaller than those for the full problem. We refer to Zhong and Qui, 1983 for details, and ADINA, 2008.

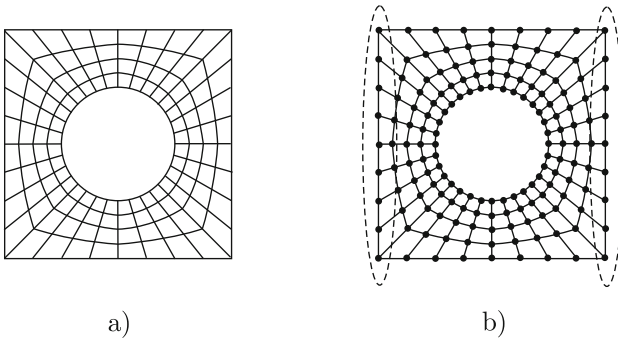
### 6.6.6 Substructures

As a motivation, consider the finite element model of the cantilever with holes shown in Figure 6.71. There is a repetition pattern in the mesh used. In Figure 6.72a we show the mesh part, which when repeated leads to the complete



**Fig. 6.71.** Finite element model of cantilever with holes

mesh. In Figure 6.72b we indicate the nodes whose degrees of freedom are shared by more than one part of the model or for which boundary conditions are assigned.



**Fig. 6.72.** Finite element mesh of part of the model

The substructuring technique consists of two steps. In the first step – the static condensation – the stiffness matrix of the repeating part is established for only the degrees of freedom which are shared with other parts or have assigned boundary conditions as exemplified below. This part with the reduced number of degrees of freedom may be interpreted as a macroelement.

In the second step the stiffness matrices of these macroelements are assembled to obtain the structure stiffness matrix using much fewer degrees of freedom than originally.

The computational advantages of the substructuring technique are twofold. The stiffness matrix evaluation effort is generally much reduced and the solution effort may also be significantly less since there are much less active degrees of freedom.

The static condensation part is detailed below. Let  $\mathbf{U}_m$  and  $\mathbf{U}_s$  be column matrices which collect the degrees of freedom that will be kept for the main structure and those that will be condensed out, respectively. Let  $\mathbf{K}^p$  be the stiffness matrix of the part. Then, we can write



$$\begin{bmatrix} \mathbf{K}_{mm}^p & \mathbf{K}_{ms}^p \\ \mathbf{K}_{sm}^p & \mathbf{K}_{ss}^p \end{bmatrix} \begin{bmatrix} \mathbf{U}_m \\ \mathbf{U}_s \end{bmatrix} = \begin{bmatrix} \mathbf{R}_m \\ \mathbf{0} \end{bmatrix}$$

which leads to

$$\mathbf{K}_{mm}^p \mathbf{U}_m + \mathbf{K}_{ms}^p \mathbf{U}_s = \mathbf{R}_m \quad (6.155)$$

$$\mathbf{K}_{sm}^p \mathbf{U}_m + \mathbf{K}_{ss}^p \mathbf{U}_s = \mathbf{0}. \quad (6.156)$$

From equation (6.156)

$$\mathbf{U}_s = -\mathbf{K}_{ss}^{p-1} \mathbf{K}_{sm}^p \mathbf{U}_m$$

which substituted into (6.155) yields

$$\left( \mathbf{K}_{mm}^p - \mathbf{K}_{ms}^p \mathbf{K}_{ss}^{p-1} \mathbf{K}_{sm}^p \right) \mathbf{U}_m = \mathbf{R}_m$$

and therefore

$$\mathbf{K}^{pr} = \mathbf{K}_{mm}^p - \mathbf{K}_{ms}^p \mathbf{K}_{ss}^{p-1} \mathbf{K}_{sm}^p$$

is the reduced stiffness matrix of the part.

Note that upon solution of this problem,  $\mathbf{U}_m$  is determined for each part and from equation (6.156)  $\mathbf{U}_s$  can be obtained using

$$\mathbf{U}_s = -\mathbf{K}_{ss}^{p-1} \mathbf{K}_{sm}^p \mathbf{U}_m$$

and then all solution variables can be determined for the whole domain. The process can be very efficient, but is not always so, see Bathe, 1996 for more details.

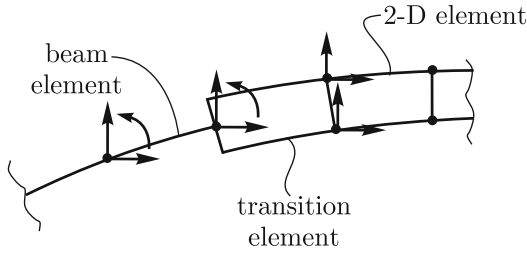
## 6.6.7 Connecting different type of elements

### Connecting beam and 2-D elements

When discussing constraint equations, we exemplified above one way of linking beam and plane elasticity elements.

In fact, the easiest way to establish constraints is to use rigid links. Referring to Figure 6.63b, we could define rigid links between nodes  $b$  and  $a$ , and  $b$  and  $c$  which would assume a rigid connection.

An alternative way is to use transition elements. In Figure 6.73 we schematically show a transition element. At one side, the transition element has the degrees of freedom of the 2-D element and at the other the degrees of freedom of the beam element, therefore, preserving displacement compatibility. Although the use of rigid links is more common in practice since it does not require a new element, the transition element concept is very attractive and provides useful elements to connect 3-D and shell elements as also



**Fig. 6.73.** 2-D transition element

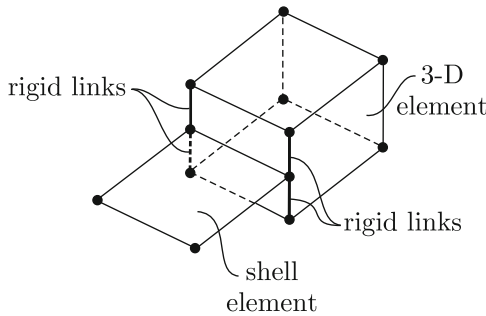
discussed below. We refer to Bathe, 1996 for the derivation of the transition element of Figure 6.73.

### Connecting beam and shell elements

We already discussed constraint equations and rigid links to connect beam and shell elements. This modeling is effective and takes into account the relative position of the beam axis with respect to the midsurface of the plate/shell.

### Connecting shell and 3-D elements

As for the connection of beam and 2-D elements, we have two approaches. The first is the use of rigid links between the shell and 3-D element nodes at the interface as summarized in Figure 6.74. The second is the transition element as shown in Figure 6.75. Shell transition elements have some top and bottom nodes with only translational degrees of freedom. We refer to Bathe and Ho, 1981 for the detailing of this transition element.



**Fig. 6.74.** Connecting a four-node shell element with an eight-node 3-D element through rigid links

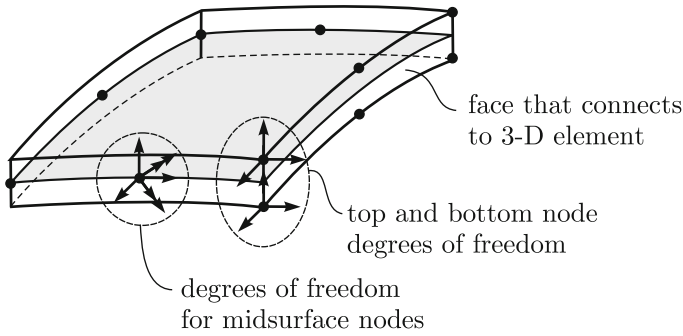


Fig. 6.75. Transition shell element

### 6.6.8 Skew systems

Frequently, it is necessary to have at a node a local reference system to assign displacement boundary conditions or to apply forces. For example, refer to Figure 6.70a, where we show the model of a cyclic part. If we align one of the sides for which displacement boundary conditions are specified with the global system, we need a local system for the other side. This local reference system, rotated with respect to the global system, to be assigned to nodes is referred to as a *skew system*.

Of course, the structure stiffness matrix has to be modified to account for these skew systems. These modifications are efficiently introduced at the element levels prior to the assemblage of the global stiffness matrix. In fact, let

$$\begin{aligned}\mathbf{u} &= \mathbf{T}_s \tilde{\mathbf{u}}_s \\ \mathbf{f} &= \mathbf{T}_s \tilde{\mathbf{f}}_s\end{aligned}$$

where  $\mathbf{u}$  is the element nodal displacement column matrix referred to the global system and  $\tilde{\mathbf{u}}_s$  is the column matrix of element nodal displacements in which some of the degrees of freedom are referred to a skew system. Analogous definitions for the element nodal force column matrices  $\mathbf{f}$  and  $\tilde{\mathbf{f}}_s$  apply. Following the derivations presented in Chapter 2, namely equations (2.30) to (2.32), we obtain the stiffness matrix of the element which takes into account the skew system as

$$\mathbf{k}_s = \mathbf{T}_s^T \mathbf{k} \mathbf{T}_s. \quad (6.157)$$

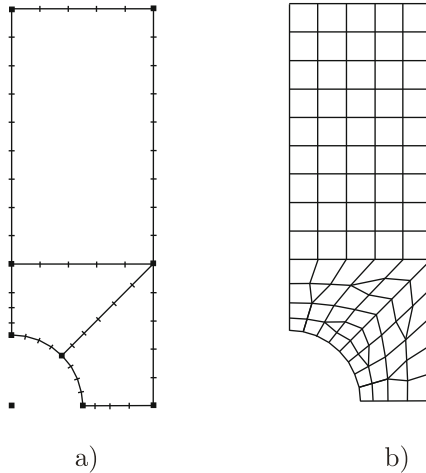
Although, equation (6.157) formally gives the transformation,  $\mathbf{k}_s$  is efficiently obtained operating only with the rows and columns of  $\mathbf{k}$  associated with the degrees of freedom for which the skew system is specified.

## 6.7 Meshing issues and error assessment

Nowadays mesh generators are widely used to obtain finite element meshes in the analysis of engineering problems. In this context, the analyst has to specify some mesh parameters which control the mesh generation process. Usually, these parameters are related to the mesh density which is desired in the different regions of the model.

To fix ideas, let us consider the plate with a hole problem described in Figure 6.68. We model one quarter of the plate as shown in Figure 6.68b. It is well known that there is a stress concentration region near the hole and the highest stress gradients for the plane stress components  $\tau_{yy}$ ,  $\tau_{zz}$ ,  $\tau_{yz}$  are expected to occur in this region.

As already exemplified for the 1-D problem, mesh grading is very efficient to capture high gradients of the variables to be predicted. Therefore, it is natural to specify smaller mesh densities for the hole region. In Figure 6.76a, we show the mesh densities at the lines of the geometric model and in Figure 6.76b the outcome of the mesh generator used. Due to the varying mesh density and the geometry, general quadrilateral and a few triangular elements have been generated. We generically refer to these quadrilateral elements as distorted elements since we have as reference the square element.



**Fig. 6.76.** Typical 2-D mesh generation

A natural question arises: Is the solution obtained with this mesh “good enough”?

To answer this question we refer to Figure 1.13 where the process of hierarchical modeling is described. In that figure we implicitly assumed that the solution of each mathematical model can be obtained exactly or as close

to the exact solution as desired. Since we are also assuming that the finite element models used comply with the convergence requirements, we can indeed obtain a finite element solution as close to the exact solution as desired by sufficiently refining the mesh. However, from an engineering perspective overrefinement of the mesh may be very expensive and a waste of resources.

We recall that the ultimate objective of the modeling is to estimate the response of the structure. We are actually interested in some variables and we are also aware that in each of the mathematical models there are assumptions that lead to some errors in the prediction of these variables when measured with respect to the predictions of the most-comprehensive mathematical model. Therefore, as part of the hierarchical modeling process, we also need to establish the precision with which each variable should be predicted in the finite element solution of a mathematical model.

Hence the above “good enough” need not mean very close to the exact solution of the mathematical model since some level of error – determined in the hierarchical modeling process – is acceptable. Nevertheless, the essence of the question remains: is the solution obtained with this mesh “within the required precision”?

A pragmatic approach could be to keep on refining the mesh until for two consecutive solutions the variables to be predicted change by less than the required precision. This might be expensive, however.

The objective of this section is to discuss some issues related to mesh quality and solution accuracy which should aid the analyst to arrive at a finite element solution of a “good enough” accuracy.

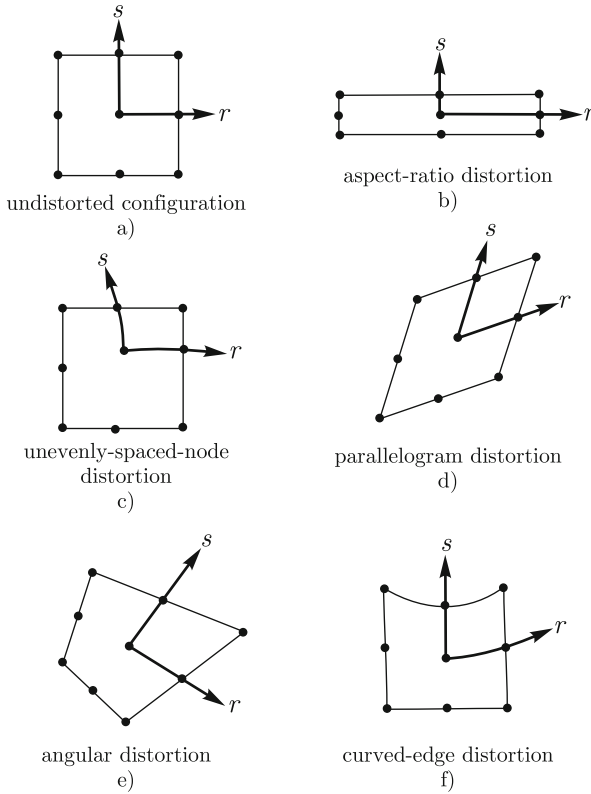
### 6.7.1 Mesh grading

In general, as in the plate with a hole problem, the analyst has an expectation about the qualitative behavior of the solution and/or in which model region a more accurate prediction is required. This information should be used to guide the selection of the first mesh.

### 6.7.2 Element shape

We assume from the start that we are using effective elements as characterized in Section 6.5. Therefore, the elements are isoparametric with the use of mixed methods to overcome locking when required.

We would like to discuss the effect of the element shape on the accuracy of the predictions. The terminology element distortion is generically used to refer to an element shape which is not a square for 2-D quadrilateral elements and not a cube for 3-D hexahedral elements. A more precise definition of distortion types is given in Figure 6.77 (see Lee and Bathe, 1993, Bathe, 1996) for 2-D quadrilateral elements. Note that the distortions (c) and (f) are not applicable to a four-node 2-D element since these are defined based on the position of the mid-side nodes.



**Fig. 6.77.** Classification of element distortions

Considering isoparametric elements, we recall that the interpolation functions are defined for the reference element using the isoparametric coordinates  $r$  and  $s$ . The interpolations in the physical coordinates depend on the element shape. For example, consider a generic four-node element as defined in Figures 6.29 and 6.30. Equations (6.111) and (6.112) show that the interpolation functions  $\tilde{h}_i(x, y)$  defined in the physical coordinates depend on the isoparametric mapping  $(r(x, y), s(x, y))$ . Therefore, the element shape which implicitly defines the isoparametric mapping through the element nodal coordinates affects the interpolation functions in the physical coordinates.

Of course, the approximation power of an element is linked to the monomials of the Pascal triangle that the element can actually represent in the physical coordinates.

Lee and Bathe (Lee and Bathe, 1993) have examined how element distortions affect the monomials which can be exactly represented in the physical coordinates. We summarize their findings in Table 6.9.

**Table 6.9.** Effect of element distortions for 2-D elements.  $Q_n, P_n$  represent all monomials of the Pascal triangle which are up to order  $n$  in each variable

Type of element	Monomials exactly represented		
	Undistorted	Angular distortion	Curved-edge distortion
4-node element	$Q_1$	$P_1$	–
8-node element	$P_2, x^2y, xy^2$	$P_1$	$P_1$
9-node Lagrangian element	$Q_2$	$P_2$	$P_1$
12-node element	$P_3, x^3y, xy^3$	$P_1$	$P_1$
16-node Lagrangian element	$Q_3$	$P_3$	$P_1$
25-node Lagrangian element	$Q_4$	$P_4$	$P_2$

We note that the 8 and 12-node elements are significantly more affected by angular distortions than the Lagrangian elements and the curved-edge distortion severely diminishes the number and order of the monomials that can be exactly represented. These observations lead to practical guidelines for mesh constructions, namely:

- When elements with angular distortion are anticipated – the usual case for engineering problems – Lagrangian elements are preferable compared to the 8 and 12-node elements.
- Unless we are modeling curved boundaries, curved edge distortions should be avoided, that is, for each edge the interior node should be placed on the straight line linking the corner nodes such that the distance between neighbouring nodes are equal.

### 6.7.3 Error estimation and adaptative procedures

Error estimation in finite element analysis is a broad field. In this section we would only like to briefly review some developments in this area with respect to their use in practical finite element analysis.

In Section 6.2, we discussed error estimates or bounds as given in (6.63) for 1-D and in (6.136) for 2-D and 3-D analyses. These error bounds are referred to as *a priori* error bounds since they give general bounds on the error even before any finite element solution is obtained. These bounds, of course, involve unknown constants. To obtain an error estimate for a specific finite element solution, the *a posteriori* error estimates are used.

*A posteriori* error estimates are useful to give the analyst an idea of how far the obtained solution is from the exact solution. Since usually the *a posteriori* error estimate is defined pointwise for the problem domain, it is also used to steer adaptative mesh refinement procedures (either  $h$  or  $p$ ).

We note that every error estimate is based on a quantity for which the error is being estimated. In the early developments this quantity was the energy norm.

More recently error estimates are being developed for specific variables of interest. These estimates are very attractive for the hierarchical modeling process, since this process is driven by the precision with which some variables are to be predicted.

Considering the voluminous amount of material which has been published regarding error estimation and the actual usage of these developments in practical finite element analysis, we observe a substantial gap. The reasons are many, but in essence the developments have still not attained a level which permit their usage in a reliable and efficient manner for practical problems. We refer the reader to Grätsch and Bathe, 2005 for a review on this subject.

Before we close this section we would like to mention a very practical procedure used in engineering analysis to assess the accuracy of finite element solutions – the isobands of stresses – as proposed in Sussman and Bathe, 1986.

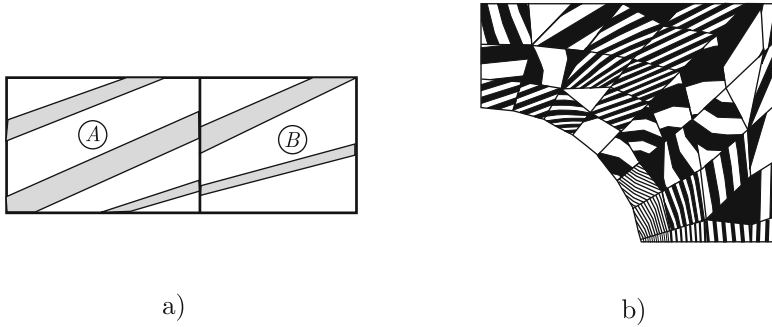
We recall that although the finite element solution always satisfies some equilibrium properties as discussed in Section 6.1, differential equilibrium is not satisfied pointwise, *i.e.*, the equations given by (3.114) are not satisfied when the stress field is obtained from the displacement finite element solution through the compatibility and constitutive relations. Also, at element boundaries, which are shared by two elements, equilibrium is, in general, violated. In fact, for a point on this boundary we can evaluate the stress (a stress component or an invariant to have a scalar value) from the displacement solution considering either element to arrive, in general, at different values. Of course, if the loads, the geometry and the material properties of the problem are smooth, there is only one stress value corresponding to the exact solution at that point and the difference in the finite element prediction is referred to as a stress jump which is a local measure of the error for the stress prediction.

By means of the stress isobands we can graphically visualize the stress jumps throughout the finite element domain. The stress isobands are constructed by plotting bands of selected stress measures (pressure, effective



stress, stress components, among others) from the displacement finite element solution.

A typical situation for two neighboring elements is shown in Figure 6.78a. Each band, black or white, represents a specified range of the stress measure.

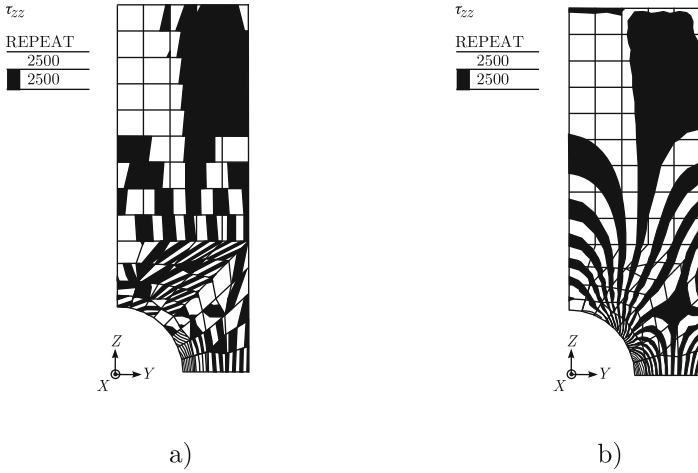


**Fig. 6.78.** a) Schematic isoband plot two neighbouring elements; b) Isobands of a mesh region

When we examine the common boundary of elements *A* and *B*, we identify some discontinuities. Selecting the magnitude of the band interval with respect to some relevant reference value for the problem, we can visualize how accurate the finite element solution is with respect to that stress measure. In Figure 6.78b we show a stress isoband plot for a region of a finite element model which we examine next. For the selected band interval we can identify all sorts of discontinuities revealing poor predictions.

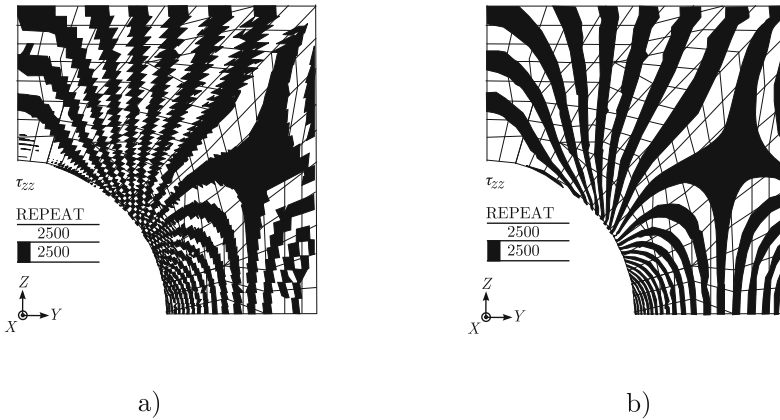
Let us consider the plate with a hole problem described in Figure 6.68. We are interested in assessing the accuracy of the prediction for the stress  $\tau_{zz}$  when using selected finite element meshes. In Figure 6.79a we show the isoband plots of  $\tau_{zz}$  obtained with 4-node quadrilateral plane stress elements. In Figure 6.79b we plot for the same mesh the analogous results obtained with 9-node quadrilateral elements. We first note that the applied uniform traction has a magnitude of  $25 \text{ N/mm}^2$  and the stress intensity factor for the component  $\tau_{zz}$  predicted by the exact solution is of the order of 4 leading to values for  $\tau_{zz}$  around  $100 \text{ N/mm}^2$  near the hole. We selected  $2.5 \text{ N/mm}^2$  as the stress band interval magnitude which is, therefore, of the order of 2.5% of the maximum  $\tau_{zz}$ . Note that for the 4-node element model we can not clearly identify a band pattern and there are very large band discontinuities revealing a poor quality prediction. For the 9-node element model we have a clear band pattern and the discontinuities are small indicating good predictions for  $\tau_{zz}$  when a  $2.5 \text{ N/mm}^2$  error is acceptable.

In order to obtain better predictions with the 4-node element a much more refined mesh is required. In Figure 6.80a, we show the isobands for a



**Fig. 6.79.** Isoband plots for  $\tau_{zz}$ . Problem data: plate width 20 mm, height 56 mm, thickness 1 mm, hole diameter 10 mm, applied traction 25 N/mm<sup>2</sup>,  $E = 7.0 \times 10^4$  N/mm<sup>2</sup> and  $\nu = 0.25$

refined mesh of 4-node elements. Of course, since the interpolations are of low-order for the 4-node element some discontinuities are unavoidable for distorted elements. If the results are smoothed by taking average values at element boundaries we obtain the isobands of Figure 6.80b. Care must be exercised when using isoband plots of smoothed results since they are always continuous at element interfaces no matter how bad the predictions might be. Therefore, smoothed results may be used to improve the visualization only when the unsmoothed results have been examined and have revealed reasonable accuracy.



**Fig. 6.80.** Isoband plots for refined 4-node element mesh

Finally, we note that the stress band plots are particularly effective in identifying incompatibilities in constructed element meshes. That is, if by a data input error, displacement incompatibilities have been created by not connecting elements properly, the stress band plots will quite likely show artificial stress gradients and stress jumps, thus indicating the regions where the mesh should be checked and repaired.

## 6.8 Finite element model construction

Before we close this chapter we would like to mention some developments that have significantly facilitated the use of the finite element method and have therefore helped to spread the use of this technology. This task is often referred to as mesh generation. In the early stages of applications of the finite element method in industry, the mesh generation was performed by defining the geometric properties of each element and its position with respect to a coordinate system. For three-dimensional problems the generation of the mesh was a major task and consumed most of the resources involved in the finite element model construction. Therefore continuous efforts have been directed to ease this burden. Nowadays, the construction of complex 3-D finite element models takes advantage of the geometric modeling of solids and makes use of automatic mesh generation algorithms which act directly on the solid models.

In order to illustrate these developments, let us briefly describe how the construction of model 3 for the carabiner (see Chapter 1 and Section 7.3) could be aided by use of geometric modeling and automatic mesh generation algorithms.

In Figure 6.81, a 3-D representation of the carabiner, *i.e.*, a geometric model is shown. These geometric models are, in general, constructed in Computer Aided Design (CAD) codes for other purposes than performing a finite element analysis. Their primary objective is usually linked with the production process of the part/equipment/structure. We note that this is the reason why some details are present in the geometric model shown in Figure 6.81 such as the letter imprints and the small hole for the pin of the superior closing part. For the kind of structural predictions generally sought, such details are not important and their modeling would lead to a much more refined finite element model than required. Therefore, it is necessary to modify the geometric model before generating the finite element model and implicitly the mesh. This process is called *defeaturing* and it corresponds to the suppression of features that have no significant impact on the prediction of the variables sought in the analysis.

In Figure 6.82, we give an illustration of the *defeaturing* process. We see that it is still performed at the level of the geometric model using, in general, the tools of the geometric modeling program. We show in Figure 6.83 the results of some steps of the finite element model construction that can still

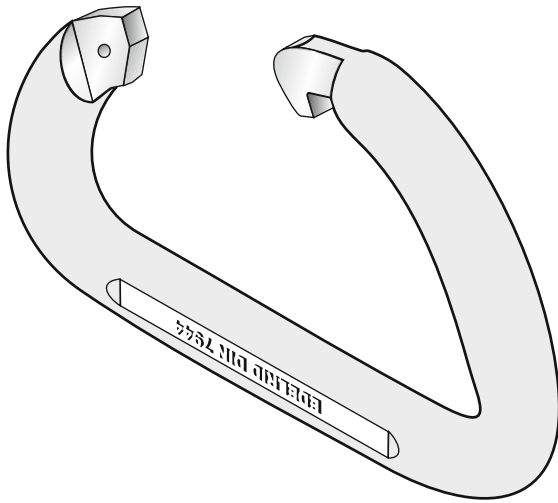


Fig. 6.81. Geometric model of the carabiner

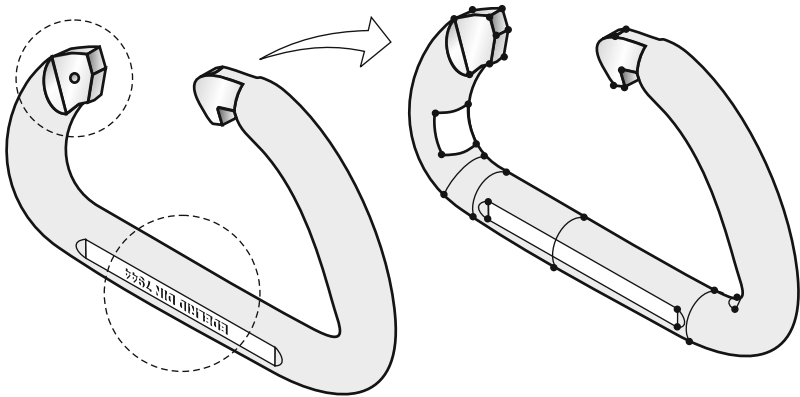
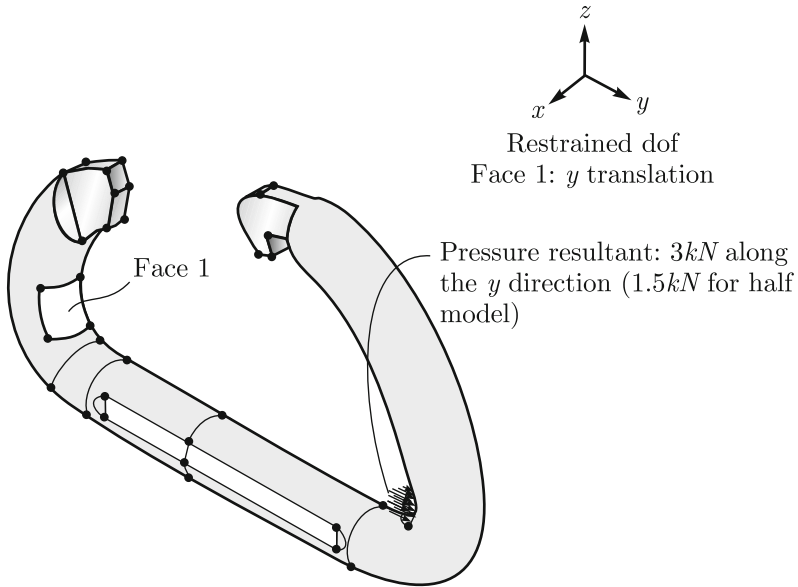
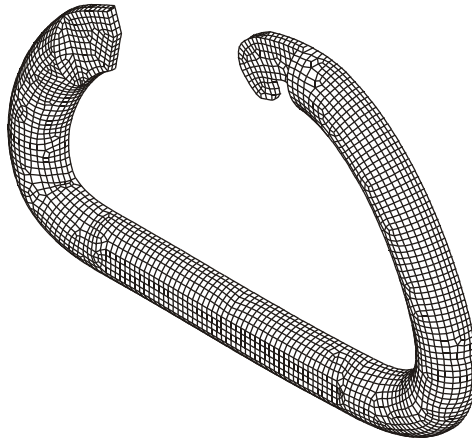


Fig. 6.82. Illustration of the defeaturing process

be made at the geometric modeling level. The surfaces to apply the pressure and to specify the displacement boundary conditions can be defined on the geometric model. Also, the representation of only half of the model due to symmetry can be introduced at the geometric modeling level. The geometric model of Figure 6.83 with the mechanical conditions already introduced is ready for the mesh generation. In Figure 6.84 an automatically constructed mesh is presented.



**Fig. 6.83.** Finite element mechanical conditions that are applied to the geometric model



**Fig. 6.84.** Finite element mesh for the carabiner

## 6.9 A finite element modeling example

We choose to end this chapter by discussing the finite element modeling of a simple problem. Actually, this example could have been included in the next chapter as one of the modeling examples. However, placed at this point

it should be interpreted as a synthesis of many concepts introduced in this chapter.

### Spherical dome subjected to its own weight

This problem was studied in Section 4.4.2 and solved with the shell mathematical models presented in that section. We consider first the situation shown in Figure 4.116 for which the dome is supported tangentially. The data of the problem is that given in Example 4.21.

The sequence of mathematical models for this problem is:

1. Membrane-bending shell model
2. Basic shell model
3. 3-D elasticity model

Of course, in case the support prevents the motion along the tangential direction only, model 1 is analytically solved using the membrane theory of shells of revolution loaded axisymmetrically as detailed in Examples 4.19 and 4.20.

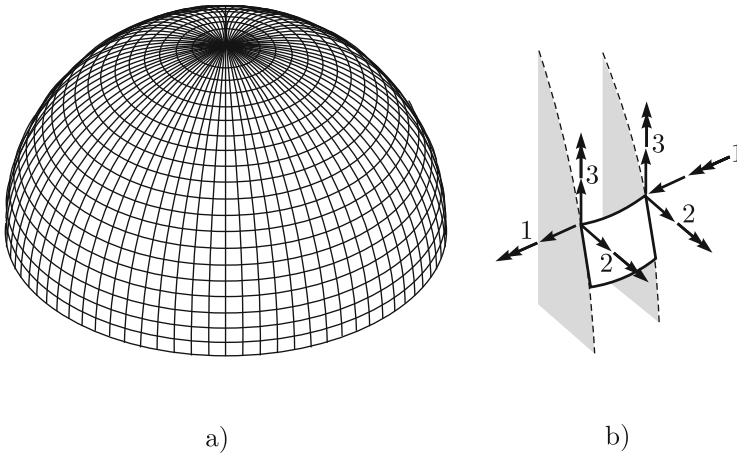
We resort to finite elements to solve models 2 and 3. The most efficient way to solve model 2 is to use the degenerated solid approach particularized to axisymmetric conditions. This procedure actually leads to axisymmetric shell elements based on the degenerated approach, see Bathe, 1996. In this study, however, we use shell elements to obtain the solution of model 2 and to exemplify their usage.

To solve model 3, we use axisymmetric 2-D elements. Of course, in this case, the solution of the axisymmetric 2-D elasticity model corresponds to the exact solution of the 3-D model as discussed in Section 4.1.3.

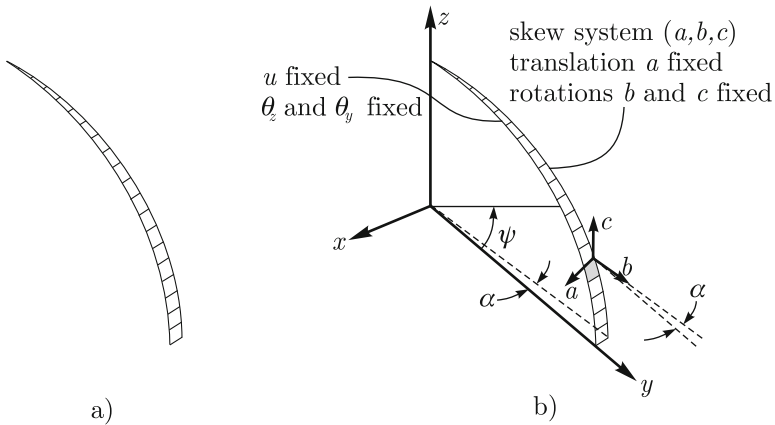
#### Model 2 – Shell model

We need to choose an initial mesh. We selected 20 elements along the meridian direction to discretize the curved geometry and no grading is used since due to the tangential support condition a membrane type solution is expected.

In Figure 6.85a we show a mesh which discretizes the whole shell domain with eighty elements along the circumferential direction. The elements in the shell apex region are degenerated triangular elements which have such a small width that they can not be seen with the scale of Figure 6.85a. In Figure 6.85b, we show a generic element and the degrees of freedom for two nodes. These degrees of freedom are selected such that two of their directions (2 and 3) lie on the meridian plane and direction 1 is orthogonal to it. Due to the symmetry conditions the rotations about directions 2 and 3 should be zero and the displacement along the direction 1 should also be zero. Therefore, considering these symmetry conditions we can select to discretize only a



**Fig. 6.85.** a) Shell model; b) Degrees of freedom for a node at the meridian



**Fig. 6.86.** a) Model of a shell wedge; b) Symmetry boundary conditions

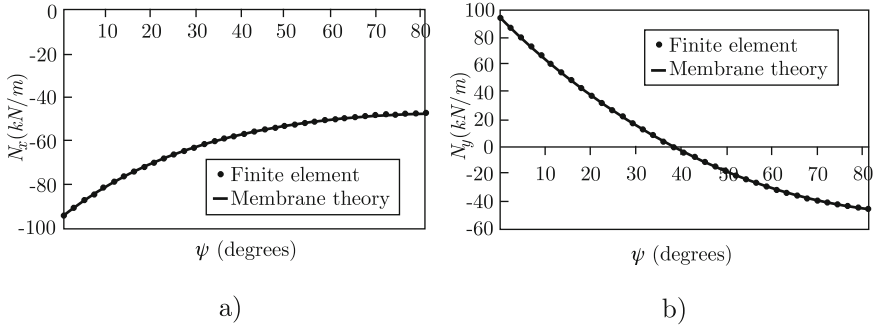
wedge of the shell as shown in Figure 6.86a instead of discretizing the whole domain.

As long as we impose the symmetry boundary conditions as detailed above for every node on the meridian planes and the elements are geometrically the same as those of the mesh of Figure 6.85a for one element along the circumferential direction, we would obtain exactly the same predictions with the models of Figures 6.85a and 6.86a.

In order to impose the boundary conditions discussed above for the model of Figure 6.86a we can position the model with respect to the global system and define a skew system as shown in Figure 6.86b. Then the appropriate boundary conditions can be imposed as detailed in Figure 6.86b.

The model of Figure 6.86 was solved with MITC9 shell elements, considering first that the shell is tangentially supported. Since our model is hemispherical, we prevent the vertical displacement at the shell edge.

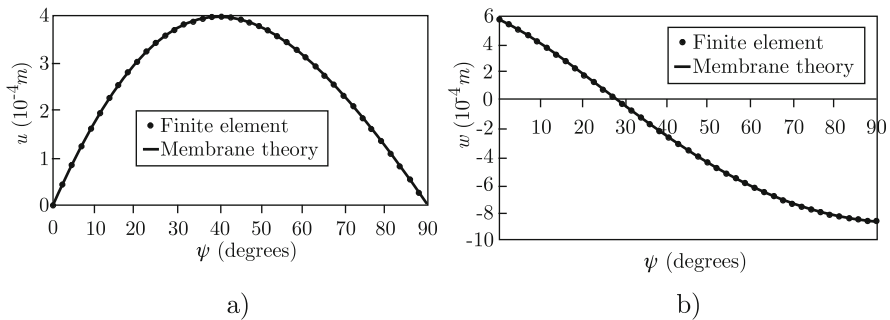
In Figure 6.87 we compare the membrane force predictions obtained with the model of Figure 6.86 to those of the membrane theory derived in Example 4.19.



**Fig. 6.87.** Membrane force predictions. The angle  $\psi$  is measured from the edge as shown in Figure 4.122

We note the very close agreement between the membrane theory solution and the finite element solution. The finite element model predictions for the bending moments lead to very small values of less than 1 kN.m/m, therefore confirming the membrane behavior of the shell for the tangential support.

In Figure 6.88 the tangential  $u$  and radial  $w$  displacement predictions are shown. We again note the very close agreement between the membrane theory solutions and the finite element model predictions.

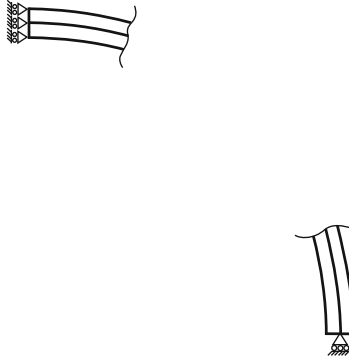


**Fig. 6.88.** Displacements of the midsurface of the shell. Finite element shell and membrane theory solutions;  $u$  and  $w$  measured as in Figure 4.115



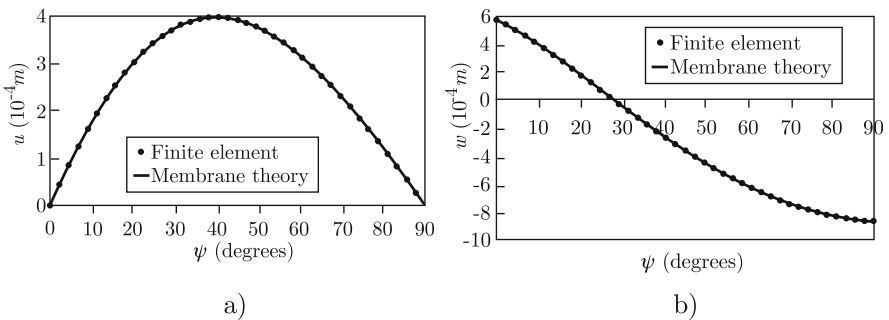
### Model 3 – 2-D axisymmetric model

In Figure 6.89, we show a close-up at the support regions of the finite element mesh for the tangentially supported shell where the model boundary conditions are shown. Again, a uniform mesh was used since we expect a membrane type solution. We used a total of eighty 9-node 2-D axisymmetric elements with two elements through the shell thickness.



**Fig. 6.89.** Axisymmetric 2-D model

We compare the nodal displacements at the line which corresponds to the midsurface of the shell to the membrane theory solution. The results are shown in Figure 6.90 and the same convention used for Figure 6.88 is adopted. We note that with the scale of the graph we can barely distinguish between the model solutions.



**Fig. 6.90.** Displacement predictions of the midsurface of the shell. Finite element 2-D and membrane theory solutions

The stress resultants such as axial forces and bending moments can be obtained through the integration of the stress fields. These resultants were

evaluated leading to predicted values which are very close to those of the membrane theory.

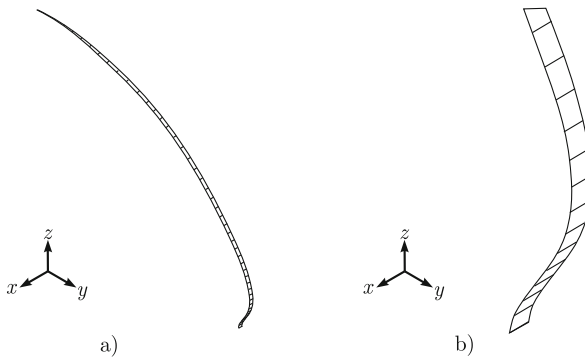
### Modeling of the clamped case

As discussed in Section 4.4.2 when a spherical dome is clamped, the shell can no longer resist the external loading through membrane internal actions alone and some bending takes place.

In Example 4.21 this problem with clamped conditions was solved. We obtained the bending moment distribution  $M_x$  reported in Figure 4.124.

Now we want to solve this problem with the shell finite element model and since we anticipate high gradients for the variables of interest near the edge, it is natural to use a graded mesh. We refined our mesh by grading it along the meridian assigning a smaller mesh density near the edge. We also refined the mesh for the circumferential direction by selecting a smaller central angle of  $1^\circ$  instead of  $4.5^\circ$  for the previous case. This is equivalent to considering a full shell model with 360 divisions in the circumferential direction.

In Figure 6.91a we show a much magnified deformed mesh and in Figure 6.91b a close-up view of the deformations near the edge.



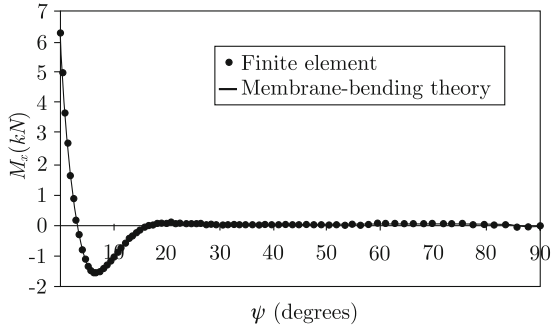
**Fig. 6.91.** Deformed mesh

In Figure 6.92 we compare the solution obtained with the shell model of Figure 6.91 with the shell theory solution derived in Example 4.21. We can see the close agreement obtained for the variable  $M_x$ .

This clamped case was also solved with the 2-D axisymmetric model. A mesh grading was also used and the stress resultants such as  $M_x$  were evaluated by integration; the calculated values were very close to those predicted by the shell theory and shell finite element model.

### Summary

In this section we detailed the modeling of a simple shell structure. Nevertheless, several issues related to model choices and finite element mesh



**Fig. 6.92.** Moment  $M_x$  predictions

constructions could be explored. We emphasize that the knowledge of the mathematical models used was an essential ingredient. Also, it was very important to be able to anticipate the nature of the solution, since this will guide the choice of mesh density. The use of symmetry and skew systems simplified a great deal the shell models, not only diminishing the computational effort but also facilitating the understanding through an easier interpretation of the results.

The three models considered led to very close predictions for displacements and internal actions showing that they are reliable for this problem.